Surface-Induced Assembly for Molecular Arrangement in Thin Film based on Porphyrin Coordination Networks

SALINTHIP LAOKROEKKIAT

Japan Advanced Institute of Science and Technology

Doctoral Dissertation

Surface-Induced Assembly for Molecular Arrangement in Thin Film based on Porphyrin Coordination Networks

SALINTHIP LAOKROEKKIAT

Supervisor: Associate Professor Dr. Yuki Nagao

School of Materials Science

Japan Advanced Institute of Science and Technology

September 2016

Referee-in-chief : Associate Professor Dr. Yuki Nagao

Japan Advanced Institute of Science and Technology

Referee : Professor Dr. Noriyoshi Matsumi

Japan Advanced Institute of Science and Technology

Professor Dr. Kohki Ebitani

Japan Advanced Institute of Science and Technology

Professor Dr. Donglin Jiang

Japan Advanced Institute of Science and Technology

Associate Professor Dr. Tatsuya Nishimura

Kanazawa University

Abstract

The development in nanostructural materials has been continuously pursued due to the higher efficiency than that of conventional materials. In recent, the engineering of nanomaterials onto the surface for device applications has been progressively promoted through the concept of coordination chemistry and surface science. In aspect of material performance, not only the molecular components but also molecular ordering and alignment direction play significant impact on it. The strategy to control the architectures is extremely important to achieve the desired properties. Surface-Induced Assembly (SIA) is considered for this achievement. The sequential immobilization between metal ions and organic building units on the surface can promote huge variety of coordination structures with controllable manner. The stepwise growth phenomena using SIA approach differs from the bulk system. The novel structures on surface can be possibly discovered by this method.

In this research, the oriented porphyrin-based multilayer thin films on amine-terminated surface substrates were synthesized using cobalt(II) ions and porphyrin building blocks via SIA approach at room temperature. The multilayer thin films exhibited the stepwise growth with compact packing and homogeneous surface morphology which were characterized by UV-Vis, AFM, IR, and XPS studies. The studies on XRR and GI-SAXS revealed that the mass density of film was almost constant throughout the multilayer formation along with the existence of periodic structure in in-plane (IP) direction. These results indicated a well-organized structure of film growth. The alignment of the porphyrin macrocycle plane in the framework has been proposed as a hexagonal packed model using single-anchor binding with tilting of approximately 60° relative to the surface substrate. This result suggested that structural arrangement on the surface can be efficiently controlled by SIA technique. The structure of the synthesized thin film was distinct from the bulk synthesis, which suggests a significant role of the surface and SIA approach for the coordination network formation.

This report of our research provides insight into the ordered porphyrin-based metal-organic coordination network thin films. The design of metal-organic coordination network thin film with controllable growth behavior represents as an important challenge that must be addressed to promote these solid state phenomena for nanoscale device. The interior perspective for the molecular growth behavior is highly necessary to elucidate the growth mechanisms along with the development of material properties for specific applications.

Keyword : Surface-Induced Assembly (SIA), Thin Film, Porphyrin, Metal-Organic, Coordination Networks

Table of Contents

Abbreviation

ALD	Atomic Layer Deposition
AFM	Atomic Force Microscope
APTMS	3-Aminopropyltrimethoxysilane
$CHCl_3$	Chloroform
$Co(OAc)_2.4H_2O$	Cobalt(II) acetate tetrahydrate
CoTCPP	Cobalt(II)- Tetrakis(4-carboxyphenyl)-porphyrin
FET	Field-Effect Transistor
FTIR-ATR	Fourier-transform infrared attenuated total reflectance
GI-SAXS	Grazing incidence small angle X-ray scattering
H_2TCPP	5,10,15,20-Tetrakis(4-carboxyphenyl)-porphyrin
H_2TPyP	5,10,15,20-tetra(4-pyridyl)porphyrin
IP	In-plane
LB	Langmuir-Blodgett
LbL	Layer-by-Layer
LPE	Liquid Phase Epitaxy
MLD	Molecular Layer Deposition
MOFs	Metal-Organic Frameworks
OP	Out-of-plane
p-MAIRS	Infrared p-polarized Multiple Angle Incidence Resolution Spectroscopy
PXRD	Powder X-ray diffraction
RMS	Root-mean-square
SAMs	Self-Assembled Monolayers
SBUs	Secondary Building Units
SEM	Scanning Electron Microscopy
SIA	Surface-Induced Assembly

SURMOFs	Surface-attached Metal-Organic Frameworks
XPS	X-ray photoelectron spectroscopy
XRR	X-ray reflectivity

List of Figures

Page

List of Tables

Page

List of Schemes

Page

Chapter 1

General Introduction

1.1 Molecular Assembly

Supramolecular chemistry involves with the study in molecular assembly, molecular recognition, and host-guest chemistry via the noncovalent interactions such as hydrogen bonding, van der Waal, π-π interaction, and metal-ligand coordination.[1, 2] These noncovalent interactions are essential to understand the process in biological system. Through the clever concept of organized structure in the nature, the inspiration to create the artificial organized material has been occurred. In light harvest complexes in natural such as chlorophyll derivatives, the molecular distance and the orientation impact to the energy transfer in this system. This leads to study in the self-assemble of molecular dye such as porphyrin derivatives to improve the efficiency in solar cell system.

In common concept, device is made from the assemblies of components. The individual component shows the simple ability, meanwhile the assemblies show more complicated and useful function.[3] The important factors for the material properties are not only its component, but also how the structure arranges. The organization of the molecular scale such as atomic level to the macroscopic scale in the system is potentially involved to the properties of its material (Figure 1.1)[4,5]. Through this concept, the supramolecular assembly plays a crucial impact to develop the organized structure.

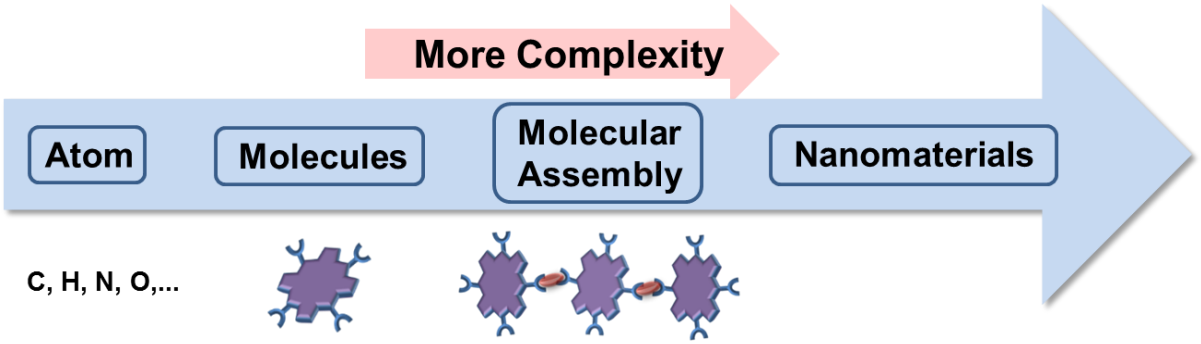

Figure 1.1 Complexity in matter.

Nanostructural materials have been continuously developed due to their higher efficiency than that of conventional materials in various research fields.[6, 7] To prepare the nanostructure materials, molecular assembly is considered which refers to the gathering of molecules to generate the array structures in nanometer size.[8] The preparing of molecular assembly in nanoscale with high tenability in structure, function and properties plays a significant role to enhance material ability.

1.2 Revolution from Bulk to Thin Film Material

As the development in technologies aims to facilitate human's life, the improvement for material preparations and processing are more extensively pursued with various protocols to create the potential applications as human demand. In general, the assembly of components to create material usually occurs in solution phase, which can produce as bulk or single crystal material. Although the uses of bulk material are already available in various applications such as adsorption-separation, sensing, catalysis, magnetic, electronic, and biomedical application, the utilization is not sufficient in all cases. This makes the limitation for the real usage. At this aspect, the immobilization of molecular assembly at the surface in nanoscale was recently intended with expectation for the improvement in utilization, especially for device development.[9, 10] Furthermore, the high surface area of nano-sized material is expected to exhibit the higher efficiency than the macroscopic bulk.

Figure 1.2 represents the revolution from bulk to thin film synthesis of the assembly between metal and organic building units through metal-organic coordination. This can solve this limitation and extend the usage in wide range of device applications in this research field[9, 11](Figure 1.3).

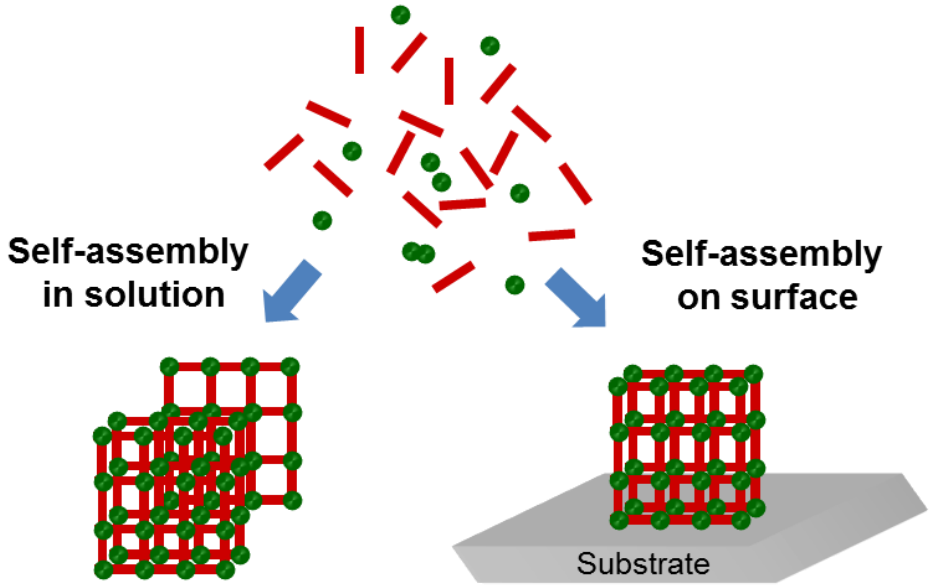

Figure 1.2 Comparison of conventional bulk Metal-Organic Frameworks (MOFs) synthesis and MOF thin film on surface through the self-assembly concept.

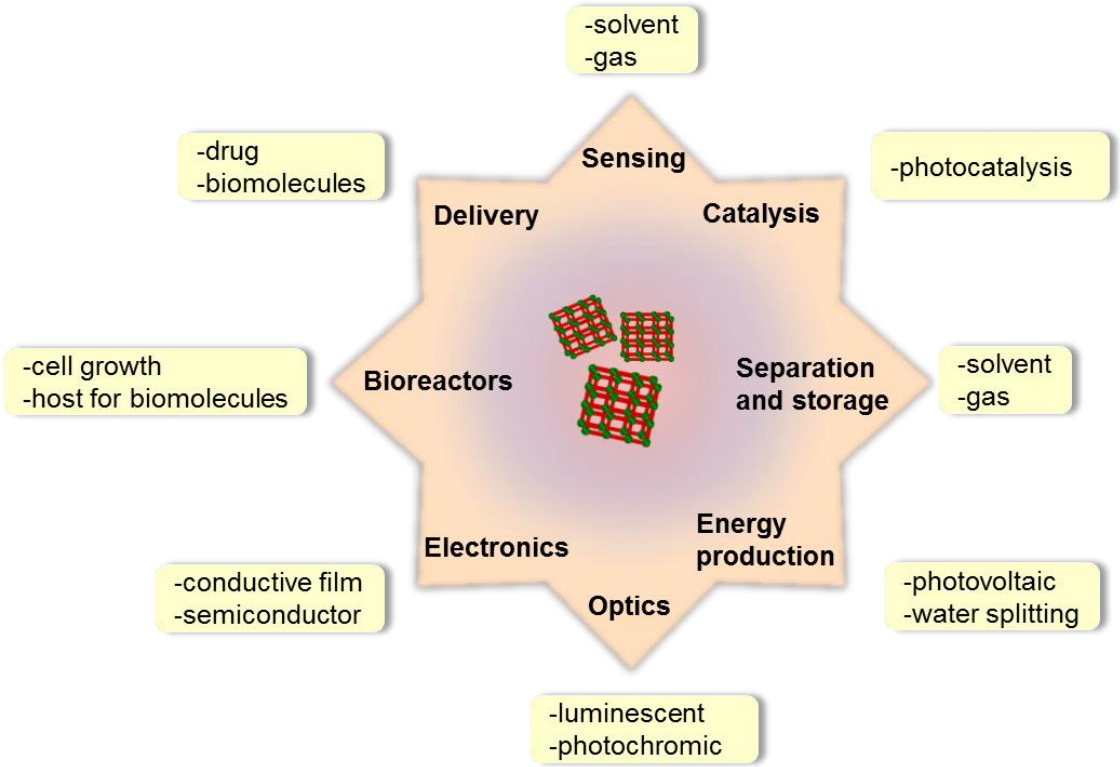

Figure 1.3 MOF-based device applications.

The engineering of molecular-based nanoarchitectures onto the surface such as thin film is recently promoted via the concept of coordination chemistry and surface science[12] in the monolayer and multilayer fashion to produce the unique material with organized features. However, the control of structural arrangement at a nanoscale level is highly challenging. The methods to manipulate the spontaneous assembly of molecular building units with well-defined structure are considered to achieve in this issue.

1.3 Structures Drive Function

The well-defined or ordered molecular alignment can control the electron and proton transfer in efficient pathway within the frameworks, which can improve the performance of materials. For examples, the proton conductivity in an oriented thin film is higher than conductivity in the random structure of bulk system[13], the ordered structure of porphyrin array fabricated by LPE in semiconductor shows the better improvement in photovoltaic device than disorder material[14] (Figure 1.4). Synergistic concern between structural arrangement and material properties presents a challenging issue for breakthrough in the required utilizations.

a)

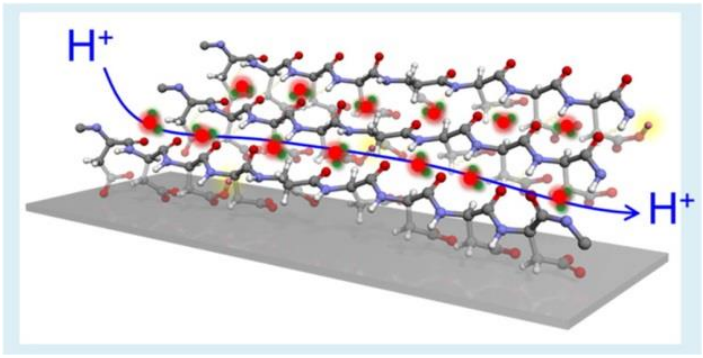

b)

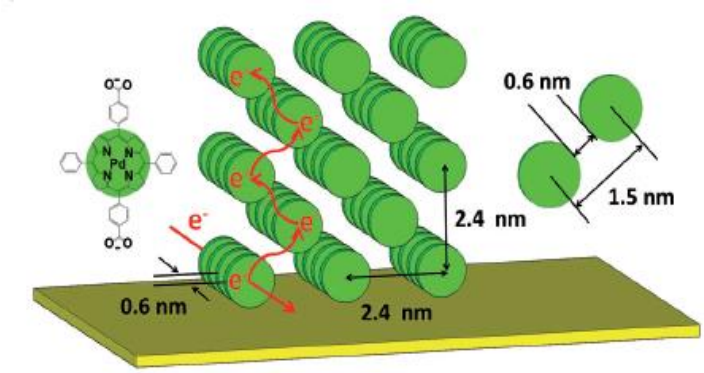

Figure 1.4 Examples of the driven functions by structures in aspect of (a) proton transport[13] and (b) electron transport in the ordered system.[14]

Not only the molecular ordering, but the alignment direction of molecule in thin film also play significant impact for performance of material. For example, the edge-on orientation of molecular arrangement on the surface is desirable for field-effect transistor (FET) devices, which the organization in in-plane improves the charge migration between the electrode. In contrast, the face-on orientation is preferred for photovoltaic devices such as solar cells[15] (Figure 1.5). Therefore, the determination of molecular alignment is essential to clarify the appropriate application. As in this point, the strategy to control the architectures on the surface is extremely important.

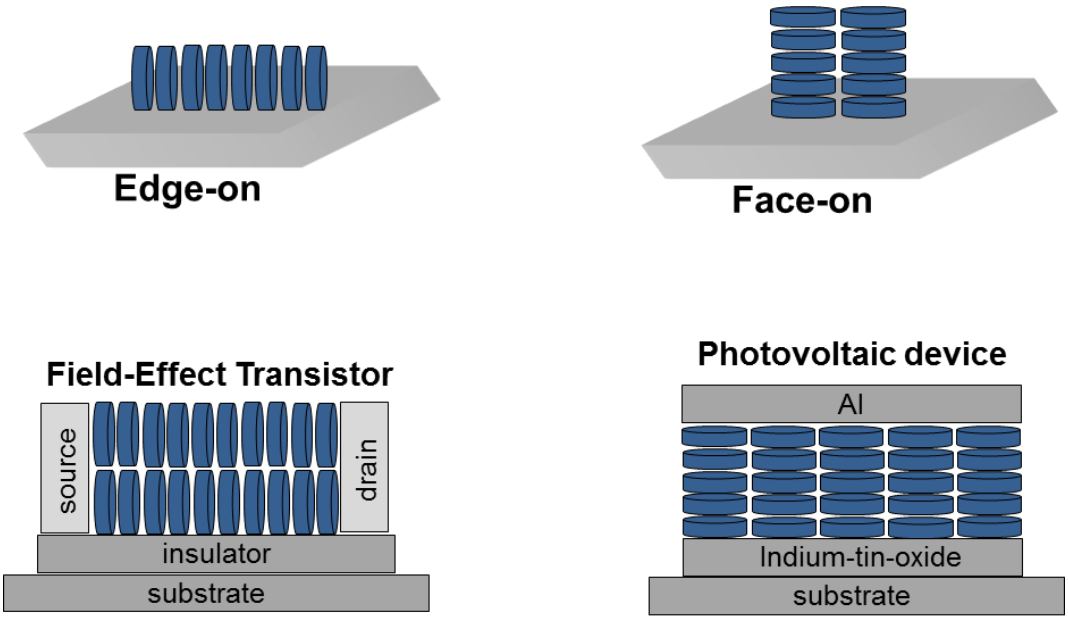

Figure 1.5 Edge-on alignment for FET and Face-on alignment for photovoltaic device (solar cell).

1.4 Build-Up Thin Film on Surface

As the huge interest in nanostructural material on the surface, the design and the capability to control molecular assembly with precise structure is significant for the properties and performance of device. To bulid up the nanostructure, two major synthetic approaches are top-down and bottom-up approach (Figure 1.6). The top-down approach uses electron beam or X-ray lithography to fabricate the device such as removing the material to achieve the smaller pattern.[16] The bottom-up approach relies on the assembly of small components such as atom or molecule to make more complexity in 2D and 3D systems.[17]

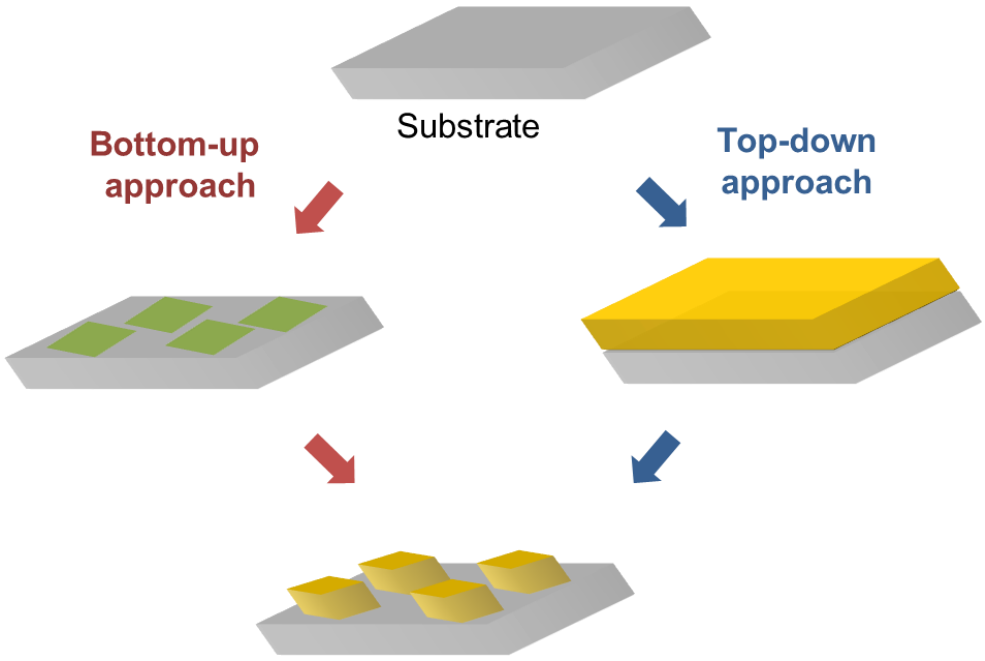

Figure 1.6 Top-down and bottom-up approach for nanostructure fabrication.

In bottom-up approach, the various techniques for thin film fabrication on the surface are described[9, 18] including Layer-by-Layer (LbL) (also Liquid Phase Epitaxy, LPE)[19], Langmuir-Blodgett (LB)[20], microwave[21], colloidal[22], electrochemical deposition[23], inkjet[24],

spray coating[25] and spin coating[26]. Among these methods, LbL is a widely used fabrication process to control the multilayer nanostructure on a surface substrate due to the controllable thickness, high structural ordering, wide variety of components, and simple operation.[4, 27] In case of another popular method, LB approach, the film is prepared at the air-liquid interface, followed with transferring to the substrate. However, LB method requires quite specific apparatus and operation procedure.

Layer-by-layer is a potential technique for thin film fabrication among bottom-up approach. In traditional LbL technique[28], the opposite charge species of polyelectrolytes such as cationic and anionic charged species were adsorbed sequentially at the surface (Figure 1.7). This method can generate the multilayer structure with controllable thickness. Although the polycation and polyanion can make the strong binding between the polymer chain, this behavior gives the less information about the arrangement in the internal structure which is limited to the study of insight growth.

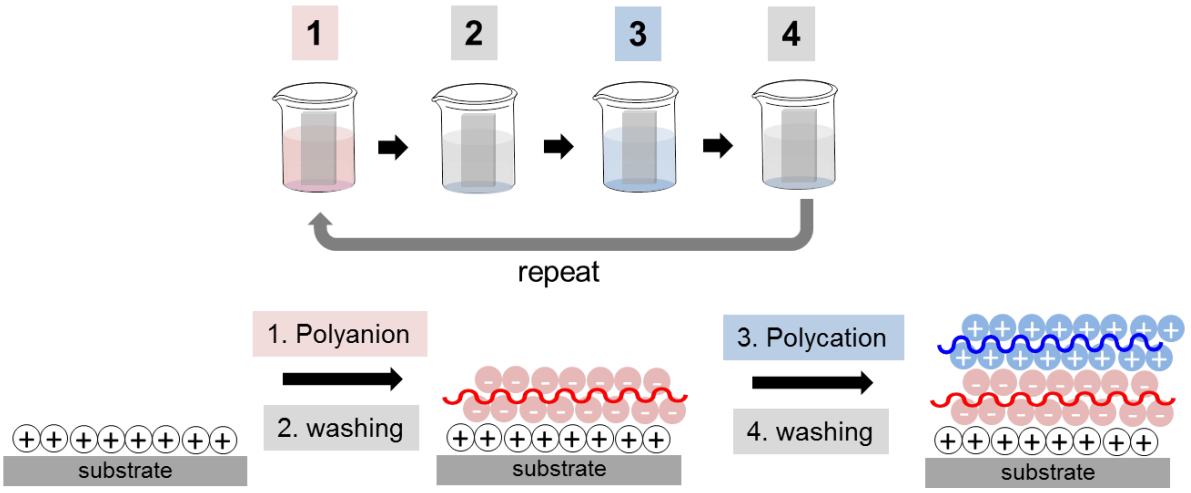

Figure 1.7 Traditional LbL technique for build-up multilayer thin film by electrostatic interaction.

The various kinds of intermolecular interactions can be used for LbL assembly such as electrostatic interaction[29], covalent bonding[30], hydrogen bonding[31], metal-organic coordination[32], and host-guest interaction[33] etc. Typical LbL is available for solution-based LbL and vapor-based LbL. The solution-based deposition process is one of the effective techniques to prepare the well-organized structure on the substrate. During each layer deposition, the physisorbed molecule is removed by solvent washing. In case of vapor-based LbL, Atomic Layer Deposition (ALD) and Molecular Layer Deposition (MLD) were generally utilized. ALD method is based on inorganic components such as metal oxide, metal nitrile, and noble metal. The unreacted precursors is removed by inert gas purging.[34] MLD technique is used for bi- or multi-functional organic molecules, which can lead to prepare the crosslinking of organic thin film.[35]

LbL is spontaneous thin film fabrication with self-limiting character of saturated surface as represented in Figure 1.8 with two different types of LbL growth[36]. In Figure 1.8 (a), the material deposits as a layer without any significant binding at specific point likewise random distribution. In contrast, Figure 1.8 (b) represents the binding of components at the specific point on the surface, which can make the specific arrangement likely the ordered structure. Figure 1.8 (b) refers to the LbL in particular with functionalized substrate (self-assembled monolayers (SAMs)), which is considered as the promising strategy to build-up the ordered structure of multilayer film on the surface in nanoscale level with simple and versatility of components.

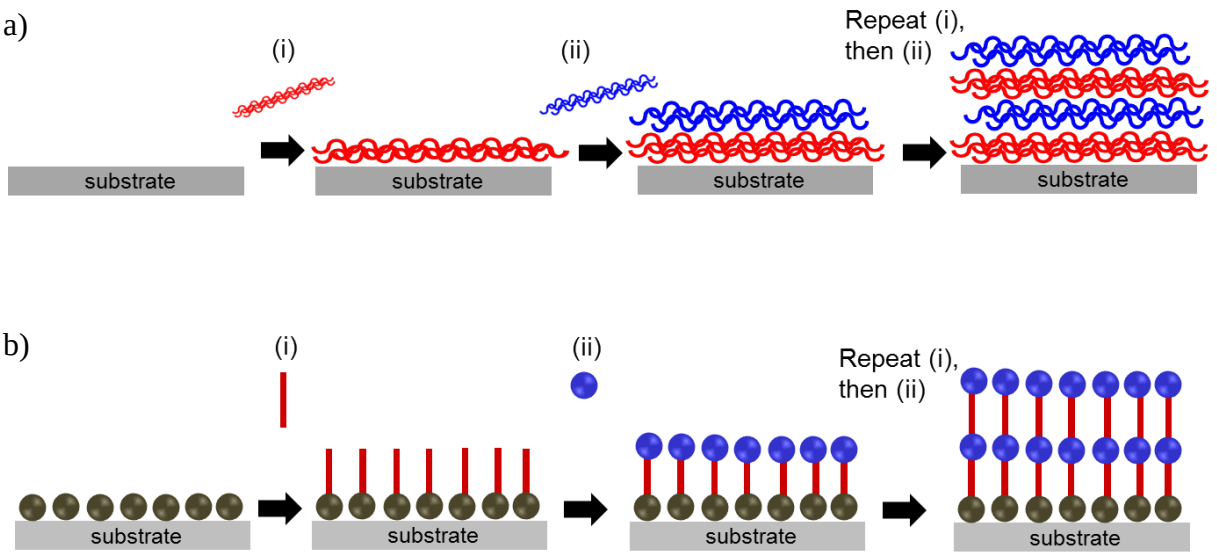

Figure 1.8 Two types of Layer-by-Layer (LbL) growth (a) no specific binding point, and (b) with specific binding point.

In this research, we consider that the surface is strongly important for the growth phenomena of thin film. We determine "Surface-Induced Assembly (SIA)" as a technique to control the molecular arrangement on the surface. The sequential immobilization between two components such as metal ion and organic building units onto the specific functionalized surface can promote the variation of coordination network structures in a controllable manner with high alignment and homogeneity at molecular level. This stepwise growth phenomenon is dissimilar to that of bulk. The coordination is simultaneously driven in the bulk system, which easily leads to generate the random or non-crystalline structure. From this aspect, novel structures on the surface can be possibly discovered by the SIA approach. For the detail in growth process of SIA, it is expected that the size of molecular building unit effectively determines the structure on the surface. For an example, the large molecular unit such as porphyrin macromolecule can strongly dominate the coordination structure on the surface rather than the small unit of metal ions.

1.5 Engineering of Metal-Organic Coordination Network Thin Film

The coordination complexes are typically acquired by the combination between metal and ligand precursors to create the metal-ligand bonding. As mentioned about the methods to fabricate thin film on surface in the previous part, we intend at sequential immobilization of components with the presence of SAMs on the surface. The research on metal-organic coordination-based multilayer assemblies on the substrates by bottom-up feature via LbL approach has been rapidly studied with the interest in surface chemistry at the solid-liquid interface.[37-42] Furthermore, self-assembled monolayers (SAMs)[43, 44] were effectively used as a nucleated template to control the oriented growth of metal-organic network on the surface with bottom-up style[45-50] as shown in Figure 1.9. It was mentioned that the types and the density of functional group on SAMs surface can affect to the orientation of structure on surface.[51, 52] The detail of SAMs will be displayed in the chapter 3.

Wöll, Fischer and co-workers introduced the LbL method to generate MOF films on surface.[19, 53] The particular MOF thin films in multilayer fashion with nanometer range are recently referred to surface-attached Metal-Organic Frameworks (SURMOFs). The SURMOFs are particularly beneficial because of their highly oriented structure, homogeneous morphology with a smooth surface, precisely controllable thickness via deposition cycle, and less defective framework than bulk synthesis.[54] These qualities were required for the device utilization.

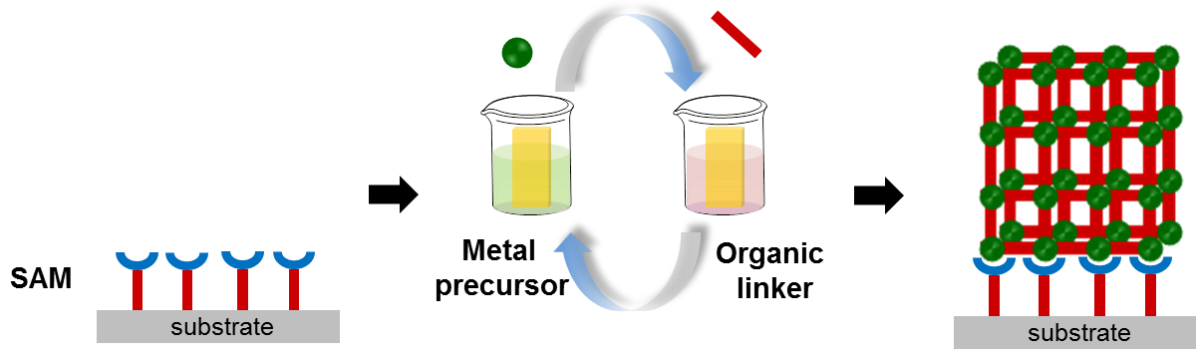

Figure 1.9 The growth of SURMOFs on SAMs surface via step-by-step method.

The crystal engineering development[55] was pursued to control the polymeric networks with the desired topology according to the building units. Not only the molecular components, but also the arrangement within the crystal lattice can contribute to the properties. Van der Boom pointed out the importance of surface-confined assembly that the binding site at the surface can determine the structure of metal-organic assembly on that surface. This refers that the variety of structures on the surface can be possibly obtained by changing of active functional group on the surface.[56]

The choice of organic building unit and metal ion combined with the particular surface functionality and also the assembly method are concomitantly important to define the structure. The state of the art for the coordination chemistry is highly scoped on the surface. The heterogeneous structures can be possibly achieved by this sequential deposition method which was reported in recent.[57] The alteration of sequence in assemblies can provide not only the multi-components, but also the possibilities of different functions in single thin film (Figure 1.10). The variety of coordination between transition metal ions and organic ligands

leads to the creation of 2D and 3D metal-organic coordination networks for various applications including gas storage, separation, sensing, catalyst, and drug delivery.

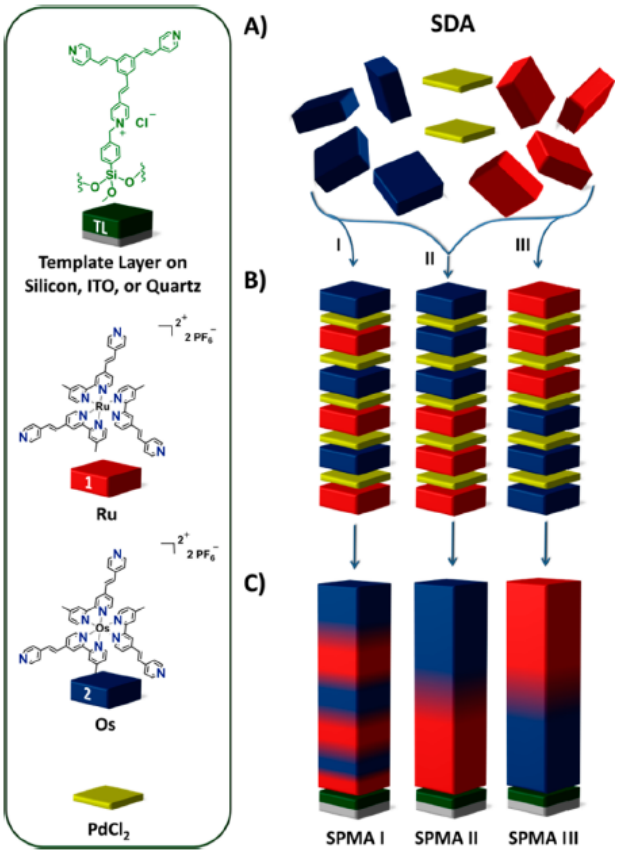

Figure 1.10 The different sequences of molecular assemblies providing the heterogeneous structures.[57]

The strategy for nanoscale assemblies is critically considered to achieve the organized structure with high performance. One of the challenging issues is to produce the controllable arrangement of molecule on the surface at room temperature. The author decided to take the advantage of SIA technique to promote the arrangement of metal-organic coordination networks on the surface using porphyrin as molecular building unit. The unique characteristics and the diversity of functions in porphyrin such as photosynthesis, oxygen

transport, and catalytic properties attract to build up the artificial material based on porphyrin building unit. Although the numerous bulk porphyrin-based MOFs have been reported, the thin films have been less explored.[58] In recent, porphyrin-based MOFs thin films on substrate have been more investigated such as Hupp group using LbL technique [59, 60], Kitagawa group using LB-LbL technique[20, 61, 62], and other groups.[63-65] Nevertheless, the insight investigations of the ordered porphyrin-based metal-organic thin films are still needed to explore the growth behavior of thin film materials.

This research potentially declares how importance of the surface through metal-organic coordination chemistry and surface science. The control of growth, orientation and also confined position on the surface support is still interesting issue which may contribute to the discovery in novel types of metal-organic coordination structures on the surface.

1.6 Research Objectives

Nanostructural materials have been continuously developed due to their higher efficiency than that of conventional materials. The engineering of nanomaterials onto the surface is recently promoted via the concept of coordination chemistry and surface science. However, the control of structural arrangement at a nanoscale level is highly challenging.

The objective in this research is to use the surface-induced assembly (SIA) method for pursuing the molecular arrangement of porphyrin-based coordination network thin film on the substrate surface. This research was mainly addressed in two parts as following :

1) The preliminary investigation of bulk synthesis of porphyrin-based coordination networks at room temperature condition.
2) The study of thin film synthesis of porphyrin-based coordination networks on amine-functionalized surface by SIA approach, especially in these aspects:
    - Growth phenomena, morphology, and molecular arrangement
    - Structural comparison between bulk and thin film

1.7 Outline of thesis

In chapter 1, the general introduction of this thesis was mentioned in the scope of assembly of components from the bulk to thin film material.

In chapter 2, the bulk of porphyrin-based coordination networks was successfully synthesized at room temperature. The preliminary investigation of bulk properties suggests that the presence of crystalline structure can be achieved under this synthetic system. The finding in this chapter motivated to the study of thin film preparation on the surface by SIA technique in chapter 3.

In chapter 3, the thin film of porphyrin-based coordination networks on amine-functionalized surface substrate was synthesized using SIA technique at room temperature. The growth phenomena and thin film properties were examined. It was found that the organized structure of multilayer thin film can be obtained even in mild synthetic condition. The different structures between bulk and thin film were observed, which suggests about the role of surface and SIA process for the molecular arrangement on surface.

In chapter 4, general conclusion and future prospects of this research were presented. The finding in this research can contribute to the study of coordination chemistry on the surface which may promote the understanding in solid state phenomena and extend to prepare the various nanostructure systems for application in nanoscale device.

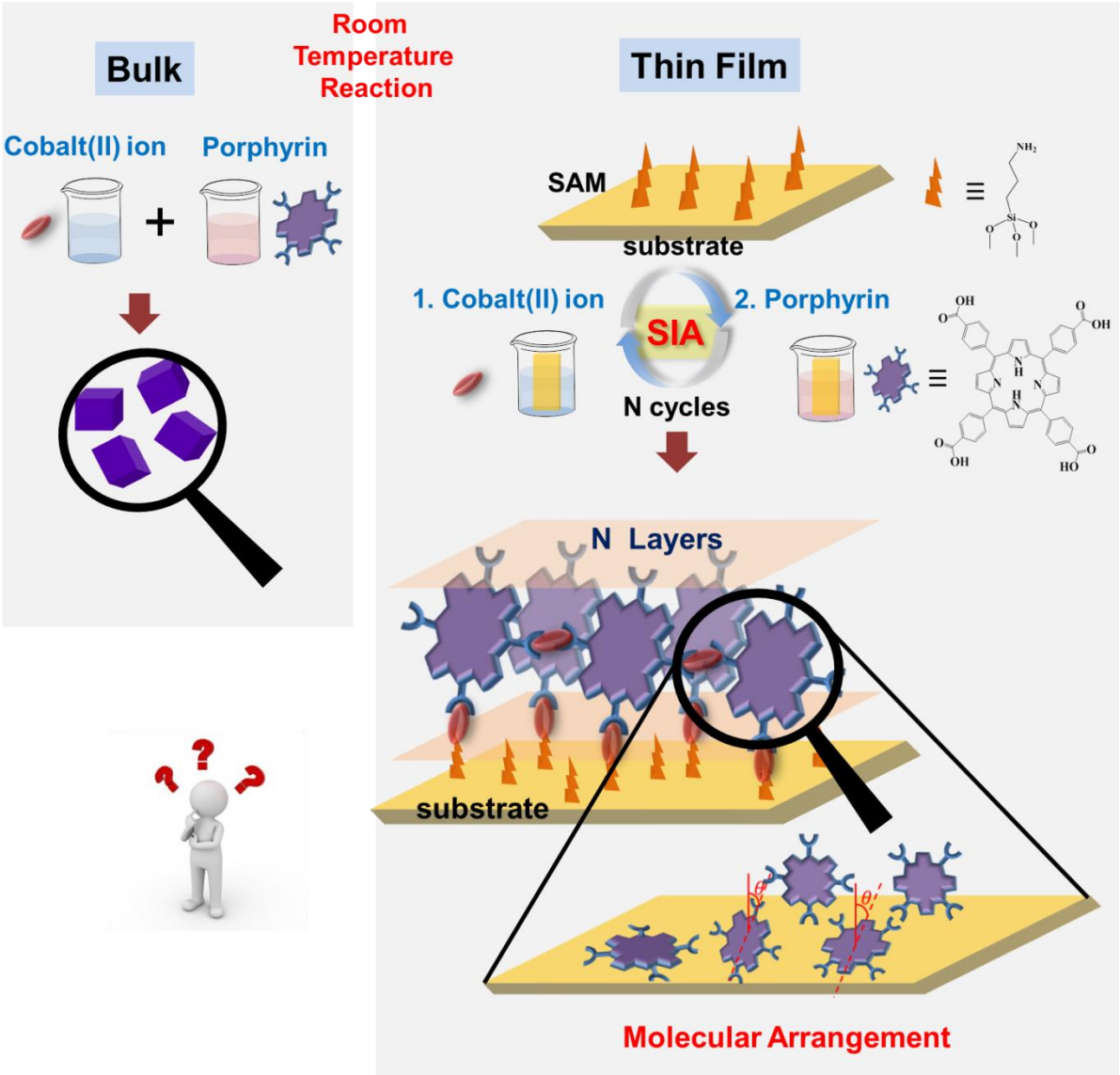

Figure 1.11 Schematic representation of research strategies.

References

1. Elemans, J. A. A. W.; Lei, S.; Feyter, S. D. Molecular and Supramolecular Networks on Surfaces: From Two-Dimensional Crystal Engineering to Reactivity. *Angew. Chem. Int. Ed.* **2009**, *48*, 7298-7332.
2. Lehn, J.-M. Supramolecular Chemistry, VCH, Weinheim, 1995.
3. Balzani, V.; Credi, A.; Venturi, M. *Molecular Devices and Machines : Concepts and Perspectives for the Nanoworld, Second ed.;* Wiley-VCH Verlag GmbH & Co. KGaA: Germany, 2008.
4. Decher, G.; Schlenoff, J. B. *Multilayer Thin Films: Sequential Assembly of Nanocomposite Materials*, Second ed.; Wiley-VCH Verlag GmbH & Co. KG AA: Germany, 2012.
5. Decher, G. Layerd Nanoarchitectures via directed assembly of anionic and cationic molecules. In *Templating, Self-Assembly and Self-Organization*; Sauvage, J.-P.; Hosseini, M. W., Eds., Pergamon Press: Oxford, 1996; pp 507-528.
6. Nguyen, T.-D.; Dinh, C.-T.; Do, T.-O. Tailoring the Assembly, Interfaces, and Porosity of Nanostructures toward Enhanced Catalytic Activity. *Chem. Commun.* **2015**, *51*, 624–635.
7. Carné, A.; Carbonell, C.; Imaz, I.; Maspoch, D. Nanoscale metal-organic materials. *Chem. Soc. Rev.* **2011**, *40*, 291-305.
8. Whitesides, G. M.; Mathias, J. P.; Seto, C. T. Molecular Self-Assembly and Nanochemistry: A Chemical Strategy for the Synthesis of Nanostructures. *Science* **1991**, *254*, 1312-1319.
9. Falcaro, P.; Ricco, R.; Doherty, C. M.; Liang, K.; Hill, A. J.; Styles, M. J. MOF Positioning Technology and Device Fabrication. *Chem. Soc. Rev.* **2014**, *43*, 5513–5560.

10. Ariga, K.; Sakakibara, K.; Richards, G. J.; Hill, J. P. Dynamic Supramolecular Systems at Interfaces. *Supramol. Chem.* **2011**, *23*, 183-194.
11. Ariga, K.; Hill, J. P.; Lee, M. V.; Vinu, A.; Charvet, R.; Acharya, S. Challenges and Breakthroughs in Recent Research on Self-Assembly. *Sci. Technol. Adv. Mater.* **2008**, *9*, 1-96.
12. Barth, J. V. Fresh Perspectives for Surface Coordination Chemistry. *Surf. Sci.* **2009**, *603*, 1533–1541.
13. Nagao, Y.; Matsui, J.; Abe, T.; Hiramatsu, H.; Yamamoto, H.; Miyashita, T.; Sata, N.; Yugami, H. Enhancement of Proton Transport in an Oriented Polypeptide Thin Film. *Langmuir*, **2013**, *29*, 6798-6804.
14. Liu, J.; Zhou, W.; Liu, J.; Howard, I.; Kilibarda, G.; Schlabach, S.; Coupry, D.; Addicoat, M.; Yoneda, S.Tsutsui, Y.; Sakurai, Wöll, C. Photoinduced Charge-Carrier Generation in Epitaxial MOF Thin Films: High Efficiency as a Result of an Indirect Electronic Band Gap. *Angew. Chem. Int. Ed.* **2015**, *54*, 7441-7445.
15. Müller, S.; Müllen, K. Expanding Benzene to Giant Graphenes: Towards molecular Devices. *Phil. Trans. R. Soc. A* **2007**, *365*, 1453-142.
16. Doherty, C. M.; Grenci, G.; Riccò, R.; Mardel, J. I.; Reboul, J.; Furukawa, F.; Kitagawa, S.; Hill, A. J.; Falcaro, P. Combining UV Lithography and an Imprinting Technique for Patterning Metal-Organic Frameworks. *Adv. Mater.* **2013**, *25*, 4701-4705.
17. Teo, B. K.; Sun, X. H. From Top-Down to Bottom-Up to Hybrid Nanotechnologies: Road to Nanodevices. *J. Cluster Sci.* **2006**, *17*, 529-540.
18. Bétard, A.; Fischer, R. A. Metal-Organic Framework Thin Films: From Fundamentals to Applications. *Chem. Rev.* **2012**, *112*, 1055–1083.

19. Zacher, D.; Yusenko, K.; Bétard, A.; Henke, S.; Molon, M.; Ladnorg, T.; Shekhah, O.; Schüpbach, B.; de los Arcos, T.; Krasnopolski, M.; Meilikhov, M.; Winter, J.; Terfort, A.; Wöll, C.; Fischer, R. A. Liquid-Phase Epitaxy of Multicomponent Layer-Based Porous Coordination Polymer Thin Films of [M(L)(P)0.5] Type: Importance of Deposition Sequence on the Oriented Growth. *Chem. Eur. J.* **2011**, *17*, 1448–1455.
20. Makiura, R.; Motoyama, S.; Umemura, Y.; Yamanaka, H.; Sakata, O.; Kitagawa, H. Surface Nano-Architecture of a Metal-Organic Framework. *Nat. Mater.* **2010**, *9*, 565–571.
21. Li, Z.-Q.; Zhang, M.; Liu, B.; Guo, C.-Y.; Zhou, M. Rapid Fabrication of Metal-Organic Framework Thin Film Using in situ Microwave Irradiation and Its Photocatalytic Property. *Inorg. Chem. Commun.* **2013**, *36*, 241-244.
22. Horcajada, P.; Serre, C.; Grosso, D.; Boissière, C.; Perruchas, S.; Sanchez, C.; Férey, G. Colloidal Route for Preparing Optical Thin Films of Nanoporous Metal-Organic Frameworks. *Adv. Mater.* **2009**, *21*, 1931-1935.
23. Wade, C. R.; Li, M.; Dincá, M. Facile Deposition of Multicolored Electrochromic Metal-Organic Framework Thin Films. *Angew. Chem. Int. Ed.* **2013**, *52*, 13377-13381.
24. Zhuang, J.-L.; Ar, Z.; Yu, X.-J.; Liu, J.-X.; Terfort, A. Patterned Deposition of Metal-Organic Frameworks onto Plastic, Paper, and Textile Substrates by Inkjet Printing of a Precursor Solution. *Adv. Mater.* **2013**, *25*, 4631-4635.
25. Arslan, H. K.; Shekhah, O.; Wohlgemuth, J.; Franzreb, M. High-Throughput Fabrication of Uniform and Homogenous MOF Coatings. *Adv. Funct. Mater.* **2011**, *21*, 4228-4231.
26. Zhuang, J.-L.; Ceglarek, D.; Pethuraj, S.; Terfort, A. Rapid Room-Temperature Synthesis of Metal-Organic Framework HKUST-1 Crystals in Bulk and as Oriented and Patterned Thin Films. *Adv. Funct. Mater.* **2011**, *21*, 1442–1447.

27. Ariga, K.; Hill, J. P.; Ji, Q. Layer-by-Layer Assembly as a Versatile Bottom-up Nanofabrication Technique for Exploratory Research and Realistic Application. *Phys. Chem. Chem. Phys.* **2007**, *9*, 2319–2340.
28. Borges, J.; Mano, J. F. Molecular Interactions Driving the Layer-by-Layer Assembly of Multilayers. *Chem. Rev.* **2014**, *114*, 8883-8942.
29. Dubas, S. T.; Schlenoff, J. B. Swelling and Smoothing of Polyelectrolyte Multilayers by Salt. *Langmuir* **2001**, *17*, 7725-7727.
30. Kohli, P.; Blanchard, G. J. Applying Polymer Chemistry to Interfaces: Layer-by-Layer and Spontaneous Growth of Covalent Bound Multilayers. *Langmuir* **2000**, *16*, 4655-4661.
31. Zhang, H.; Fu, Y.; Wang, D.; Wang, L.; Wang, Z.; Zhang, X. Hydrogen-Bonding-Directed Layer-by-Layer Assembly of Dendrimer and Poly(4-vinylpyridine) and Micropore Formation by Post-Base Treatment. *Langmuir* **2003**, *19*, 8497-8502.
32. Wanunu, M.; Vaskevich, A.; Shanzer, A.; Rubinstein, I. Divergent Growth of Coordination Dendrimers on Surfaces. *J. Am. Chem. Soc.* **2006**, *128*, 8341-8349.
33. Crespo-Biel, O.; Dordi, B.; Reinhoudt, D. N.; Huskens, J. Supramolecular Layer-by-Layer Assembly: Alternating Adsorptions of Guest- and Host-Functionalized Molecules and Particles Using Multivalent Supramolecular Interactions. *J. Am. Chem. Soc.* **2005**, *127*, 7594-7600.
34. Jiang, X.; Bent, S. F. Area-Selective ALD with Soft Lithographic Methods: Using Self-Assembled Monolayers to Direct Film Deposition. *J. Phys. Chem. C* **2009**, *113*, 17613-17625.
35. Du, Y.; George, S. M. Molecular Layer Deposition of Nylon 66 Films Examined Using in Situ FTIR Spectroscopy. *J. Phys. Chem. C* **2007**, *111*, 8509-8517.

36. Amabilino, D. B. Layer-byLayer Growth. In *Supramolecular Chemistry at Surfaces.* Gale, P.; Steed, J., Ed.; The RSC: UK, 2016; Chapter6, pp.303-339.
37. Altman, M.; Shukla, A. D.; Zubkov, T.; Evmenenko, G.; Dutta, P.; van der Boom, M. E. Controlling Structure from the Bottom-Up: Structural and Optical Properties of Layer-by-Layer Assembled Palladium Coordination-Based Multilayers *J. Am. Chem. Soc.* **2006**, *128*, 7374-7382.
38. Ren, X.-B.; Chen, M.; Qian, D.-J. Pd(II)-Mediated Triad Multilayers with Zinc Tetrapyridylporphyrin and Pyridine-Functionalized Nano-TiO_2 as Linkers: Assembly, Characterization, and Photocatalytic Properties. *Langmuir* **2012**, *28*, 7711-7719.
39. Tong, B.; Yang, H.; Xiong, W.; Xie, F.; Shi, J.; Zhi, J.; Chan, W. K.; Dong, Y. Controlled Fabrication and Optoelectrical Properties of Metallosupramolecular Films Based on Ruthenium(II) Phthalocyanines and 4,4′-Bipyridine Covalently Anchored on Inorganic Substrates. *J. Phys. Chem. B* **2013**, *117*, 5338-5344.
40. Choudhury, J.; Kaminker, R.; Motiei, L.; de Ruiter, G.; Morozov, M.; Lupo, F.; Gulino, A.; van der Boom, M. E. Linear vs Exponential Formation of Molecular-Based Assemblies. *J. Am. Chem. Soc.* **2010**, *132*, 9295-9297.
41. Kanaizuka, K.; Hahuki, R.; Sakata, O.; Yoshimoto, M.; Akita, Y.; Kitagawa, H. Construction of Highly Oriented Crystalline Surface Coordination Polymers Composed of Copper Dithiooxamide Complexes. *J. Am. Chem. Soc.* **2008**, *130*, 15778-15779.
42. Haga, M.-a.; Kobayashi, K.; Terada, K. Fabrication and Function of Surface nanomaterials based on multilayered or nanoarrayed assembly of metal complexes. *Coord. Chem. Rev.* **2007**, *251*, 2688-2701.

43. Haensch, C.; Hoeppener, S.; Schubert, U. S. Chemical Modification of Self-Assembled Silane Based Monolayers by Surface Reactions. *Chem. Soc. Rev.* **2010**, *39*, 2323-2334.
44. Ulman, A. Formation and Structure of Self-Assembled Monolayers. *Chem. Rev.* **1996**, *96*, 1533-1554.
45. Shekhah, O.; Wang, H.; Zacher, D.; Fischer, R. A.; Wöll, C. Growth Mechanism of Metal-Organic FrameworksL: Insights Into the Nucleation by Employing a Step-by-Step Route. *Angew. Chem. Int. Ed.* **2009**, *48*, 5038-5041.
46. Yu, X.-J.; Zhuang, J.-L.; Scherr, J.; Abu-Husein, T.; Terfort, A. Minimization of Surface Energies and Ripening Outcompete Template Effects in the Surface Growth of Metal-Organic Frameworks. *Angew. Chem. Int. Ed.* **2016**, *55*, 1-6.
47. Otsubo, K.; Haraguchi, T.; Sakata, O.; Fujiwara, A.; Kitagawa, H. Step-by-Step Fabrication of a Highly Oriented Crystalline Three-Dimensional Pillared-Layer-Type Metal-Organic Framework Thin Film Confirmed by Synchrotron X-ray Diffraction. *J. Am. Chem. Soc.* **2012**, *134*, 9605-9608.
48. Liu, N.; Yao, Y.; Cha, J. J.; McDowell, M. T.; Han, Y.; Cui, Y. Functionalization of Silicon Nanowire Surfaces with Metal-Organic Frameworks. *Nano Res.* **2012**, *5*, 109-116.
49. Shekhah, O. Layer-by-Layer Method for the Synthesis and Growth of Surface Mounted Metal-Organic Frameworks (SURMOFs). *Materials* **2010**, *3*, 1302-1315.
50. Munuera, C.; Shekhah, O.; Wang, H.; Wöll, C.; Ocal, C. The Controlled Growth of Oriented Metal-Organic Frameworks on Functionalized Surfaces as Followed by Scanning Force Microscopy. *Phys. Chem. Chem. Phys.* **2008**, *10*, 7251-7261.
51. Liu, J.; Shekhah, O.; Stammer, X.; Arslan, H. K.; Liu, B.; Schüpbach, B.; Terfort, A.; Wöll, C. Deposition of Metal-Organic Frameworks by Liquid-Phase Epitaxy: The

Influence of Substrate Functional Group Density on Film Orientation. *Materials* **2012**, *5*, 1581-1592.

52. Zhuang, J.-L.; Kind, M.; Grytz, C. M.; Farr, F.; Diefenbach, M.; Tussupbayev, S.; Holthausen, M. C.; Terfort, A. Insight into the Oriented Growth of Surface-Attached Metal-Organic Frameworks: Surface Functionality, Deposition Temperature, and First Layer Order. *J. Am. Chem. Soc.* **2015**, *137*, 8237-8243.

53. Shekhah, O.; Wang, H.; Strunskus, T.; Cyganik, P.; Zacher, D.; Fischer, R.; Wöll, C. Layer-by-Layer Growth of Oriented Metal Organic Polymers on a Functionalized Organic Surface. *Langmuir* **2007**, *23*, 7440−7442.

54. Heinke, L.; Tu, M.; Wannapaiboon, S.; Fischer, R. A.; Wöll, C. Surface-Mounted Metal-Organic Frameworks for Applications in Sensing and Separation. *Micropor. Mesopor. Mat.* **2015**, *216*, 200−215.

55. Evans, O. R.; Lin, W. Crystal Engineering of NLO Materials Based on Metal-Organic Coordination Networks. *ACC. Chem. Res.* **2002**, *35*, 511-522.

56. Motiei, L.; Feller, M.; Evmenenko, G.; Dutta, P.; van der Boom, M. E. Controlling growth of self-propagating molecular assemblies. *Chem. Sci.* **2012**, *3*, 66-71.

57. Ruiter, G.; Lahav, M.; Evmenenko, G.; Dutta, P. Cristaldi, D. A.; Gulino, A.; van der Boom, M. E. Composite Molecular Assemblies: Nanoscale Structural Control and Spectroelectrochemical Diversity. *J. Am. Chem. Soc.* **2013**, *135*, 16533-16544.

58. Gao, W-Y.; Chrzanowski, M.; Ma, S. Metal-Metalloporphyrin Frameworks: a Resurging Class of Functional Materials. *Chem. Soc. Rev.* **2014**, *43*, 5841−5866.

59. So, M. C.; Jin, S.; Son, H-J.; Wiederrecht, G. P.; Farha, O. K.; Hupp, J. T. Layer-by-Layer Fabrication of Oriented Porous Thin Films Based on Porphyrin-Containing Metal-Organic Frameworks. *J. Am. Chem. Soc.* **2013**, *135*, 15698−15701.

60. So, M. C.; Beyzavi, M. H.; Sawhney, R.; Shekhah, O.; Eddaoudi, M.; Al-Juaid, A. S.; Hupp, J. T.; Farha, O. K. Post-Assembly Transformations of Porphyrin-Containing Metal-Organic Framework (MOF) Films Fabricated via Automated Layer-by-Layer Coordination. *Chem. Commun.* **2015**, *51*, 85–88.

61. Motoyama, S.; Makiura, R.; Sakata, O.; Kitagawa, H. Highly Crystalline Nanofilm by Layering of Porphyrin Metal-Organic Framework Sheets. *J. Am. Chem. Soc.* **2011**, *133*, 5640–5643.

62. Makiura, R.; Kitagawa, H. Porous Porphyrin Nanoarchitectures on Surfaces. *Eur. J. Inorg. Chem.* **2010**, 3715-3724.

63. Gough, D. V.; Lambert, T. N.; Wheeler, D. R.; Rodriguez, M. A.; Brumbach, M. T.; Allendorf, M. D.; Spoerke, E. D. Controlled Nucleation and Growth of Pillared Paddlewheel Framework Nanostacks onto Chemically Modified Surfaces. *ACS Appl. Mater. Interfaces* **2014**, *6*, 1509-1514.

64. Ahrenholtz, S. R.; Epley, C. C.; Morris, A. J. Solvothermal Preparation of an Electrocatalytic Metalloporphyrin MOF Thin Film and its Redox Hopping Charge-Transfer Mechanism. *J. Am. Chem. Soc.* **2014**, *136*, 2464–2472.

65. Joyce, J. T.; Laffir, F. R.; Silien, C. Layer-by-Layer Growth and Photocurrent Generation in Metal-Organic Coordination Films. *J. Phys. Chem. C* **2013**, *117*, 12502–12509.

Chapter 2

Bulk of Porphyrin-based Coordination Networks

Abstract

The bulk synthesis of metal-organic coordination networks was reported in this chapter. The synthesized bulk was proceeded using 5,10,15,20-tetrakis(4-carboxyphenyl)-porphyrin and cobalt (II) ion at room temperature with no catalyst. The obtained bulk was preliminary characterized by FTIR-ATR, XPS, and PXRD. The results revealed that the coordination network-based porphyrin can be achieved, which can provide both of the crystalline and amorphous phase at room temperature synthetic condition. This finding inspired to prepare the thin film-based this coordination system in the chapter 3.

2.1 Introduction

In the introduction in this chapter, the background of metal-organic coordination networks and the porphyrin building unit will be introduced. Then, the construction and the characterization of porphyrin-based metal-organic coordination networks will be mentioned and discussed.

2.1.1 Metal-Organic Coordination Networks

The development in hybrid inorganic-organic framework materials has been continued over decades to pursue the multifunctional nanomaterial-based molecular components for the next-generation utilization. This leads to promote the research of coordination polymer in aspects of design and control the structures for the desirable properties. The coordination polymer shows the stronger bonding than hydrogen bond in the pure organic system and also provides more network dimension rather than π-π stacking.[1]

There are some terminologies that usually use in this research fields as coordination polymers, coordination networks and Metal-Organic Frameworks (MOFs). The classification by IUPAC[2] recommends that the most common term is coordination polymers, while the coordination networks presents as subclass of coordination polymers. MOFs present as further subclass of coordination networks with the potential porosity. The diagram of order in these materials is simplified in Figure 2.1. [3]

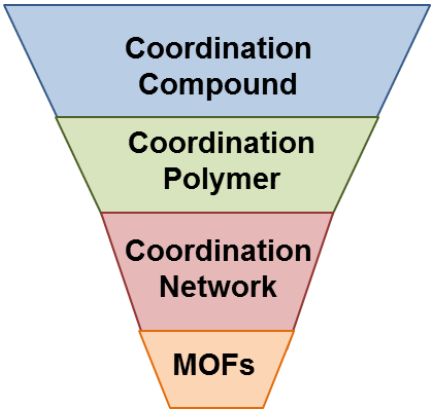

Figure 2.1 The classification of coordination polymers, coordination networks and Metal-Organic Frameworks (MOFs).

The IUPAC book suggests that the "coordination compound" contains coordination entity, which means an ion or neutral molecule such as metal attaches to the surrounding array such as ligands.[4] A "coordination polymer" provides the repeating coordination entities of coordination compound in one, two or three dimension. For example, the structures of nickel(II) cyanide[5] and Cd(II)-(4,4'-bipyridine)[6] are shown in Figure 2.2.

a) b)

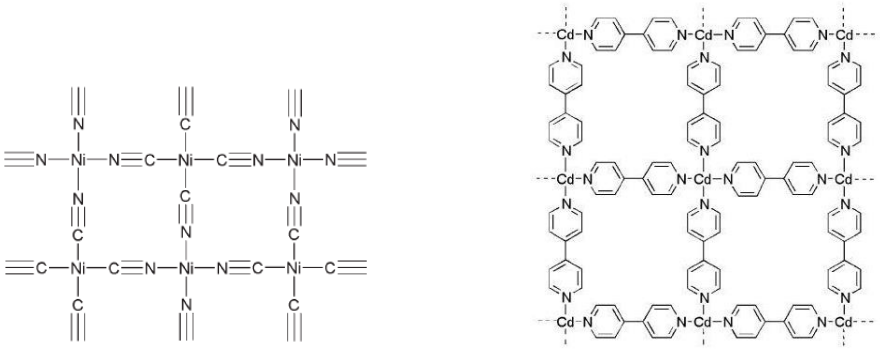

Figure 2.2 Examples of coordination polymers (a) nickel(II) cyanide[5] and (b) Cd(II)-(4,4'-bipyridine).[6]

The classification of coordination polymers[7] is based on dimensionality in one, two or three dimension, which relies on the amount of extended directions as shown in Figure 2.3.

a) 1D coordination polymer (extension in x direction)

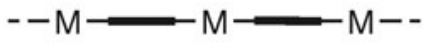

b) 2D coordination polymer (extension in x and y directions)

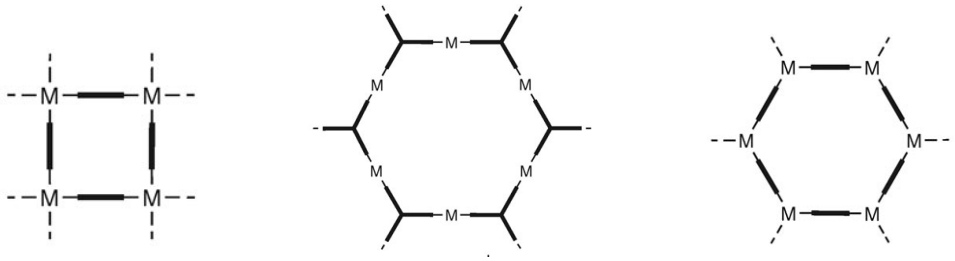

c) 3D coordination polymer (extension in x, y, and z directions)

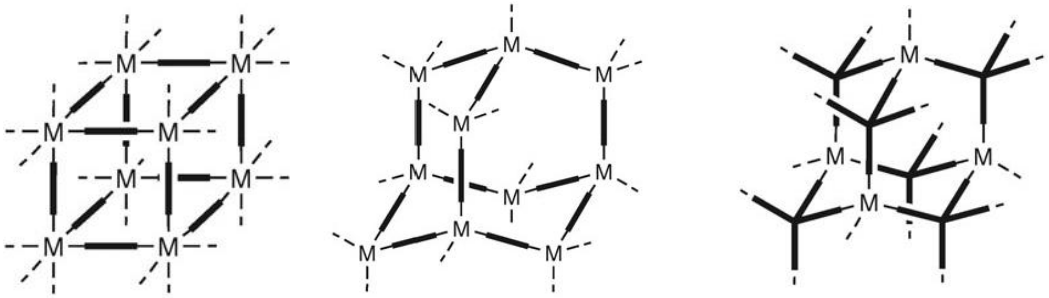

Figure 2.3 Typical types of coordination polymers based on dimensionality; M = metal ion, and black line = organic bridging ligand.[7]

In case of "coordination network", it is definite to a coordination compound which extends through repeating coordination units in 1D with crosslink between the chains or the coordination compound extending through 2D, 3D.[2]

Metal-Organic Frameworks (MOFs)[8-10] are hybrid porous materials composed of a metal cluster connecting with organic linkers. This material is considered as the coordination network with the potential void.[2] MOFs are exploited in extensive applications including gas adsorption and separation, sensing, optoelectronic, biomedical and catalysis.[11-16] The first word of Metal-organic frameworks was introduced in 1995 by Yaghi[17] to report the porous 3D structure $[Cu(4,4'\text{-bipyridine})_{1.5}].NO_3(H_2O)_{1.25}$.

Transition metals are usually used for MOFs preparation such as Mn^{2+}, Fe^{2+}, Co^{2+}, Cu^{2+}, Zn^{2+} and so on. The coordination geometry of metal varies with its oxidation state. The common coordination geometries are linear, trigonal planar, square planar or tetrahedral, trigonal bipyramidal, and octahedral represented in Figure 2.4 respectively. Such an example in Co^{2+}, the versatility of geometry is ranged from tetrahedral, trigonal bipyramidal to octahedral.[18]

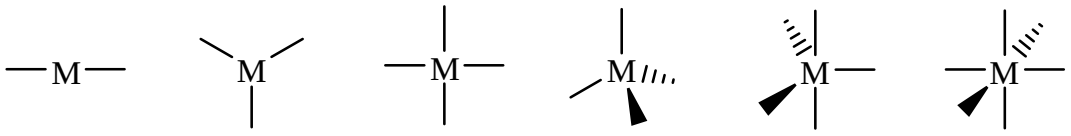

Figure 2.4 Metal ions (M) with different coordination features.

For the organic ligand, oxygen- and nitrogen-donor ligands are usually used in MOFs synthesis such as the carboxylic acid ligands. The coordinations between carboxylate ligand to metal ions are possible in various forms such as unidentate, bidentate, and bidentate chelating (Figure 2.5)[19].

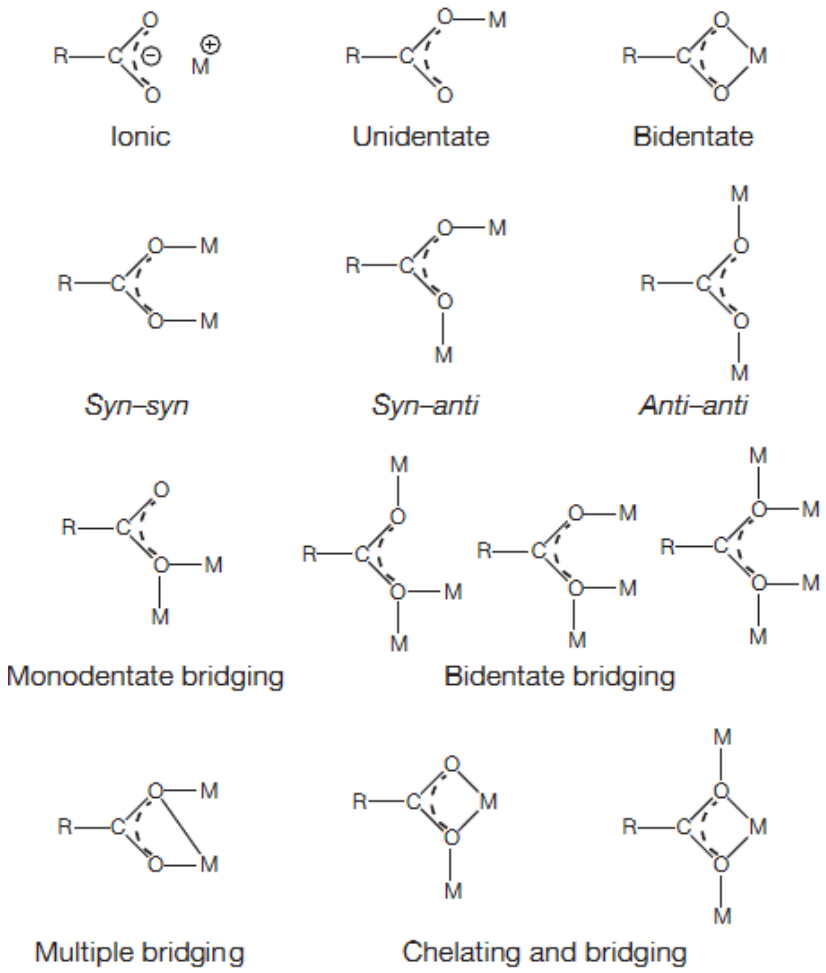

Figure 2.5 Coordination modes of carboxylate ligand to metal (M).[19]

The metal and organic ligand can combine to promote the periodic array using the coordination chemistry concept. The common secondary building units (SBUs), which refer to the used metal node and cluster in the array of assembly are shown in Figure 2.6.

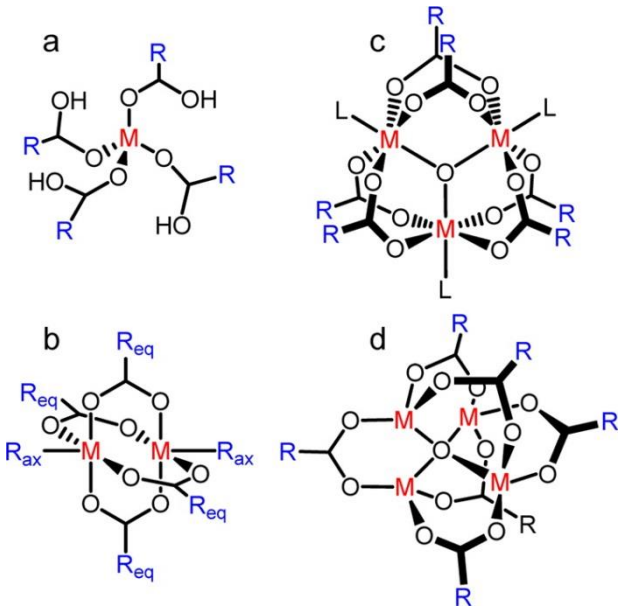

Figure 2.6 The common SBUs in MOFs synthesis: (a) mononuclear, (b) dinuclear paddlewheel, (c) trinuclear cluster, and (d) tetranuclear cluster.[9]

The various topologies can be tunable through the selection of metal-organic components along with reaction condition such as solvent, concentration, reaction time, temperature and synthetic method.[20] Many synthetic methods are available for MOFs synthesis such as diffusion method, hydro/solvothermal method, microwave-assisted method, and mechanochemical method, however the solvothermal method are generally utilized. Some reports of the room temperature synthesis have been mentioned. This indicated that some MOF systems do not require the heating to produce the crystalline MOFs material.[21] The synthesis at the room temperature condition is still a challenging issue to promote the well-defined structure.

The development in coordination chemistry is still going on to make the versatility of structures and functions. The enhancement in complexity and functionality is recently proceed by the multicomponents and the post-synthetic modification process such as metal ion or ligand exchange, incorporation of metal, and covalent modification.[9]

2.1.2 Porphyrin Building Unit

Porphyrin is macrocyclic aromatic compound with tetrapyrrolic system. In nature, metalloporphyrins are relevant to the human life in photochemical and biochemical aspects such as porphyrin derivative in chlorophyll for photosynthesis in plant, porphyrin complexes in hemoglobin for oxygen transport in red blood cell and catalytic properties.[22] This motivates the extensive studies in this attractive molecule to create the novel analogues for numerous applications.

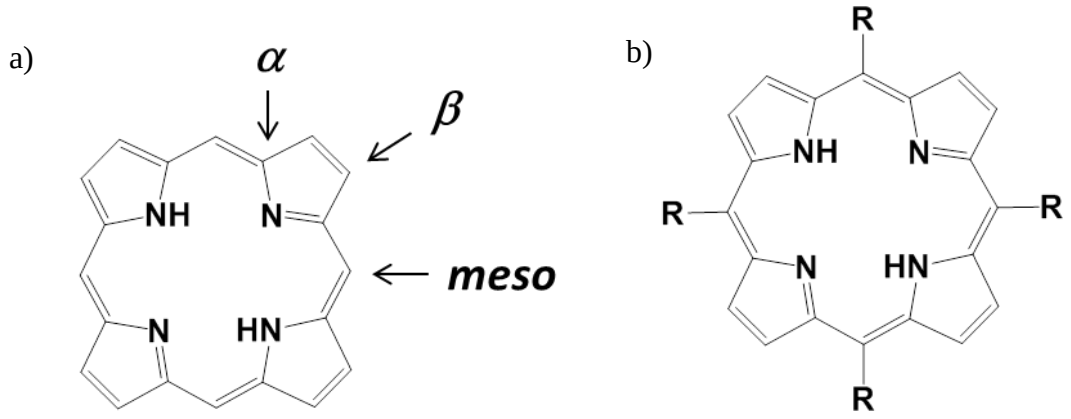

Figure 2.7 (a) Porphin, the parent macrocycle of porphyrins, and (b) Porphyrin, porphine with peripheral substituents (R = phenyl, pyridyl etc.).

Porphin is the parent compound of porphyrin. This composes of four pyrrole units with the methin linkage (=CH-) (Figure 2.7). Porphyrins are porphin with peripheral substituents (R). Porphyrins are one of the great candidates to use as a linker backbone in molecular networks. Some of unique and great properties impact to prepare the artificial material based on porphyrin derivatives such as high molecular symmetry with π-conjugated system exhibiting the unique photochemical and electrochemical behavior, high thermal and oxidative stability.[23] The various functional properties of porphyrin-based materials have

been reported with variety of applications, including photosensitizing, optoelectronic, magnetic, molecular recognition, selective gas sorption, and catalytic properties.[24, 25]

2.1.3 Porphyrin-based Metal-Organic Coordination Networks

As we mentioned about the coordination networks, the assembly of metal ions and the organic ligands can provide the various kinds of structures in 1D, 2D and 3D. The buildup of porphyrin-based coordination structure promotes the different topological structures with unique properties. The common used porphyrin building units to construct the networks contain the carboxyphenyl and pyridyl peripheral group (R)[26] as shown in Figure 2.8.

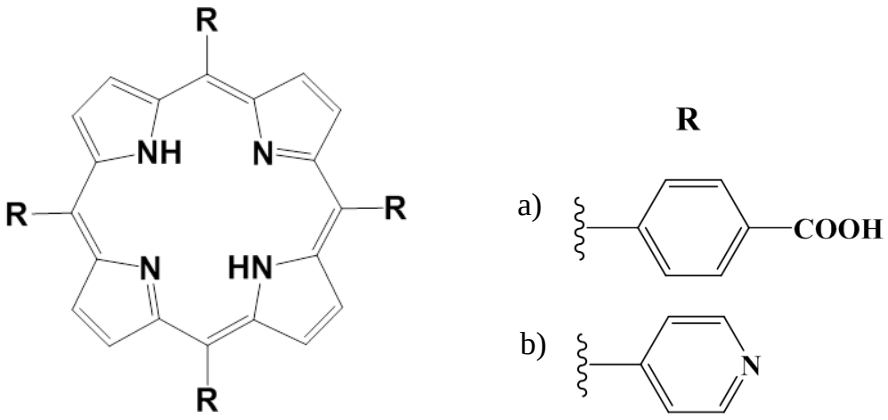

Figure 2.8 The common used porphyrin building units to construct the assembly networks with the peripheral group (R) (a) tetra(4-carboxyphenyl)porphyrin (H_2TCPP), and (b) tetra(4-pyridyl)porphyrin (H_2TPyP).

The studies of porphyrin-based frameworks using porphyrin ligands and metal building units have been intensively studied in many research groups such as Goldberg[27], Suslick[28], Hupp[29], Choe[30], Wu[31], Ma[32], and others.[33] Some metalloporphyrin-based frameworks were mentioned that the conformation of porphyrin ring such as flat, bowl-shape

can provide the different framework structures, which can affect to the optical, electronic or catalytic properties.[34]

Suslick and co-workers[35] reported the metalloporphyrin frameworks, PIZA-1, which was synthesized by $CoCl_2$ and free-base H_2TCPP under the solvothermal condition. The framework exhibited the distortion of porphyrin plane from the planar due to the cobalt metalation at the porphyrin core and the cobalt cluster (Figure 2.9). This 3D framework showed the zeolite-like structure with the unique pore channel for molecular sieve character.

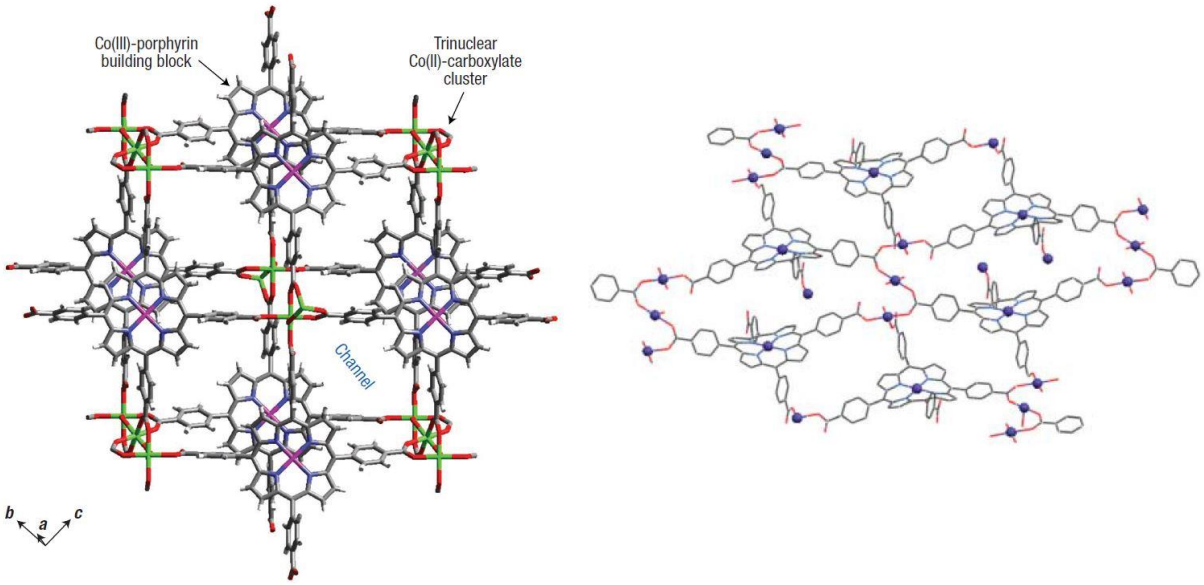

Figure 2.9 TCPP-based framework solid, PIZA-1 (C, Grey; O, red; N, blue; Co(II) in trinuclear clusters, green ; and Co(III), purple.[23, 35]

The core of porphyrin unit can be metalated with the various kinds of metal ions, thus it also make the variety for this materials. The post-synthetic modification process can be applied to the frameworks for tailoring the variety to the framework. The study of porphyrin-based MOFs using free-base type as a precursor with further following by post-metalation or trans-metalation process[32, 33] (Figure 2.10) may provide the valuable information about the

coordination structure comparing to the pre-metalated one. The versatile coordination frameworks can be anticipated from the free-base form.

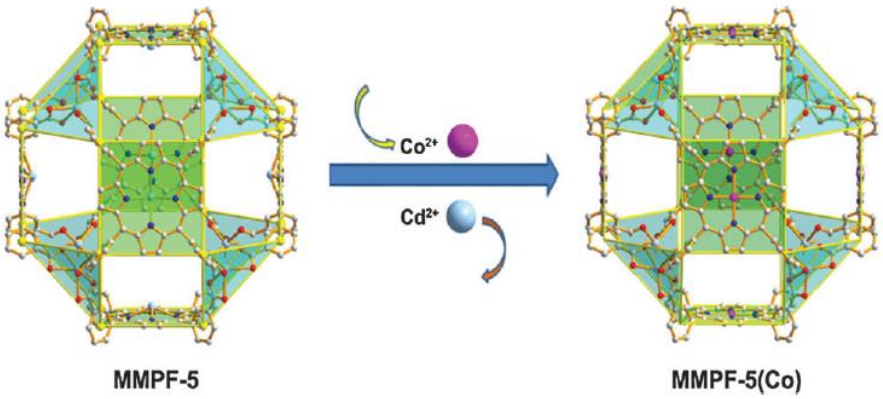

Figure 2.10 The trans-metalation process to exchange the Cadmium(II) in MMPF-5 to Cobalt(II).[32, 33]

The objective in this chapter is to investigate the bulk synthesis of porphyrin-based metal-organic coordination networks at room temperature. We expected that the crystallinity of bulk product can be obtained under mild synthetic condition.

2.2 Experimental Section

2.2.1 Chemicals

5,10,15,20-Tetrakis(4-carboxyphenyl)-porphyrin (H_2TCPP) (purity 98%) was purchased from Strem Chemical Inc., USA. Cobalt(II) acetate tetrahydrate ($Co(OAc)_2.4H_2O$) was purchased from Wako Pure Chemical Industries Ltd. AR grade of solvents such as chloroform ($CHCl_3$), methanol, and 2-propanol were used. All solvents were purchased from Wako Pure Chemical Industries Ltd. All chemicals were used as received without further purification.

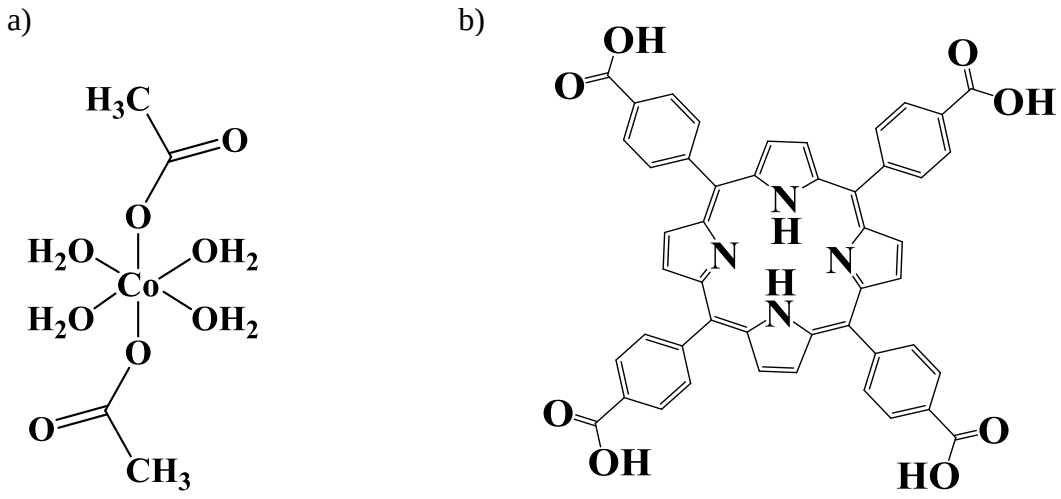

Figure 2.11 Structure of Chemical precursors (a) $Co(OAc)_2.4H_2O$, and (b) H_2TCPP.

2.2.2 Characterization Techniques

Fourier-transform infrared attenuated total reflectance (FTIR-ATR) was used to obtain the molecular vibration of chemical bond in chemical precursors and the bulk sample. The IR spectrum was acquired using an FT-IR spectrometer (Nicolet 6700; Thermo-Fisher

Scientific) equipped with a deuterated triglycine sulfate (DTGS) detector. All spectra were recorded with 64 scans and 4 cm^{-1} resolution.

X-ray photoelectron spectroscopy (XPS) was used to determine the elemental composition of chemical precursors and the bulk sample. The powder samples were fixed on the double sticky carbon-tape to the sample holder. The XPS experiment was conducted using a spectrometer (Axis-Ultra DLD; Kratos Analytical Ltd.) with an Al Kα radiation source (1486.6 eV). The binding energies were calibrated using C1s peak at 284.5 eV as a standard. Curve fitting was performed by processing software (Vision) using a Gaussian envelope with Shirley background correction.

Powder X-ray diffraction (PXRD) was used to investigate the crystalline properties of a synthesized bulk sample. The measurement was performed using a high-resolution X-ray diffractometer (ATX-G; Rigaku Corp.) equipped with a Cu Kα radiation source (λ= 0.1542 nm.) at the step size of 0.02°.

2.2.3. Synthesis and Characterization of Bulk ($(Co/H_2TCPP)_{Bulk}$)

$Co(OAc)_2.4H_2O$ (0.125 mmol) was clearly dissolved in solvent mixture of methanol and chloroform (1:9, v/v) 100 ml. H_2TCPP (0.401 mmol) was dissolved in 2-propanol 50 ml. Then, cobalt salt solution was added gradually to the free-base porphyrin solution with stirring at room temperature. The dark red precipitation rapidly formed. The suspension was continuously stirred under room temperature for 1 day ($(Co/H_2TCPP)_{Bulk-1}$) and 3 days ($(Co/H_2TCPP)_{Bulk-2}$). The precipitate was collected by centrifugation and then washed with 2-propanol (4 times) and mixture solvent of $1MeOH:9CHCl_3$ (4 times). The $(Co/H_2TCPP)_{Bulk}$ products were then dried under vacuum at room temperature in order to measure ATR-IR, XPS, and PXRD.

a)

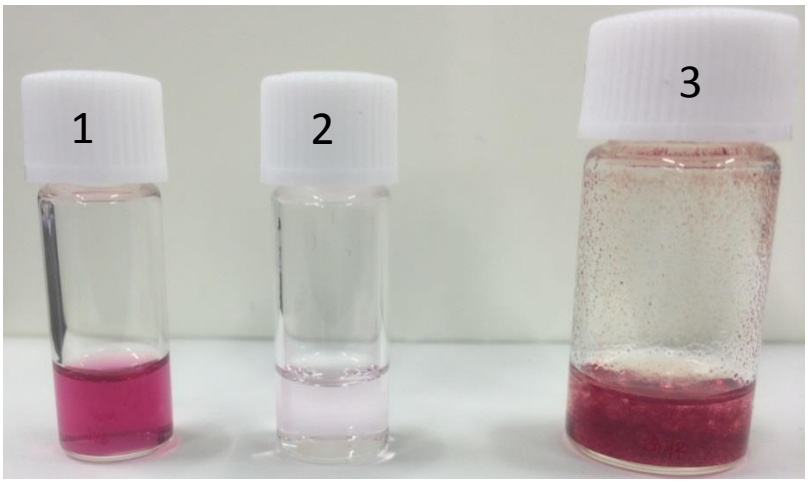

b)

Figure 2.12 Bulk synthesis of **(**$Co/H_2TCPP)_{Bulk}$. (a) H_2TCPP solution (1), Cobalt (II) acetate solution (2), and the precipitation of reaction between (1) and (2) at room temperature, and (b) **(**$Co/H_2TCPP)_{Bulk}$.

2.3 Results and Discussion

In order to characterize the synthesized bulk ($(Co/H_2TCPP)_{Bulk}$), we divided the detail in 3 parts as the FTIR-ATR, XPS and PXRD analysis as following :

2.3.1) Investigation of Chemical Bond by FTIR-ATR

2.3.2) Elemental Composition Analysis by XPS

2.3.3) Structural Investigation by PXRD

2.3.1 Investigation of Chemical Bond by FTIR-ATR

In the bulk synthesis, the rapid precipitation from the reaction was a primary evidence for the production of coordination networks at room temperature condition. The IR spectra of synthesized bulk ($(Co/H_2TCPP)_{Bulk}$) were compared with other chemical precursors such as H_2TCPP and $Co(OAc)_2.4H_2O$ as shown in Figure 2.13. The assignment of each functional group was declared in the Table 2.1. The decreasing of carboxylic (COOH) peak intensity at 1688 cm^{-1} [36, 37] with the presence of asymmetric and symmetric stretching of carboxylate (COO^-) suggested that carboxylate moieties of porphyrin can react with the cobalt ions to generate the coordination networks without any additional basic precursor such as trimethylamine.[38] However, the remaining of unreacted COOH group inferred to the incomplete reaction between cobalt ions and carboxylate from porphyrin unit in this bulk synthesis. It was noted that the extension of reaction time from one day to three days, the amount of carboxylic acid group tended to decrease. This result indicated that the long reaction time was required for the bulk synthesis to consume the reactive moieties for network construction at the room temperature.

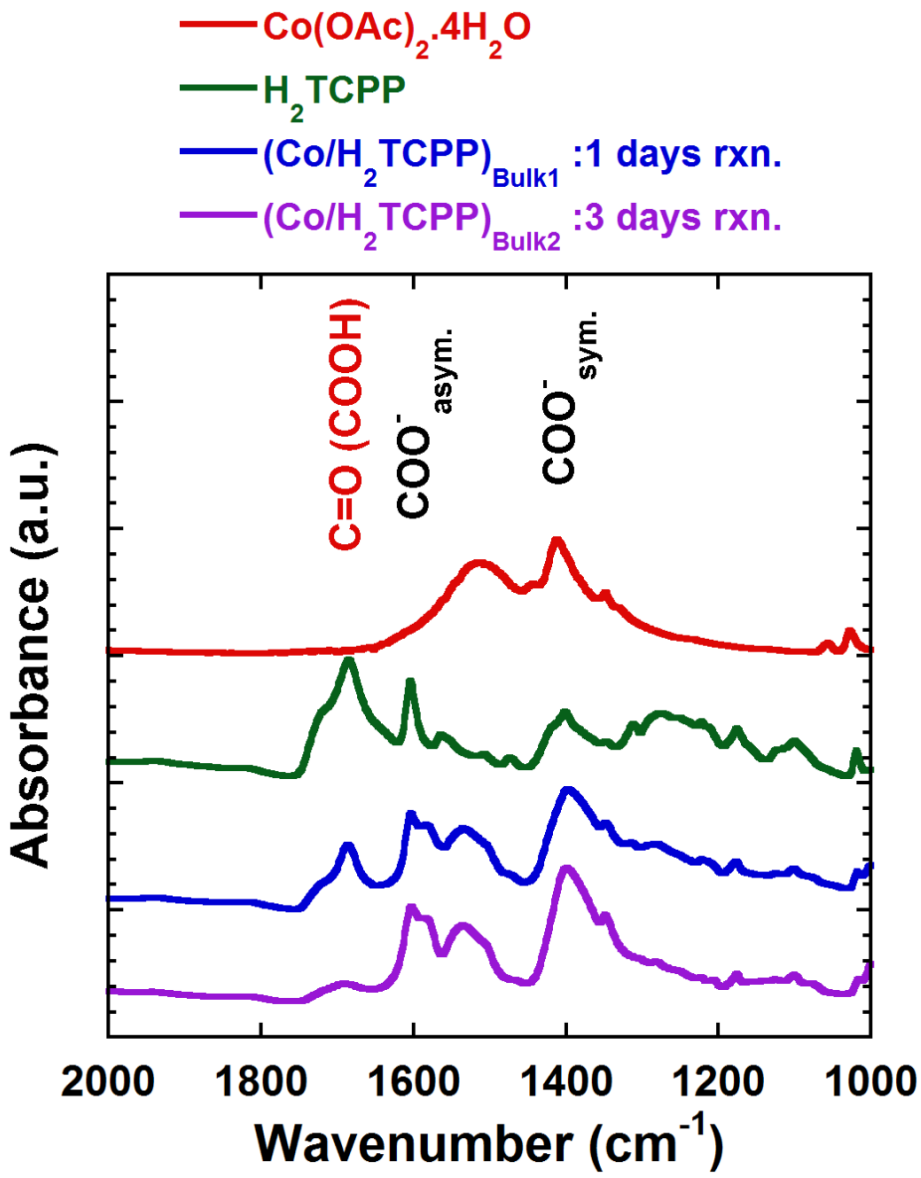

Figure 2.13 ATR-IR spectra of $Co(OAc)_2.4H_2O$, H_2TCPP, bulk samples($(Co/H_2TCPP)_{Bulk-1}$), ($(Co/H_2TCPP)_{Bulk-2}$)).

Table 2.1 The peak assignment of characteristic bands in IR spectra.

	C=O (COOH)	**C=C aromatic ring**	**C-O (COOH)**	**COO^- asym**	**COO^- Sym**
H_2TCPP	1685 [36,37]	1605 [39]	1401	N.A.	N.A.
$Co(OAc)_2.4H_2O$	N.A.	N.A.	N.A.	1513	1412
$(Co/H_2TCPP)_{Bulk}$	1688 (unreacted COOH)[40, 41]	1582 [42]	N.A.	1530 [39] 1603 [42]	1389 [39, 42]

2.3.2 Elemental Composition Analysis by XPS

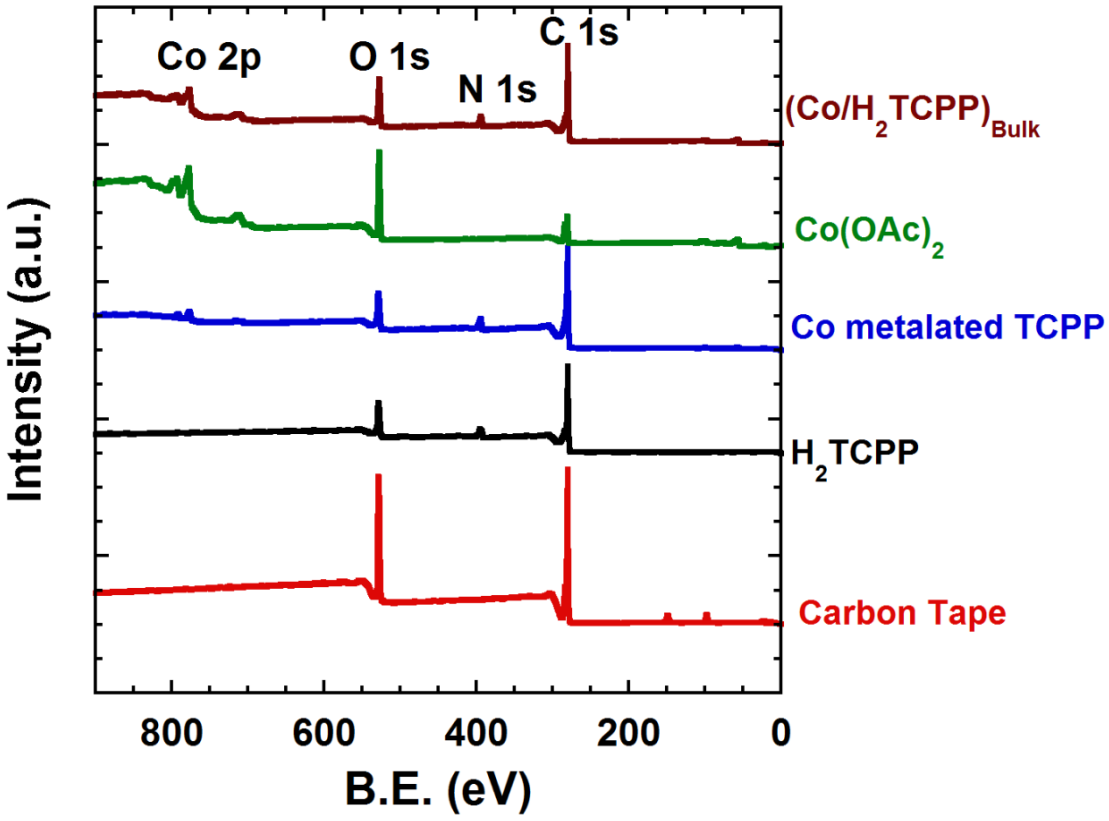

Figure 2.14 XPS survey spectra of H_2TCPP, Co metalated TCPP, $Co(OAc)_2$ and $(Co/H_2TCPP)_{bulk}$ on carbon tape.

The elemental composition of chemical precursors and $(Co/H_2TCPP)_{Bulk}$ were revealed by XPS analysis. The survey scans have been primarily showed the change in elemental composition of bulk sample comparing with the precursors as presented in Figure 2.14. The presence of N1s and Co2p peaks of $(Co/H_2TCPP)_{Bulk}$ referred to the availability of porphyrin and cobalt in this bulk material. To investigate the detail of N1s and Co2p, the fine scan spectra were discussed as presented in Figure 2.15 and Figure 2.17.

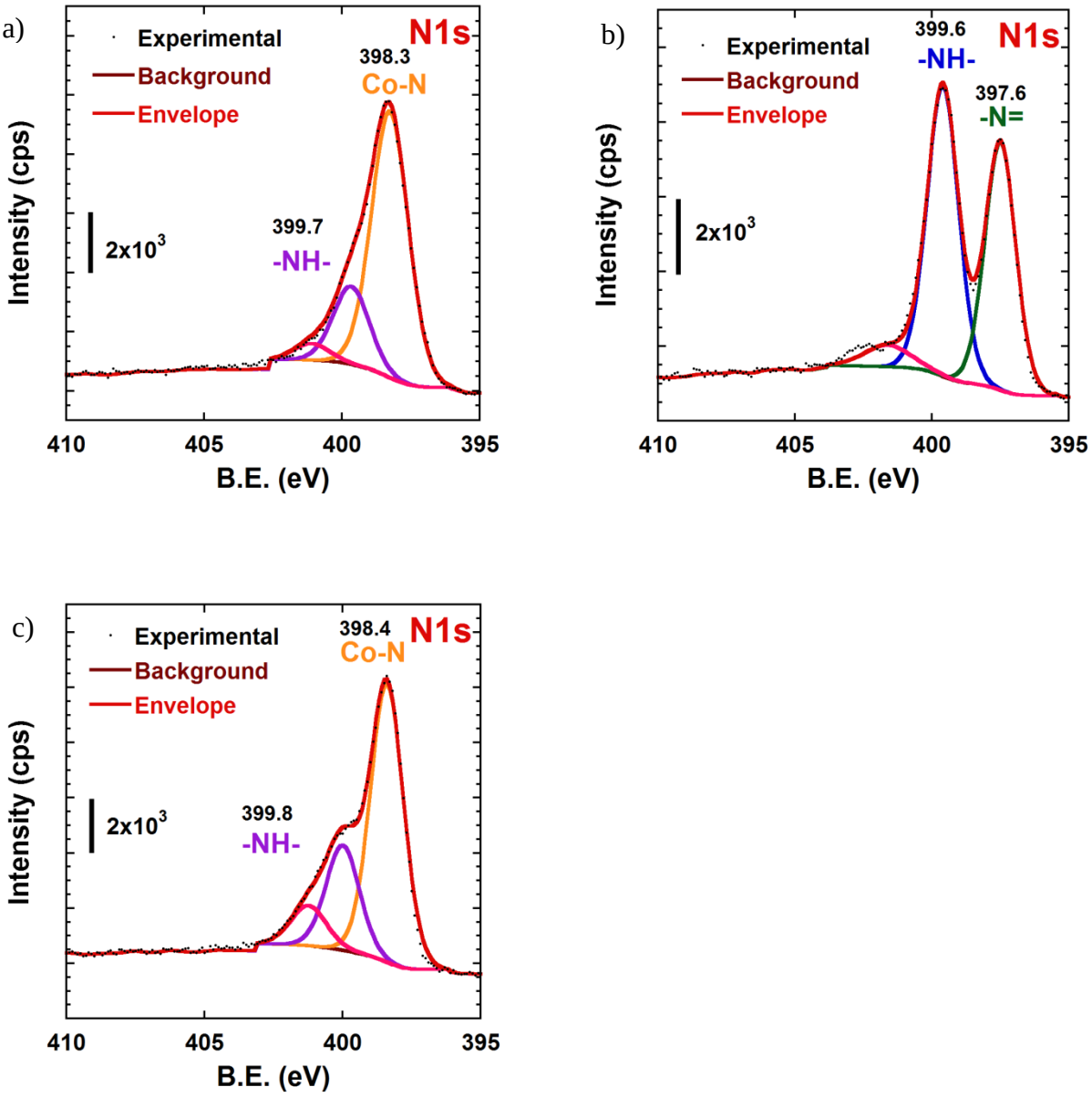

Figure 2.15 Comparison of N1s spectra between (a) $(Co/H_2TCPP)_{Bulk}$, (b) H_2TCPP, and (c) Co metalated TCPP.

In N1s case, the N1s spectra of $(Co/H_2TCPP)_{Bulk}$ (Figure 2.15a) were compared with the free-base porphyrin precursors, H_2TCPP as shown in Figure 2.15b. The spectrum of N1s in ligand H_2TCPP showed the two obvious peaks. These were protonated and non-protonated form, which were ascribed to the pyrrolic (-NH-) and iminic (-N=) species, respectively[43]

(Figure 2.16). The difference of N1s deconvolution between ligand H_2TCPP and $(Co/H_2TCPP)_{Bulk}$ indicated that the N species at the porphyrin core of this bulk are not be the free-base form. The N 1s spectrum of $(Co/H_2TCPP)_{Bulk}$ was relatively similar with the Co metalated TCPP feature (Figure 2.15c), therefore we supposed that cobalt ion metalated to the center of porphyrin macrocycle in this network during the bulk synthesis. Some bulk porphyrin-based MOFs synthesis using the free-base porphyrin as the organic ligand also mentioned the same metalation phenomena at the center of porphyrin macrocycle.[44, 45]

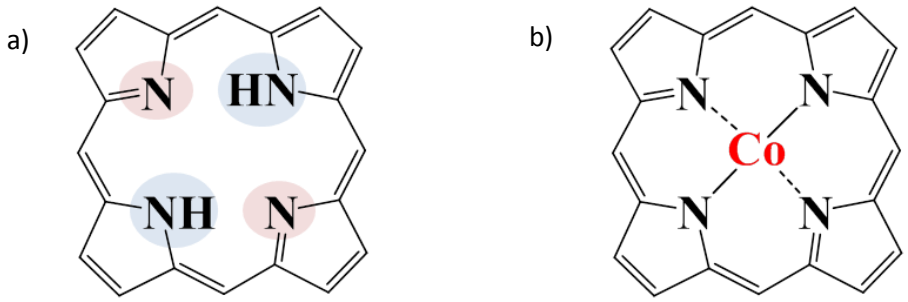

Figure 2.16 Porphyrin core unit (a) H_2TCPP; pyrrolic (-NH-) and iminic (-N=) species (b) Co metalated TCPP.

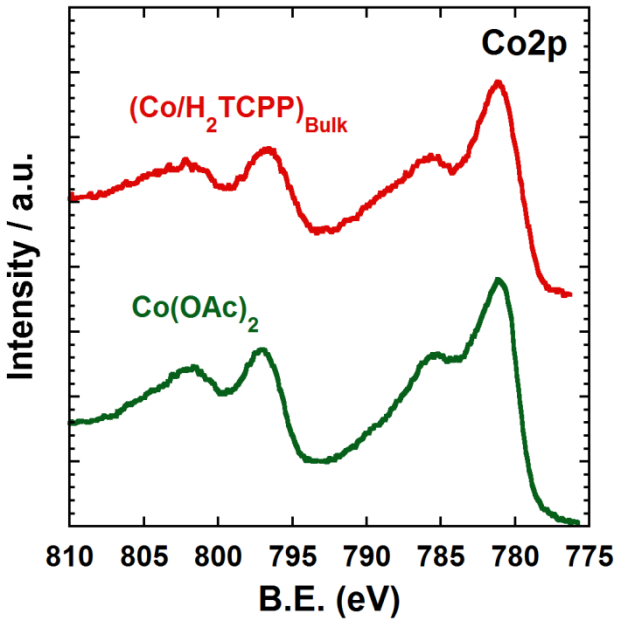

Figure 2.17 Comparison of Co2p spectra $(Co/H_2TCPP)_{Bulk}$ and $Co(OAc)_2$.

The presence of cobalt in $(Co/H_2TCPP)_{Bulk}$ can be declared by the Co2p spectra in comparison with metal salt precursor as $Co(OAc)_2$. The peaks of Co2p with two strong satellite peaks in both bulk samples and metal salt represented the oxidation state of cobalt ion as +2 [46] as displayed in Figure 2.17.

From these XPS results, it was concluded that the metalation of free-base porphyrin core can occur during the bulk synthesis and the oxidation state of cobalt moieties in the bulk networks represented as +2. The single crystal was not obtained from bulk synthesis at room temperature, therefore the chemical compositions of the bulk sample are considered from XPS analysis in Figure 2.14. The actual composition using peak areas approximately revealed ratio as $1Co^{2+}$:2N or $2Co^{2+}$:1Porphyrin, which was in close agreement with the expected value ($2Co^{2+}$:1Porphyrin).

2.3.3 Structural Investigation by PXRD

The PXRD and d-value of main three peaks in the $(Co/H_2TCPP)_{Bulk}$ were exhibited in Figure 2.18 and Table 2.2, respectively. The single crystal cannot be obtained under room temperature condition. These results suggest that not only the crystalline phase (sharp peaks), but also the amorphous phase (broad peaks) are obtainable in this bulk system. The quick precipitation of bulk product may lead to the amorphous phase. Furthermore, the remaining free carboxylic acid moieties of porphyrin from FT-IR result represented the incomplete reaction (defect) in this bulk system. However, it is possible to synthesize this metal-organic coordination networks under room temperature. Base on the information from bulk system, we intensively focus our research at the thin film preparation based on this coordination network system, which will be declared in the next chapter.

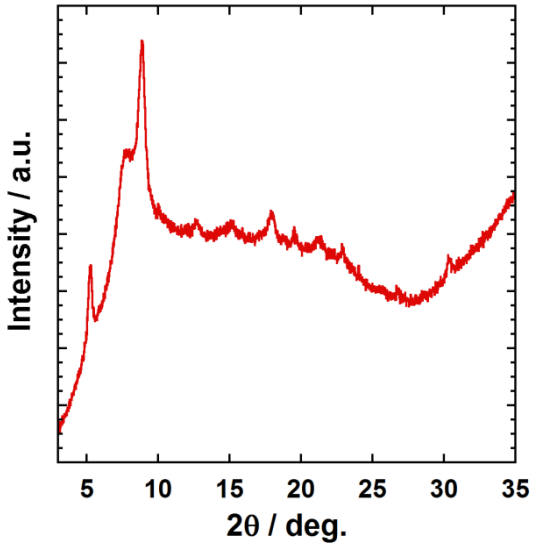

Figure 2.18 PXRD pattern of the synthesized bulk ($(Co/H_2TCPP)_{Bulk}$).

Table 2.2 The calculated d-value from PXRD of bulk sample by Bragg's law equation ($2d \sin\theta = n\lambda$) ; $\lambda = 0.1542$ nm.

2theta (degree)	**d-value (nm)**
5.28	1.67
7.84	1.13
8.84	1.00

2.4 Conclusion

In this chapter, the metal-organic coordination networks which composed of 5,10,15,20-tetrakis(4-carboxyphenyl)-porphyrin and cobalt (II) ion have been successfully synthesized at room temperature as denoted as bulk, $(Co/H_2TCPP)_{Bulk}$. The characterization techniques for this bulk were proceeded including FTIR-ATR, XPS, and PXRD. The chemical bonds in the synthesized bulk were investigated by FTIR-ATR, which suggested that the remained COOH reactive groups were presented in the bulk product. The long time reaction was needed to consume these reactive moieties in this bulk synthesis. The elemental composition analysis by XPS suggested that cobalt (II) ions can bind to porphyrin unit, not only at the carboxylic acid groups of porphyrin to promote the network formation but the cobalt (II) ions can also metalate at the center of porphyrin core under this mild condition. Furthermore, the availability of crystalline feature and amorphous phase can be obtained under room temperature synthesis, which was confirmed by PXRD.

From the survey study of bulk synthesis, we can confirm that the metal-organic coordination networks of this porphyrin and cobalt (II) ion system can efficiently occur under room temperature condition. The results in this chapter motivate the study of thin film preparation on the surface using the similar chemical precursors in the next chapter.

References

1. Janiak, C. Engineering Coordination Polymer Towards Applications. *Dalton Trans.* **2003**, 2781-2804.
2. Batten, S. R.; Champness, N. R.; Chen, X.-M.; Garcia-Martinez, J.; Kitagawa, S.; Öhrström, L.; O'Keeffe, M.; Suh, M. P.; Reedijk, J. Terminology of Metal-Organic Framworks and Coordination Polymers (IUPAC Recommendations 2013). *Pure Appl. Chem.* **2013**, *85*, 1715-1724.
3. Batten, S. R.; Champness, N. R.; Chen, X.-M.; Garcia-Martinez, J.; Kitagawa, S.; Öhrström, L.; O'Keeffe, M.; Suh, M. P.; Reedijk, J. Coordination Polymers, Metal-Organic Frameworks and the Need for Terminology Guidelines. *Cryst. Eng. Comm.* **2012**, *14*, 3001-3004.
4. IUPAC. *Nomenclature of Inorganic Chemistry, IUPAC Recommendations* Connelly, N.; Damhus, T.; Harshorn, R. M.; RSC Publishing. Cambridge, UK, 2005.
5. Bailar, J. C. Jr. Coordination Polymers. *Prep. Inorg. React.***1964**, *1*, 1-57.
6. Fujita, M.; Kwon, Y. J.; Washizu, S.; Ogura, K. Preparation, Clathration Ability, and Catalysis of a Two-Dimensional Square Network Material Composed of Cadmium(II) and 4,4'-Bipyridine. *J. Am. Chem. Soc.* **1994**, *116*, 1151-1152.
7. Janiak, C.; Vieth, J. K. MOFs, MILs and more: concepts, properties and applications for porous coordination networks (PCNs). *New J. Chem.* **2010**, *34*, 2366-2388.
8. Furukawa, H.; Cordova, K. E.; O′Keeffe, M.; Yaghi, O. M. The Chemistry and Applications of Metal-Organic Frameworks. *Science* **2013**, *341*, 1230444.
9. Cook, T. R.; Zheng, Y-R.; Stang, P. J. Metal-Organic Frameworks and Self-Assembled Supramolecular Coordination Complexes: Comparing and Contrasting the Design, Synthesis, and Functionality of Metal-Organic Materials. *Chem. Rev.* **2013**, *113*, 734–777.

10. Mueller, U.; Schubert, M.; Teich, F.; Puetter, H.; Schierle-Arndt, K.; Pastre, J. Metal-Organic Frameworks-Prospective Industrial Applications. *J. Mater. Chem.* **2006**, *16*, 626-636.
11. Falcaro, P.; Ricco, R.; Doherty, C. M.; Liang, K.; Hill, A. J.; Styles, M. J. MOF Positioning Technology and Device Fabrication. *Chem. Soc. Rev.* **2014**, *43*, 5513–5560.
12. Qiu, S.; Zhu, G. Molecular engineering for synthesizing novel structures of metal-organic frameworks with multifunctional properties. *Coordin. Chem. Rev.* **2009**, *253*, 2891–2911.
13. Li, J. R.; Kuppler, J. R.; Zhou, H. C. Selective gas adsorption and separation in metal–organic frameworks. *Chem. Soc. Rev.* **2009**, *38*, 1477-1504.
14. Farrusseng, D.; Aguado, S.; Pinel, C. Metal–Organic Frameworks: Opportunities for Catalysis. *Angew. Chem. Int. Ed.* **2009**, *48*, 7502-7513.
15. McKinlay, A. C.; Morris, R. E.; Horcajada, P.; Ferey, G.; Gref, R.; Couvreur, P.; Serre, C. BioMOFs: Metal–Organic Frameworks for Biological and Medical Applications. *Angew. Chem. Int. Ed.* **2010**, *49*, 6260-6266.
16. Kreno, L. E.; Leong, K.; Farha, O. K.; Allendorf, M.; Van Duyne, R. P.; Hupp, J. T. Metal-Organic Framework Materials as Chemical Sensors. *Chem. Rev.* **2011**, *112*, 1105-1125.
17. Yaghi, O. M.; Li, H. Hydrothermal Synthesis of a Metal-Organic Framework Containing Large Rectangular Channels. *J. Am. Chem. Soc.* **1995**,*117*, 10401-10402.
18. Cheetham, A. K.; Rao, C. N. R.; Feller, R. K. Structural Diversity and Chemical Trends in Hybrid Inorganic-Organic Framework Materials. *Chem. Commun.* **2006**, 4780-4795.

19. Ward, A. J.; Masters, A. F.; Maschmeyer, T. Cobalt (II) Carboxylate Chemistry and Molecular Magnetism. In *Comprehensive Inorganic Chemistry II : From Elements to Applications*, 2nd ed; Reedijk, J., Poeppelmeier, K., Eds.; Elsevier : Oxford, 2013; Vol.8, pp 191-228.
20. Stock, N.; Biswas, S. Synthesis of Metal-Organic Frameworks (MOFs): Routes to Various MOF Topologies, Morphologies, and Composites. *Chem. Rev.* **2012**, *112*, 933-969.
21. Tranchemontagne, D. J.; Hunt, J. R.; Yaghi, O. M. Room Temperature Synthesis of Metal-Organic Frameworks: MOF-5, MOF-74, MOF-177, MOF-199, and IRMOF-0. *Tetrahedron* **2008**, *64*, 8553-8557.
22. Beletskaya, I.; Tyurin, V. S.; Tsivadze, A. Y.; Guilard, R.; Stern, C. Supramolecular Chemistry of metalloporphyrins. *Chem. Rev*. **2009**, *109*, 1659-1713.
23. Goldberg, I. Crystal engineering of Porphyrin Framework Solids. *Chem. Commun.* **2005**, 1243-1254.
24. Drain, C. M.; Varotto, A.; Radivojevic, I. Self-Organized Porphyrinic Materials. *Chem. Rev*. **2009**, *109*, 1630–1658.
25. Day, N. U.; Wamser, C. C.; Walter, M. G. Porphyrin Polymers and Organic Frameworks. *Polym. Int.* **2015**, *64*, 833–857.
26. Zha, Q.; Rui, X.; Wei, T.; Xie, Y. Recent Advances in the Design Strategies for Porphyrin-based Coordination Polymers. *Cryst. Eng. Comm.* **2014**, *16*, 7371-7384.
27. Muniappan, S.; Lipstman, S.; George, S.; Goldberg, I. Porphyrin Framework Solids. Synthesis and Structure of Hybrid Coordination Polymers of Tetra(carboxyphenyl)porphyrins and Lanthanide-Bridging Ions. *Inorg. Chem.* **2007**, *46*, 5544-5554.

28. Smithenry, D. W.; Wilson, S. R.; Suslick, K. S. A Robust Microporous Zinc Porphyrin Framework Solid. *Inorg. Chem.* **2003**, *42*, 7719-7721.
29. Farha, O. K.; Shultz, A. M.; Sarjeant, A. A. Nguyen, S. T.; Hupp, J. T. Active-Site-Accessible, Porphyrinic Metal-Organic Framework Materials. *J. Am. Chem. Soc.* **2011**, *133*, 5652-5655.
30. Barron, P.M.; Son, H. T.; Hu, C.; Choe, W. Highly Tunable Heterometallic Frameworks Constructed from Paddle-Wheel Units and Metalloporphyrins. *Cryst. Growth Des.* **2009**, *9*, 1960-1965.
31. Yang, X.-L,; Xie, M.-H.; Zou, C.; He, Y.; Chen, B.; ÓKeeffe, M.; Wu, C.-D. Porous Metalloporphyrinic Frameworks Constructed from 5,10,15,20- Tetrakis(3,5-biscarboxyphenyl)porphyrin for Highly Efficient and Selective Catalytic Oxidation of Alkylbenzene. *J. Am. Chem. Soc.* **2012**, *134*, 10638-10645.
32. Wang, X.-S.; Chrzanowski, M.; Kim, C.; Gao, W.-Y.; Wojtas, L.; Chen, Y.-S.; Zhang, X. P.; Ma, S. Quest for Highly Porous Metal-Metalloporphyrin Framework Based Upon a Custom- Designed Octatopic Porphyrin Ligand. *Chem. Commun.* **2012**, *48*, 7173-7175.
33. Gao, W-Y.; Chrzanowski, M.; Ma, S. Metal-Metalloporphyrin Frameworks: a Resurging Class of Functional Materials. *Chem. Soc. Rev.* **2014**, *43*, 5841–5866.
34. Zou, C.; Xie, M.-H.; Kong, G.-Q.; Wu, C.-D. Five Porphyrin-Core-Dependent Metal-Organic Framework-Dependent Fluorescent Properties. *Cryst. Eng. Comm.* **2012**, *14*, 4850-4856.
35. Kosal, M. E.; Chou, J-H.; Wilson, S. R.; Suslick, K. S. A Functional Zeolite Analogue Assembled From Metalloporphyrins. *Nat. Mater.* **2002**, *1*, 118–121.

36. Alben, J. O. Infrared Spectroscopy of Porphyrins. In The Porphyrins, Physical Chemistry Part A; Dolphin, D., Ed.; Academic Press Inc.: New York, 1978; Vol.3, Chapter 7, pp 323–345.
37. Zhuang, J. L.; Lommel, K.; Ceglarek, D.; Andrusenko, I.; Kolb, U.; Maracke, S.; Sazama, U.; Fröba, M.; Terfort, A. Synthesis of a New Copper-Azobenzene Dicarboxylate Framework in the Form of Hierarchical Bulk Solids and Thin Films without and with Patterning. *Chem. Mater.* **2011**, *23*, 5366–5347.
38. Tranchemontagne, D. J.; Hunt, J. R.; Yaghi, O. M. Room Temperature Synthesis of Metal-Organic Frameworks: MOF-5, MOF-74, MOF-177, MOF-199, and IRMOF-0. *Tetrahedron* **2008**, *64*, 8553–8557.
39. Rochford, J.; Chu, D.; Hagfeldt, A.; Galoppini, E. Tetrachelate Porphyrin Chromophores for Metal Oxide Semiconductor Sensitization: Effect of the Spacer Length and Anchoring Group Position. *J. Am. Chem. Soc.* **2007**, *129*, 4655–4665.
40. Ambre, R.; Chen, K.-B.; Yao, C.-F.; Luo, L.; Diau, E. W.-G,; Hung, C.-H. Effect of Porphyrinic *meso*-Substituents on the Photovoltaic Performance of Dye-Sensitized Solar Cells: Number and Position of *p*-Carboxyphenyl and Thienyl Groups on Zinc Porphyrins. *J. Phys. Chem. C* **2012**, *116*, 11907-11916.
41. Ambre, R. B.; Mane, S. B.; Chang, G.-F.; Hung, C.-H. Effects of Number and position of Meta and Para Carboxyphenyl Group of Zinc Porphyrin in Dye-Sensitized Solar Cells: Structure-Performance Relationship. *ACS Appl. Mater. Interfaces* **2015**, *7*, 1879-1891.
42. Fateeva, A.; Clarisse, J.; Pilet, G.; Grenèche, J-M.; Nouar, F.; Abeykoon, B. K.; Guegan, F.; Goutaudier, C.; Luneau, D.; Warren, J. E.; Rosseinsky, M. J.; Devic, T. Iron and Porphyrin Metal-Organic Frameworks: Insight into Structural Diversity, Stability, and Porosity. *Cryst. Growth. Des.* **2015**, *15*, 1819–1826.

43. Joyce, J. T.; Laffir, F. R.; Silien, C. Layer-by-Layer Growth and Photocurrent Generation in Metal-Organic Coordination Films. *J. Phys. Chem. C* **2013**, *117*, 12502–12509.
44. Shultz, A. M.; Farha, O. K.; Hupp, J. T.; Nguyen, S. T. A catalytically Active, Permanently Microporous MOF with Metalloporphyrin Struts. *J. Am. Chem. Soc.* **2009**, *131*, 4204-4205.
45. Wang, X.-S.; Chrzanowski, M.; Wojitas, L.; Chen, Y.-S.; Ma, S. Formation of a Metalloporphyrin-Based Nanoreactor by Postsynthetic Metal-Ion Exchange of a Polyhedral-Cage Containing a Metal-Metalloporphyrin Framework. *Chem. Eur. J.* **2013**, *19*, 3297-3301.
46. Makiura, R.; Motoyama, S.; Umemura, Y.; Yamanaka, H.; Sakata, O.; Kitagawa, H. Surface Nano-Architecture of a Metal-Organic Framework. *Nat. Mater.* **2010**, *9*, 565–571.

Chapter 3

Thin Film of Porphyrin-based Coordination Networks by SIA

Abstract

As reported in chapter 2, we have successfully prepared bulk of coordination network-based porphyrin at room temperature. In this chapter, we prepared the multilayer film through the same chemical precursors on the amine-functionalized surface substrate using surface-induced assembly (SIA) technique at room temperature. The obtained thin film showed that the organized structure with periodic structure in in-plane (IP) can occur under this mild synthetic condition. This result suggested that molecular arrangement on the surface can be controlled by SIA method. Furthermore, the structural distinction between bulk and thin film was declared in this chapter, which suggested the different growth phenomena of thin film on substrate surface and bulk in solution. The post-modification was mentioned to extend the research for further applications.

3.1 Introduction

The development for the diversities of coordination networks might be extended by the preparation method. The combination of the surface science and coordination chemistry leads to the revolution from bulk synthesis to the thin film on the surface. The engineering of the organized structure through the assembly of coordination chemistry on the surface in the nanostructure level opens the new venue to discover the unique nano-devices for future applications such as photovoltaic device for solar cell, electrochromic device, memory device, and energy storage device for battery.

In this chapter, we focus at the multilayer film formation of coordination networks on the functionalized surface using stepwise growth Surface-Induced Assembly (SIA) method. The introduction in this chapter presents the surface modification of solid substrate by self-assembled monolayers (SAMs) and the growth of metal-organic coordination networks on the surface. Moreover, the SIA technique for the multilayer film formation on the functionalized surface will be mentioned.

3.1.1 Modification of Solid Substrate Surface

Surface chemistry is an important research field to create the variety of functional groups at the surface via the chemical modification. Since the study of self-assembled monolayers (SAMs) has been reported for several decades[1], the various kinds of device fabrication has been promoted by this technique.[2, 3] Such an example for the electronic application, the assembly of organic molecule on the semiconductor surface provides the tunable properties such a charge transfer and transport in the hybrid system for improvement in device performance.[4]

The surface modification technique by SAMs is powerful to tailor the surface properties by combination of molecule and the surface. SAMs are molecular assemblies of

molecule from solution or vapor phase to the surface (Figure 3.1). The head group is functionalized at the surface substrate, while the terminal group is available at the topmost on the surface. The idealistic SAMs fabrication is densely packed monolayer with homogeneity of molecule absorbed on the surface. Two common uses of SAMs are thiols and silane. Thiol type[5] is used for gold (Au) or silver (Ag) surface. The silane type[6] is used for hydroxyl surface such as glass, silicon oxide substrate : silicon wafer and quartz slide.[7]

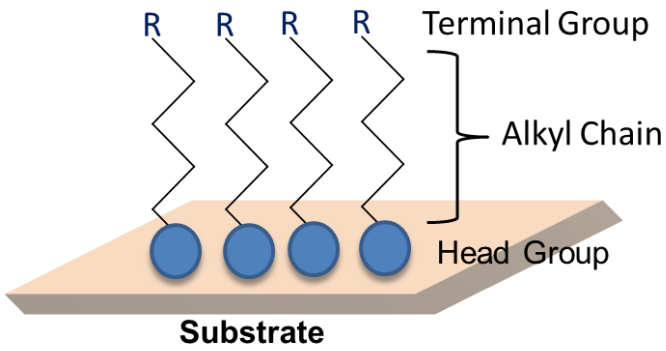

Figure 3.1 Schematic representation of SAMs structure.

In alkylsilane SAMs system, it composes of three sections (Figure 3.1) :

1. the head group : such as trichloro-, trimethoxy-, triethoxysilane, etc.
2. alkyl chain : affect to the stability of SAMs by van der Waals interaction.
3. terminal group : such as halide, methyl, carboxyl, hydroxyl, amino, etc. This terminal part is very important for further modification with the appropriate functionality to tailor the active surface for tunable properties.

To prepare the silane on the surface, two methods are available as solution and vapor phase reaction. The room temperature reaction can occur for the solution phase, while higher temperature (50-120^{o}C) is needed to use for vapor phase condition. Eventhough, the vapor

phase can provide more dense packing, the monolayer with uniform silane is quite difficult to control.[8]

The amine-terminated silane coupling reagent is widely used to functionalize the hydroxyl-terminated surface for the wide range of applications such as immobilizing of ionic nanoparticle, metal ion sensing.[9, 10] As the silanization reaction between methoxy group of silane coupling reagent and the silanol-terminated silicon surface (-OH), many forms are possible to obtain as shown in Figure 3.2. [11, 12] The preferable configuration of amine group should be leaving away from the surface to promote the further growth.[13] The advantage of SAMs on surface is the stability due to the covalent network on the surface.

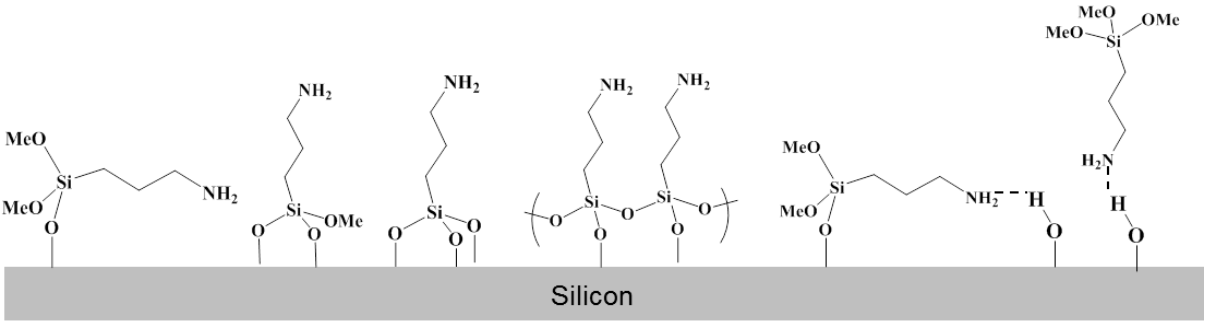

Figure 3.2 The possible orientations of APTMS on Si surface.

3.1.2 The Growth of Metal-Organic Coordination Networks on the Surface

Taking the advantage of the various functional groups on the SAMs surface, the various molecular systems on SAMs surface can be anticipated. At this point, the tailoring of molecular arrangement onto SAMs via step-by-step growth method becomes highly possible. The extension from monolayer to multilayer fashion can be likely combine the function in one system. As roughly mentioned in the first chapter, this step-by-step fabrication is based on the sequential deposition process between the opposite charge components (in this

research refers to metal ion and organic ligand), providing the growth of number of layers with self-limiting and resulting in the uniform deposition layers. This bottom-up self-assembly has high potential to control the structure on the surface in multilayer fashion with wide range of applicable components, simplicity and cost-effective system.[14] Besides, it also promotes the variety of coordination architectures at the different functionalized surfaces by SAMs.[1, 8]

The development of MOFs on the surface especially at nanoscale level is one of the great challenging issues to the realistic application in the future. To enlarge the application fields of MOFs materials, the evolution of synthetic methods has been created to generate the MOFs on the surface as known as MOF thin film and SURMOFs.[15] This can increase the variety of MOFs for device applications as mentioned in the first chapter. In case of bulk powder obtained by traditional solvothermal method, the polycrystalline and non-homogeneous layer are not suitable for device. To fulfill the requirements for device utilization, the thin film preparation is the great choice due to the continuous growth of film leading to the homogeneous and controllable thickness.[16] The key point for the device application is the control of material deposition on the surface at the nanoscale.

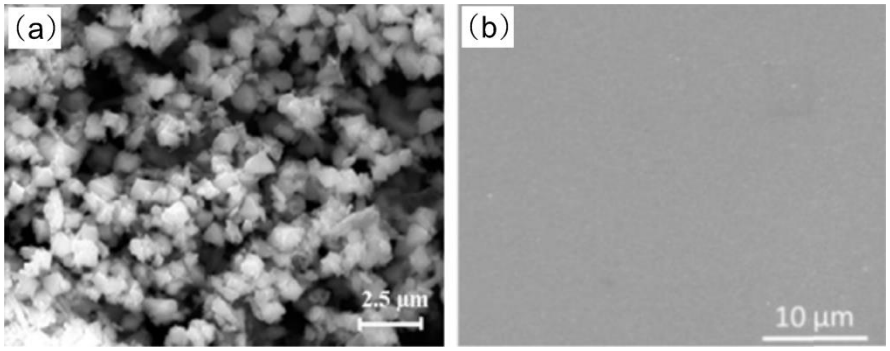

Figure 3.3 The SEM images for comparison of (a) MOF powder, and (b) SURMOFs by LbL method.[16]

The classification of MOF thin films was divided as polycrystalline MOFs and SURMOFs.[15, 17] The polycrystalline MOF thin film (Figure 3.4 (a-1)), which is synthesized on bare or SAMs surface via the direct synthesis such as solvothermal, shows the micrometer scale thickness and exhibits the disordered structure as similar structure with bulk character.[18] While SURMOFs (Figure 3.4 (b), which are synthesized by LB or LbL (LPE) method on SAMs surface, show the oriented structure in the nanoscale thickness, which may differ from the bulk structure. This suggests that the functionalized species at the surface play an important role to control the structure. This can lead to structural diversities by different preparation methods even in the similar set of components. The SURMOFs synthesis requires the fast kinetic for the chemical reaction and favorable coordination for interaction. Some of the bulk MOFs that required the harsh synthetic condition in solvothermal method may not be achieved by the mild synthesis as LbL technique.[15]

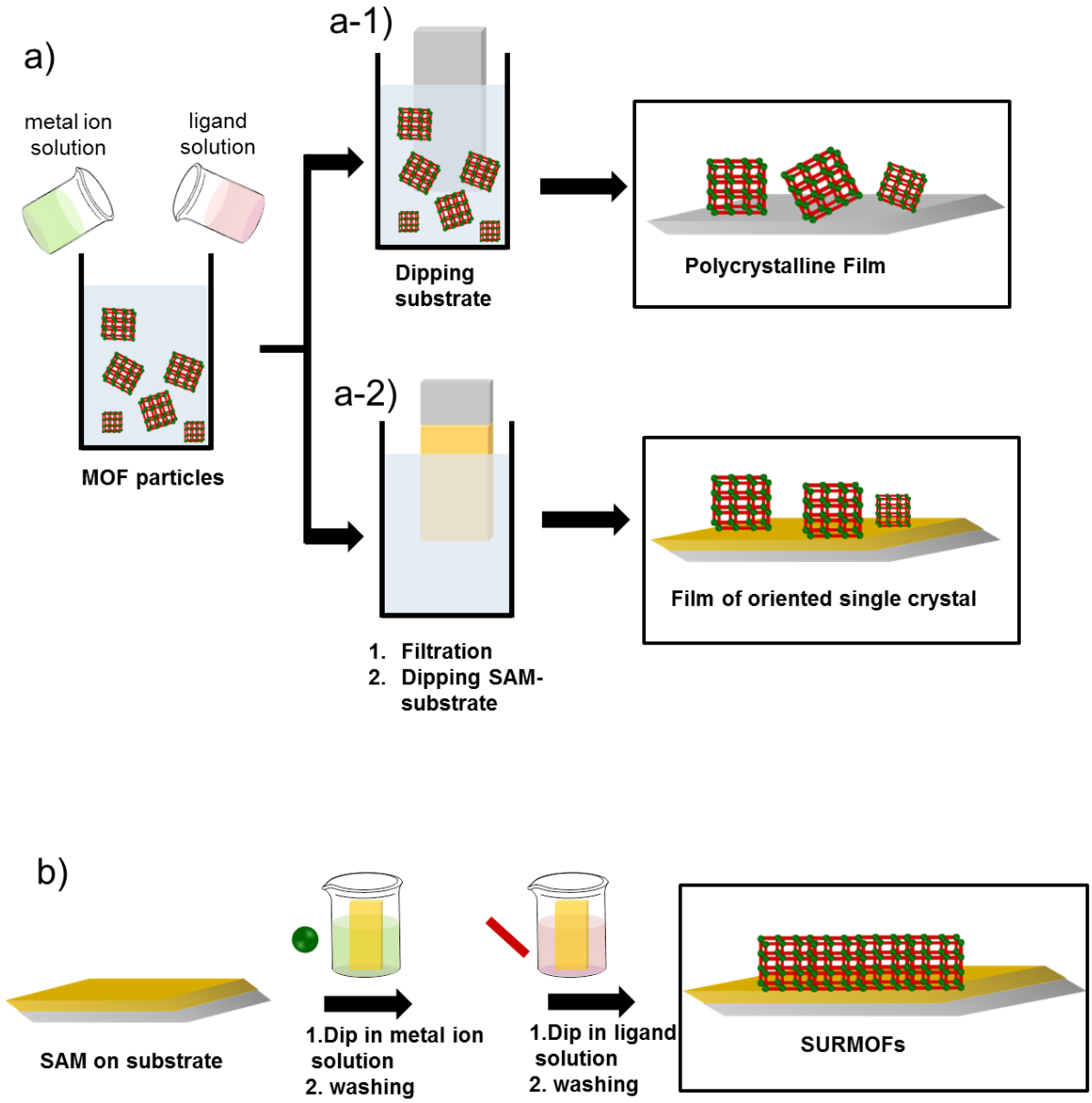

Figure 3.4 (a) the growth of MOF thin film ; (a-1) the growth of the polycrystalline film, (a-2) the growth of MOF crystal on SAMs surface, and (b) the growth of SURMOFs on SAMs

Shekhah mentioned about the growth of MOF HKUST-1, which is one of the most studied MOFs, on gold surface at room temperature. It was reported that the different functionalized SAMs on the surface such as COOH-, OH- terminated SAMs can provide the different orientations of HKUST-1 on the surface.[19] The CH_3-terminated SAMs cannot

provide thin film growth via LbL method,[20] while thin film can be prepared on CH_3-terminated SAMs using solvothermal method. This strongly points out that as SAMs have been employed to the surface likewise the template, it can strongly impact the structure and orientation of MOFs growth. In bare surface or inappropriate terminated group of SAMs (such as CH_3- terminated SAMs), the heterogeneous nucleation sites can occur, leading to the isotropic growth phenomena. In contrast, the COOH- or OH- terminated SAMs can provide the oriented behavior film. An example of amine-terminated silane, 3-aminopropyltrimethoxysilane (APTMS), it has been reported to use as SAMs for the growth of coordination networks on the surface.[21, 22] This represents that the NH_2- terminated SAMs can also promptly react with the suitable chemical component to promote and control the framework growth.

Using SIA method, the stepwise process is considered. As the SAMs surface is immersed to the metal ion solution, the anchoring groups on SAMs make coordination bonding to the metal. In ideal, the monolayer of metal moieties will occur at the surface, while the physisorption is removed by solvent rinsing. Next step, the immersion to the organic linker solution makes the coordination bond to the deposited metal units on the surface. The physisorption is removed by solvent rinsing. The repeating procedure is continued for metal-organic thin film. Ideally, one deposition cycle provides one periodic layer. This stepwise leads to the low roughness thin film with highly homogeneous feature.[23] The thickness can be precisely adjusted by the number of deposited cycles. Moreover, the growth pattern of multilayer film is likely affected by the packing density of SAM moieties at the initial surface, the flexibility of silane coupling layer as well as substrate roughness.[24]

Attention at the well-defined structure, the choice of rigid organic ligand is considered. Porphyrin is rigid conjugated ligand which can reduce the complicated packing due to the flexibility of ligand conformation. These offer the great possibilities to prepare the artificial

materials using tetracarboxyphenylporphyrin derivatives (H_2TCPP or MTCPP; M = metal ion) with different metal nodes.

We mentioned in chapter 2 that the numerous bulk porphyrin-based MOFs have been reported, while the thin films of porphyrin-based MOFs have been less explored.[25] In recent, porphyrin-based MOFs thin films on substrate in both of the presence and absence of SAMs have been more investigated such as Hupp group using LbL technique[21, 26], Kitagawa group using LB-LbL technique[27-29], and other groups.[18, 30, 31] However, the insight investigations of the ordered porphyrin-based metal-organic thin films are still needed to explore the growth behavior of porphyrin thin film materials.

Due to the large π-conjugated system, porphyrin molecule can display the intense absorption properties in visible region. The metal-free, or called free-base form exhibits the intense absorption band near 400-450 nm as denoted as soret band and also contains four less intensity bands around 450 and 700 nm as referred as Q-band.[32, 33] The porphyrin core is available for metal ions. Several processes including pre-metalation, *in situ* metalation and post-metalation can be applied to provide the metaled form, which strongly impacts to the different electronic properties by each metal species. The metalated porphyrin has higher symmetry comparing to free-base form and providing two Q-bands, which is different from the free-base form. In general, the reactivity of porphyrin is dominant by the metal in core unit.[34] This unique character can promote the tremendous applications due to the variation of metal properties.

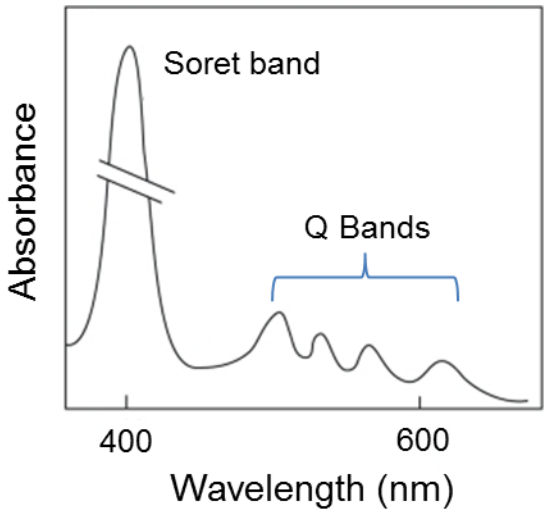

Figure 3.5 Typical UV-absorption spectra of porphyrin

In case of metal ion building unit, Co (II) cation was reported that it can effectively coordinate to amino ligands.[35, 36] In this research, we selected the amine-functionalized SAMs surface (on Si wafer and Quartz slide) as platform for promoting the growth of coordination networks between Co(II) ion and carboxyl group of porphyrin (H_2TCPP). It was expected that the growth in multilayer fashion of this system can stepwise occur via SIA process at the room temperature.

The choice of substrate is important for thin film characterization, especially XRR and GI-SAXS measurement to determine the structural detail. Due to the very thin layer of nanoscale film, the flat surface is more preferable than other substrates to use for film growth and suitable for characterization techniques. Moreover, the crystallinity of film also relates to the surface substrate. Si(100) substrate was selected to use as the substrate in this research.[27] In some metal-organic ultrathin film reports suggested that the inappropriate substrate with the very low thin film thickness leads to the difficulties for structural determination by X-ray diffraction technique.[37]

3.2 Experimental Section

3.2.1 Chemicals and Materials

3.2.1.1 Chemicals

3-Aminopropyltrimethoxysilane (APTMS, >96%) was purchased from Tokyo Chemical Industry Co. Ltd. (TCI). 5,10,15,20-Tetrakis(4-carboxyphenyl)-porphyrin (H_2TCPP) (purity 98%) was purchased from Strem Chemical Inc., USA. Cobalt(II) acetate tetrahydrate ($Co(OAc)_2.4H_2O$) was purchased from Wako Pure Chemical Industries Ltd. HPLC and AR grade of 2-propanol and ethanol were used for surface modification. Chloroform ($CHCl_3$), methanol and 2-propanol as superdehydrated solvents were used with a syringe to prepare solutions for SIA deposition. All solvents were purchased from Wako Pure Chemical Industries Ltd. All chemicals were used as received without further purification.

a)

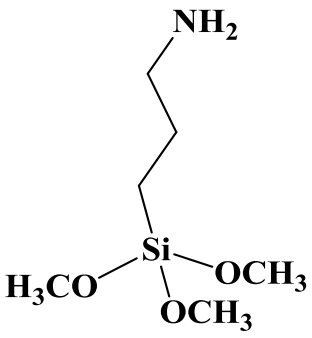

APTMS

b)

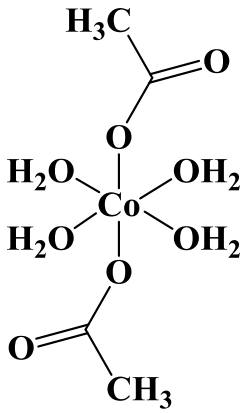

$Co(OAc)_2.4H_2O$

c)

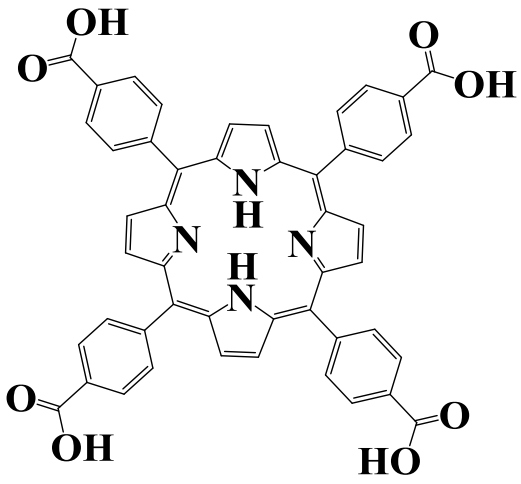

H_2TCPP

Figure 3.6 Structures of Chemicals in SIA synthesis. (a) APTMS, (b) $Co(OAc)_2.4H_2O$, and (c) H_2TCPP

3.2.1.2 Materials

Silicon wafer (100, p-type) substrates (40×25 mm^2) were purchased from Electronics and Materials Corp. Ltd. Transparent quartz plate substrates (25×15 mm^2) were purchased from Sendai Sekiei Glass Seisakusho Y.K. Both substrates were used for SIA deposition.

3.2.2 Cleaning Process for Substrate

Prior to use, silicon wafer substrates and quartz substrates were cleaned using 2-propanol two times with sonication for 10 minutes. Then, they were dried immediately and kept on a clean bench.

3.2.3 Modification of Surface Substrate with Silane Coupling Agent (APTMS)

To obtain the amine-functionalized substrates, all cleaned substrates were immersed in 10 mM ethanol solution of 3-aminopropyltrimethoxysilane (APTMS) at room temperature for 1 hour under argon atmosphere with mild shaking. After that, all substrates were washed respectively with ethanol (2 times), 2-propanol (2 times), and dried. All APTMS-modified substrates were kept in the clean sample box under argon atmosphere until use.

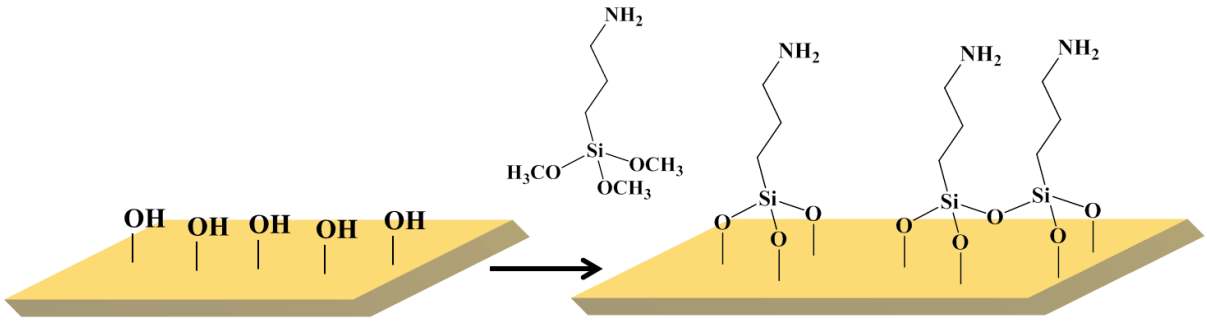

Scheme 3.1 Silanization reaction between APTMS and the hydroxylated surface on substrate

3.2.4 Fabrication of Multilayer Porphyrin-based Coordination Networks on Amine-Functionalized Substrate

The fabrication of multilayer porphyrin-based coordination networks on modified substrates was proceeded using the SIA method via an layer-by-layer (LbL) automated machine. The APTMS-modified substrates were used for all SIA experiments with the following procedures under argon atmosphere : (i) the modified substrates were immersed into 10 mM $Co(OAc)_2.4H_2O$ in the mixture solvent of superdehydrated methanol and chloroform (1:9, v/v) for 10 minutes and were then rinsed with four separated containers of the same ratio mixture solvent as those described above for each 1 minute washing to remove the remained reactants from the surface and then were dried by blowing. (ii) the metal-terminated substrates were then immersed into 0.11 mM H_2TCPP in superdehydrated 2-propanol for 10 minute following the same washing procedure in 2-propanol. The first layer of coordination networks has been created. The growth of the further multilayer was repeated by the above procedure (Scheme 3.2). The desired number of layers according to the alternate deposition of metal ion (Co(II)) and organic linker (H_2TCPP) solution is shown as the "N" layers, assigned as $(Co/\ H_2TCPP)_N$.

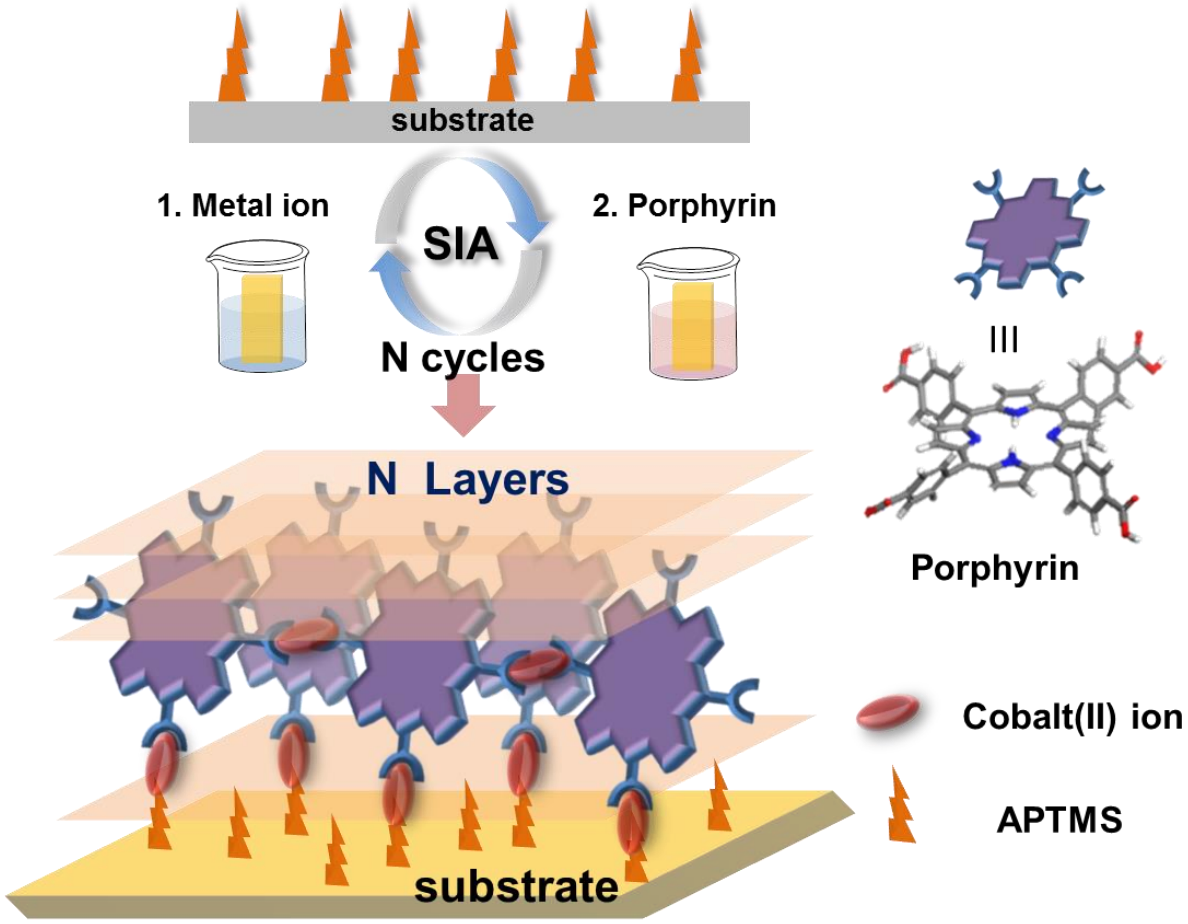

Scheme 3.2 Schematic representation for fabrication of porphyrin-based metal-organic coordination network thin films on the surface using the surface-induced assembly (SIA) process.

Figure 3.7 Thin film on quartz substrate $(Co/H_2TCPP)_5$

3.2.5 Characterization Techniques

X-ray photoelectron spectroscopy (XPS) was used to determine the elemental composition of amine-modified surface and the growth of thin film on silicon wafer. The XPS experiment was performed using a spectrometer (Axis-Ultra DLD; Kratos Analytical Ltd.) with an Al Kα radiation source (1486.6 eV). The binding energies were calibrated using C1s peak at 284.5 eV as a standard. Curve fitting was done by processing software (Vision) using a Gaussian envelope with Shirley background correction.

UV-Visible absorption spectra of the multilayer film on quartz substrates were measured as a function of number of layers in absorption mode using a spectrophotometer (V-630; Jasco Corp.) at room temperature. The APTMS-modified quartz was used as a background to subtract from each spectrum.

X-ray reflectivity (XRR) was use to determine the thickness, roughness and mass density of the thin film using a high-resolution X-ray diffractometer (ATX-G; Rigaku Corp.). The diffractometer was equipped with a Cu Kα radiation source (λ= 0.1542 nm). The X-rays were generated from a Cu rotating anode (50 kV, 300 mA). The reflective oscillation spectra from the experiment were fitted using software (GXRR; Rigaku Corp.). The fitting curve was varied from 0.2° to 3°. The difference of the fringe between SAM layer (APTMS) and Si wafer could not be observed (Figure 3.14a). The SAM layer thickness has little effect on the overall thickness of film. Thus, the thickness of APTMS and thin film was estimated as a single layer model.

An atomic force microscope (AFM) with tapping mode was used to examine the surface morphology and roughness of thin film. AFM images were collected by a digital AFM system (Nanoscope IIIa; Veeco Instruments). Silicon cantilevers (SI-DF3FM; Nanosensors Corp.) with a spring constant between 2.8 N/m and 4.4 N/m and a resonance

frequency of 79-89 kHz were used. The measurement was proceeded at scanned area of 1×1 μm^2under air atmosphere with a scan rate of 0.4 Hz.

The thickness measurement was conducted using AFM (VN-8000; Keyence Co.) with DFM/SS mode cantilever (OP-75041; Keyence Co.). Before the measurement, the thin film on Si wafer substrate was removed by sharp blaze with no damaging the hard substrate surface. The analysis was investigated across the scratched line in at least five different positions to estimate the average film thickness comparing with XRR measurement.

Infrared p-polarized multiple angle incidence resolution spectroscopy (p-MAIRS)[38, 39] was used to clarify the molecular vibration of chemical bond in both of in-plane (2×IP) and out-of-plane (OP) orientation of thin film sample. The p-MAIRS measurements were conducted on a FT-IR spectrometer (Nicolet 6700; Thermo-Fisher Scientific) equipped with a mercury-cadmium-telluride (MCT) detector. Single-beam spectra were collected from 38° to 8° by means of 6° steps in a range of angle of incidence with 64 scans and 4 cm^{-1} resolution. The aperture was fully opened (size of 150). A metal plate with small pores was placed in the light path of the incident beam to prevent saturation. A ZnSe polarizer was used to obtain the p-polarized light. The APTMS-modified silicon wafer substrate was used as a background in p-MAIRS measurement. All p-MAIRS measurements were done under N_2 atmosphere at room temperature.

Grazing incidence small angle X-ray scattering (GI-SAXS) measurement was carried out to observe the interior thin film structure. Measurement was taken using X-ray diffractometer (FR-E; Rigaku Corp.) with two-dimensional (2D) detector (R-AXIS IV; Rigaku Corp.). The sample stage included the goniometer and a vertical stage (ATS-C316-EM/ALV-300-HM; Chuo Precision Industrial Co. Ltd.). The Cu Kα radiation source (λ= 0.1542 nm.) with beam size of approx. 300 μm × 300 μm and camera length of 300 mm was

used. The angle of incidence was varied from 0.21° to 0.22°. The diffraction patterns of in-plane (IP) and out-of-plane (OP) directions were acquired.

3.3 Results and Discussion

The contents in this chapter are mainly divided in 4 parts :

3.3.1) Modification of surface substrate with silane coupling reagent (APTMS)

3.3.2) Multilayer formation of Porphyrin-based Coordination Networks on Amine-Functionalized Substrate

3.3.3) Comparison of structure between bulk and thin film

3.3.4) Opportunity to extend this research for further applications

3.3.1 Modification of Surface Substrate with Silane Coupling Reagent (APTMS)

The elemental compositions on the surface substrate can be revealed by XPS analysis. To investigate the detail in silanization of APTMS on silicon substrate, the fine scan with deconvolution of N1s peak and Si2p spectra were mainly emphasized (Figure 3.8 a). In case of N1s, two nitrogen species were observed at 399.3 and 401.5 eV which corresponded to the free aliphatic amino ($-NH_2$) and protonated aliphatic amino group (NH_3^+), respectively.[11, 40] These two different components may relate to the interaction between aminosilane group and silicon substrate as mentioned in the introduction of this chapter.[11, 12] In case of Si2p, the aminosilane (Si-O) was presented at 101.7 eV (Figure 3.8 b). The other Si2p peak components also can be detectable such as Si-Si bond in bulk silicon wafer ($Si2p_{1/2}$ and $Si2p_{3/2}$) and silicon oxide layer (SiO_2). These XPS results indicated that amino-modified silicon wafer surface can successfully bond to the silicon surface. Thus, the multilayer growth of coordination network on this amine-modified surface was then proceeded.

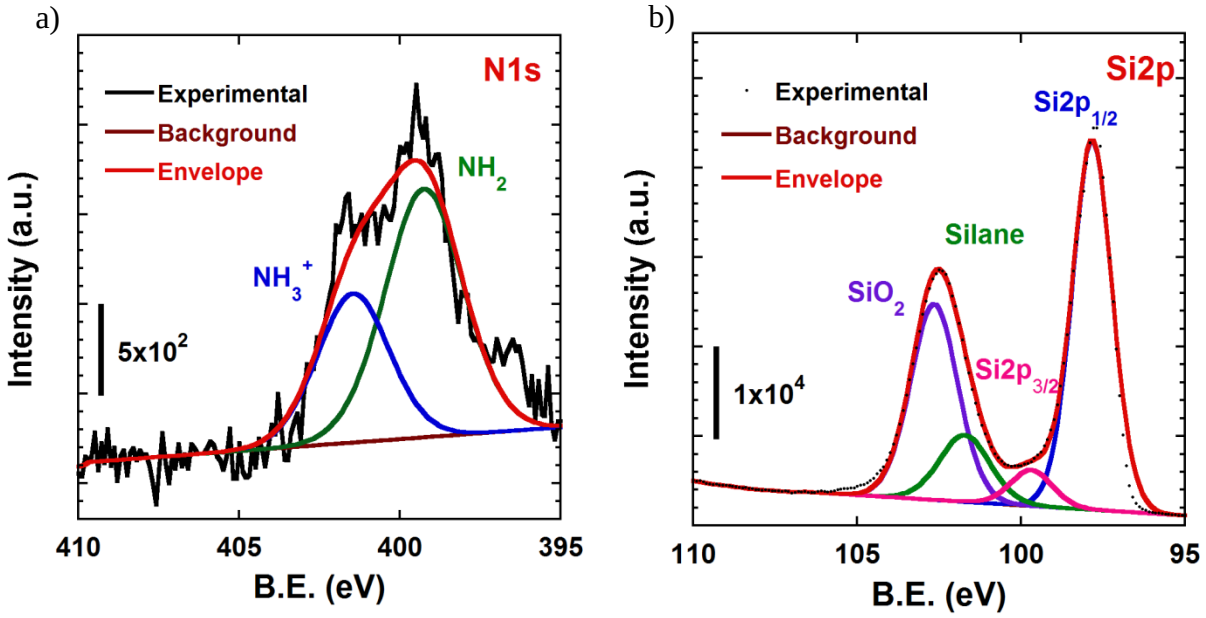

Figure 3.8 The deconvolution of (a) N1s and (b) Si2p spectra of APTMS-modified Si wafer substrate.

3.3.2 Multilayer Formation of Porphyrin-based Coordination Networks on Amine-Functionalized Substrate

3.3.2.1 Investigation of Step-by-Step Multilayer Growth by UV-Vis Spectroscopy

Porphyrinic compounds display the unique absorption in the UV-Vis region as determined as soret band (B-band) and Q-bands. This characteristic is beneficial to monitor the multilayer growth of thin film using UV-Vis spectroscopy.[41] The UV-Vis absorption spectra of multilayer thin film on the transparent quartz substrate exhibited the intense soret band at 418 nm with four Q-bands at 500-700 nm as shown in Figure 3.9 a. The absorbance of soret band and Q-band increased linearly with the number of deposited layers, which referred to the successive multilayer film growth[41] (Figure 3.9 b).

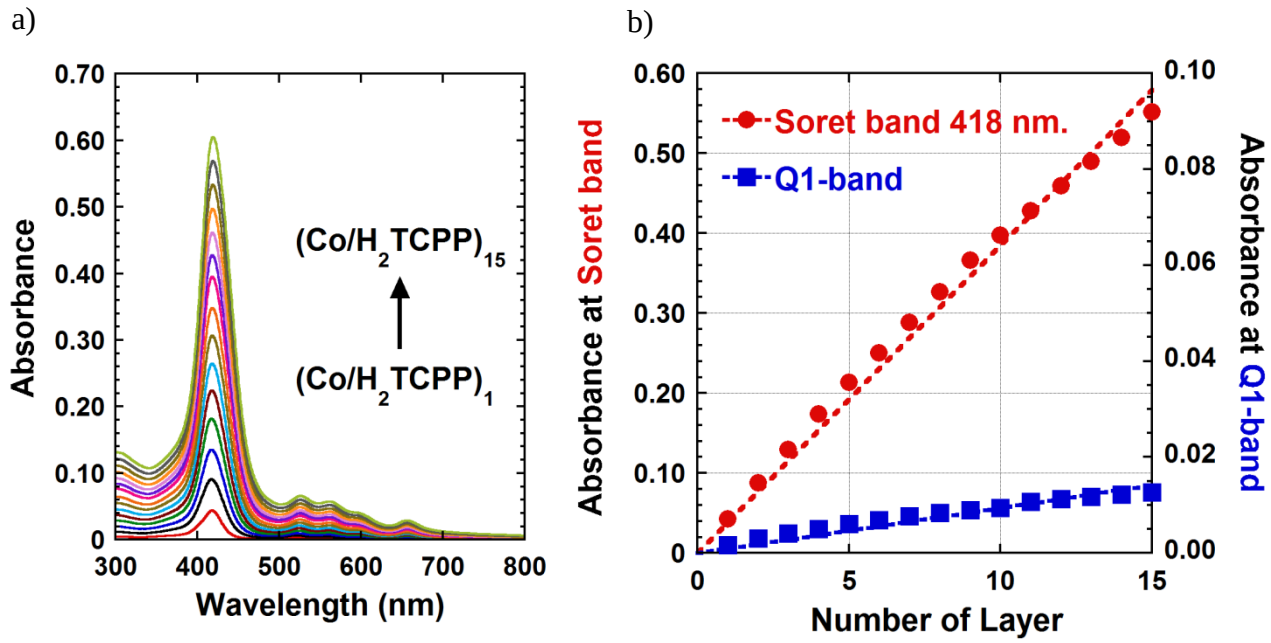

Figure 3.9 (a) UV-Vis absorption spectra of multilayer thin films with a number of deposited layers $(Co/H_2TCPP)_{1\text{-}15}$ on the APTMS-modified transparent quartz substrate. (b) The UV-Vis absorption intensity of the soret band at 418 nm and Q_1-band at 526 nm as a number of deposited layers.

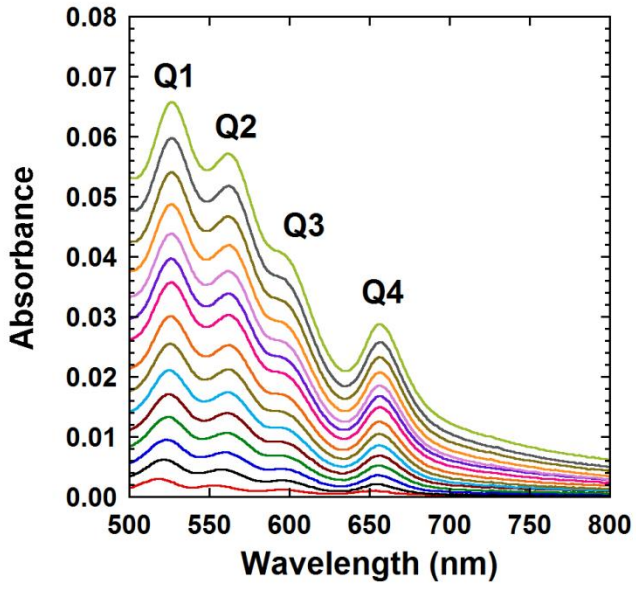

Figure 3.10 Zoom-in Q-band of $(Co/H_2TCPP)_{1\text{-}15}$ on the APTMS-modified quartz substrate.

During the stepwise reaction in film formation, the Q-bands in UV-Vis spectra have no change from four to two bands (Figure 3.10), this seems suggest the retention of the D_{2h} molecular symmetry as free-base porphyrin core.[42, 43] The plausible reason may due to the low temperature (room temperature) synthesis in the coordination network growth.[44] However, if the system contains small portion of metalated species (Co metalated TCPP), it cannot be distinguished in UV-Vis spectra. Thus, we cannot rule out the formation of Co metalated TCPP during the film growth. To consider in the metalation issue, we will discuss about the evidence for partial metalation of TCPP in this thin film, which was supported by the XPS analysis of N1s spectra (Figure 3.19d in section 3.3.2.5).

In comparison with some solvothermal bulk and thin film porphyrin-based MOFs synthesis using free-base porphyrin ligand, the metalation at center of porphyrin can easily occur. [18, 45, 46] The retaining of free-base porphyrin in the system provides the chance for post-metalation process using the variable metal species for the particular applications such as sensing and catalysis.[26]

As this multilayer film exhibited the sequential growth phenomena, it was hypothesized that cobalt ions may effectively coordinate to carboxylate group in porphyrin building unit to promote the growth. To verify this assumption, the control experiment was conducted by immersion the APTMS-modified substrate in 3 cycles assemblies without cobalt deposition step (Figure 3.11). The result showed no increasing of the absorption intensity (nearly at baseline) with the number of assembled layers. This revealed that the immersion step of metal ion solution was strongly necessary to create coordination networks. Moreover, it also inferred that the aggregation of porphyrin by physisorption on the surface did not occur in this system.

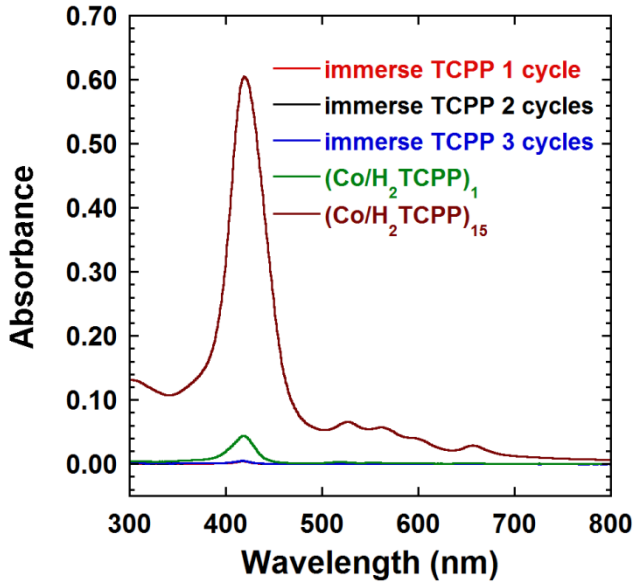

Figure 3.11 UV-Vis absorption spectra of 3 cycles assemblies on the APTMS-modified transparent quartz substrate without immersion step of cobalt ion solution, comparing with 1 layer ($(Co/H_2TCPP)_1$) and 15 layer ($(Co/H_2TCPP)_{15}$) thin film in the normal deposition process.

The soret and Q-bands of UV-Vis absorption spectra in all synthesized films displayed the broad peak with shift to longer wavelength comparing to the H_2TCPP in 2-propanol (Figure 3.12 and Table 3.1). The broaden and shifted absorption band on solid substrate comparing with solution phase represented the common phenomena when porphyrin deposited on the solid substrate.[42] This phenomenon was generally attributed to the closer packing of porphyrin assemblies in the thin film moieties rather than in solution phase.[47, 48] The shift features relate to the porphyrin aggregation types, which occur owing to the π-π interaction between porphyrin rings. The red shift (shifting to longer wavelength) refers to the J-aggregation type, which conforms as edge to edge or side to side. The blue shift (shifting to shorter wavelength) is relevant to the H-aggregation type, which displays as face to face. Many factors contribute to the shift character such as the degree of aggregation,

the distance of interplanar spacing, the monomer orientation such as tilt angle of the molecular stacking, the electronic transition probabilities and the specificity porphyrin sensitivities.[49, 50]

In our multilayer films, it was supposed that the small shift around 2 nm of soret band to longer wavelength may happen because of the high inter-planar spacing between two adjacent porphyrin rings in the networks directing to minimize the close aggregation behavior assembly.[51, 52] Another possible explanation for this phenomena is the simultaneous existence of J- and H-aggregation.[53] The aggregation character is strongly relevant to the structural arrangement of molecule in the film, which determines the properties of material such as photonic and catalytic properties.[54]

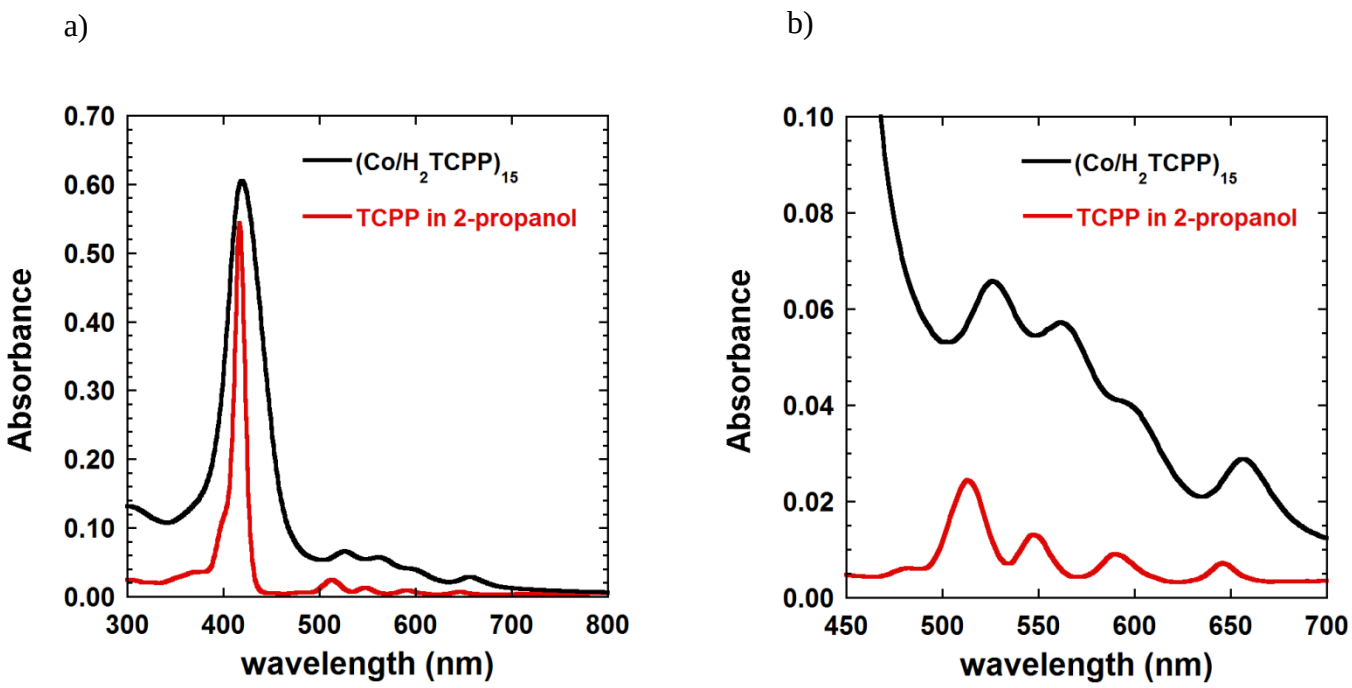

Figure 3.12 (a) Comparison of H_2TCPP in solution phase (at 1.1 μM in 2-propanol) and $(Co/H_2TCPP)_{15}$ on the APTMS-modified quartz substrate, (b) Zoom-in Q-band region.

Table 3.1 UV-Vis absorption peak position of H_2TCPP in solution phase, comparing with $(Co/H_2TCPP)_{15}$ on the APTMS-modified quartz substrate.

H_2TCPP	**Soret band (nm)**	**Q_1-band (nm)**	**Q_2-band (nm)**	**Q_3-band (nm)**	**Q_4-band (nm)**
Solution phase; in 2-propanol	417	513	547	590	646
Solid phase; $(Co/H_2TCPP)_{15}$ on the APTMS-modified Quartz	418-419	519-526	554-562	597	652-657

In general, the surface coverage of chromophore on the surface can be estimated from the absorbance of chromophore layer at surface as shown in equation 3.1.

$$\Gamma = [\left(\frac{A_\lambda}{2}\right) \varepsilon_\lambda^{-1} N_A \ ] \times 10^{-3} \quad \text{molecule/cm}^2. \ ^{55} \qquad \text{___ equation 3.1}$$

Thus, we calculated the surface coverage of porphyrin-based coordination networks (Table 3.2) by the above equation with the parameter determination as following :

A_λ = the absorbance of H_2TCPP per one deposition layer at the define wavelength (λ); in this experiment λ= 417 nm.

Factor 1/2 was used because the quartz surface was modified in two sides.

Thus, A_λ /2 = the absorbance of H_2TCPP per one deposition layer only in one side of substrate

ε_λ = extinction coefficient of H_2TCPP in 2-propanol ($M^{-1}cm^{-1}$)

ε_{417} = 489,914 $M^{-1}cm^{-1}$. The ε_λ was calculated from the calibration curve of H_2TCPP in 2-propanol as shown in Figure 3.13. It was noted that the ε_λ of H_2TCPP in the solution and at the surface were assumed to be similar.

N_A = Avogadro's number

Table 3.2 The surface coverage calculation of $(Co/H_2TCPP)_{15}$ on the APTMS-modified quartz substrate using equation 3.1.

Layer region	**Absorbance per layer (A_λ /2)**	**Surface coverage (Γ)**	
		$\times 10^{-11}$ mol/cm^2	**$\times 10^{13}$ molecule/cm^2**
L1 – L4	0.0217	4.43	2.67
L5- L9	0.0193	3.94	2.37
L10 – L15	0.0154	3.15	1.90

At the layer region; Lx ; x = number of layers

The surface coverage calculation from UV-Vis (Table 3.2) will be compared with the calculation from XRR result (Table 3.8) in the part 3.3.2.6 investigation of structural alignment in coordination networks by GI-SAXS.

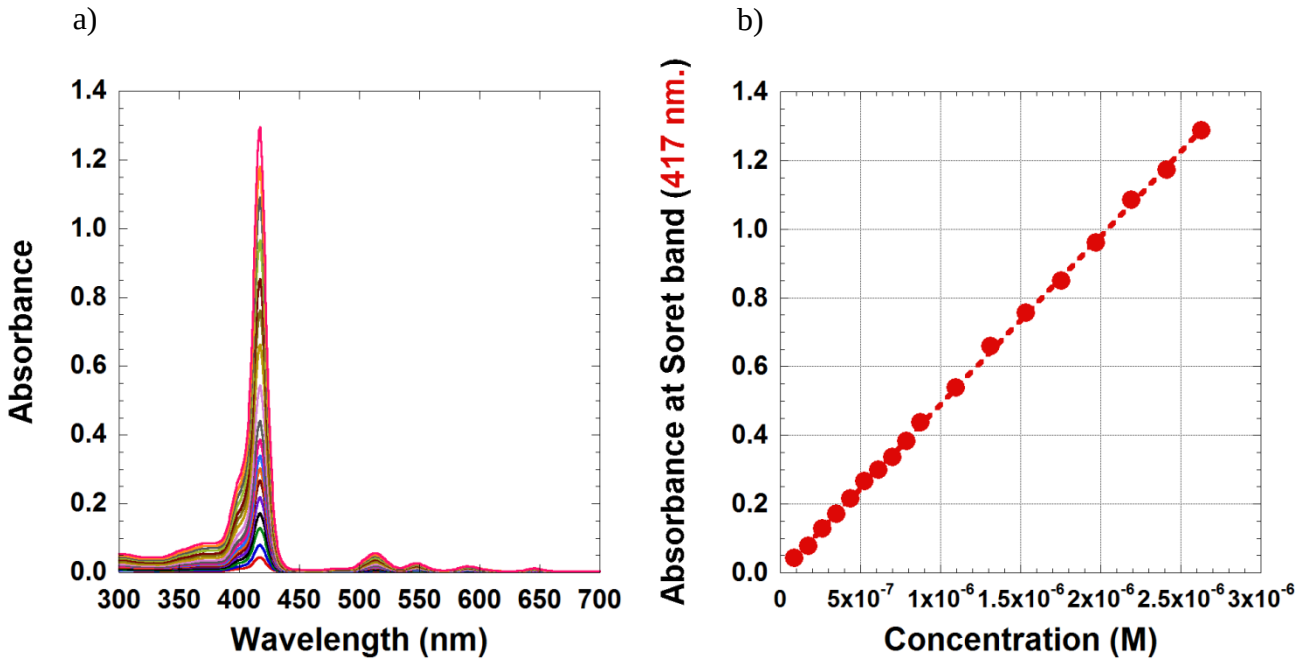

Figure 3.13 Calibration curve of H_2TCPP in 2-propanol; the extinction coefficient at 417 nm (ε_{417}) = 489,914 $M^{-1}cm^{-1}$. The ε was calculated using Beer-Lambert Law as equation 3.2.

$$A = \varepsilon c l \qquad \text{equation 3.2}$$

A = the absorbance of H_2TCPP

c = concentration of H_2TCPP in 2-propanol (mol/L)

l = path length (10 mm)

3.3.2.2 Film Thickness Measurement by XRR and AFM

X-ray reflectivity (XRR) profiles were measured as a function of growth layers, which displays the oscillation intensity (Kiessig fringes) (Figure 3.14b). The higher frequency of oscillation along with the number of growth layers indicated the increase in film thickness. The difference of the fringe between SAM layer (APTMS) and Si wafer could not be observed (Figure 3.14a). The SAM layer thickness has little effect on the overall thickness of film. Therefore, the thickness of APTMS and thin film was estimated as a single layer model. The film thickness by XRR and AFM measurements were plotted as a number of layer growth (Figure 3.14 c).[63, 64] Both cases showed the well consistent results, which exhibited a linear increase of thickness with layer growth. The average thickness per layer was approximated 1 nm with the low surface roughness as mentioned in Table 3.3.

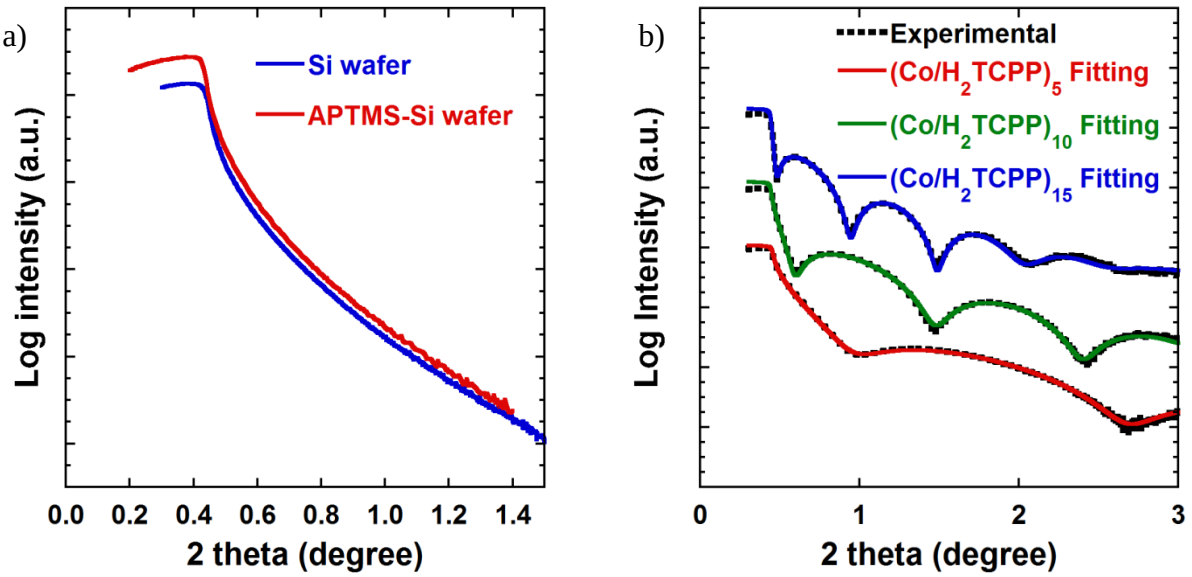

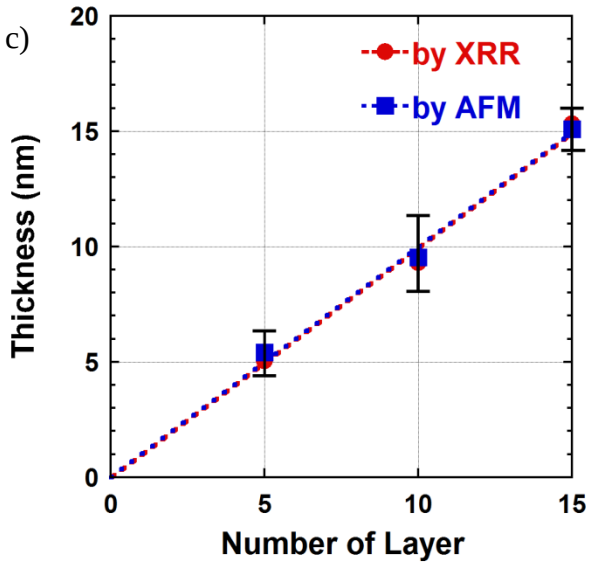

Figure 3.14 (a) XRR profiles of Si wafer and APTMS-modified Si wafer substrates, (b) XRR profiles of multilayer films $(Co/H_2TCPP)_5$, $(Co/H_2TCPP)_{10}$, and $(Co/H_2TCPP)_{15}$ on the APTMS-modified Si-wafer substrates. The experimental and fitted data were respectively displayed as dashed line and solid line, and (c) Thickness of multilayer film by XRR and AFM study with the error bar from measurement.

Table 3.3 Thickness, RMS roughness and mass density of thin film by XRR, comparing with AFM analysis. The deviation in XRR experiment was calculated from the statistical value.

Number of layer	Thickness (nm) by XRR	Thickness (nm) by AFM-Keyence	Roughness (nm) by XRR	RMS Roughness (nm) (R_q) by AFM –Veeco	Density (g/cm^3) by XRR
0 (Si-wafer)	N.A.	N.A.	0.500	0.165	2.33
5	5.031 ± 0.01	5.42 ± 0.75	0.591 ± 0.01	0.645	1.526 ± 0.01
10	9.303 ± 0.01	9.53 ± 1.48	0.826 ± 0.01	0.654	1.518 ± 0.01
15	15.329 ± 0.01	15.10 ± 0.80	1.354 ± 0.01	1.259	1.526 ± 0.01

Furthermore, the mass density of the multilayer films was also investigated by XRR. The result showed almost constant film density approximately 1.5 g/cm^3 in all thin films. This referred that growth phenomena during thin film formation was similar with uniformity. Comparing with the some reports in porphyrin-based metal-organic materials such as PIZA-1 (1.3 g/cm^3) [45], our film density value is relatively high. From this perspective, the growth of the dense coordination networks onto the porous substrate can be possible. This high density property may be considered as the advantage for some usages such as molecular separation, selective adsorption, and catalyst applications.

3.3.2.3 Examination of Surface Morphology by AFM Analysis

The surface morphology and section analysis of multilayer films were investigated by AFM (Figure 3.16). The surface morphology of thin film showed the distinction from the bare Si wafer and APTMS-modified Si wafer surface (Figure 3.15). This also presented as one evidence of thin film formation. The thin film topology showed the grain-like shape with dense packing, homogeneous morphology and smooth surface. This represented the well-deposition process during the film growth. The domain size from the 2D AFM image was estimated around 40-50 nm with small increasing in domain size from 5 to 15 layers film. The root-mean-square (RMS) roughness slightly enhanced from 0.6 to 1.3 nm as more deposited layer (Table 3.4). This showed the similar trend in porphyrin-based multilayer on Si substrate.[58]

From the XRR and AFM results, it indicated that the thickness of thin film in nanoscale level can be controllable by SIA technique with good quality of thin film production, which represented by homogeneity and low surface roughness.

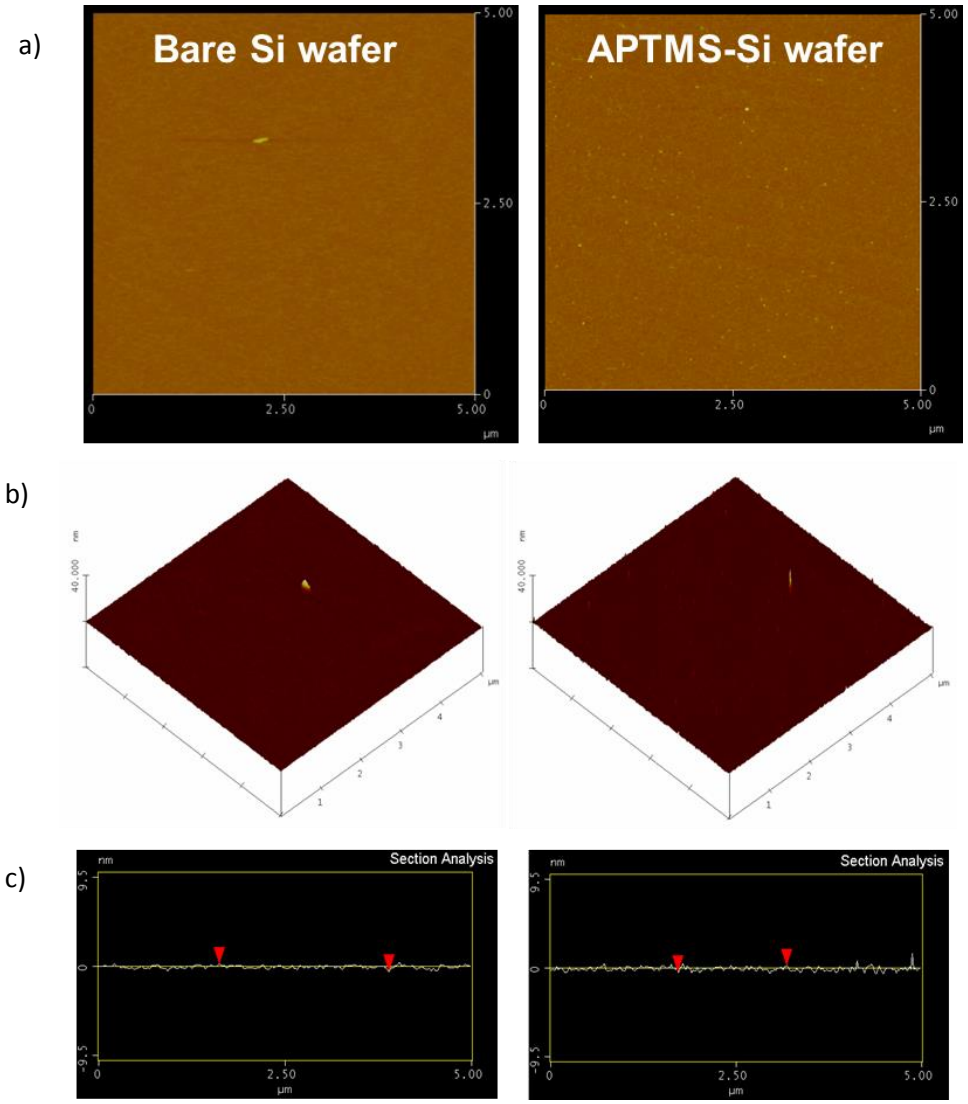

Figure 3.15 (a) surface morphology in 2D, (b) 3D AFM height image of bare Si wafer and APTMS-modified Si wafer and (c) section analysis. Scan size = 5µm × 5µm ; Data scale 20 nm.

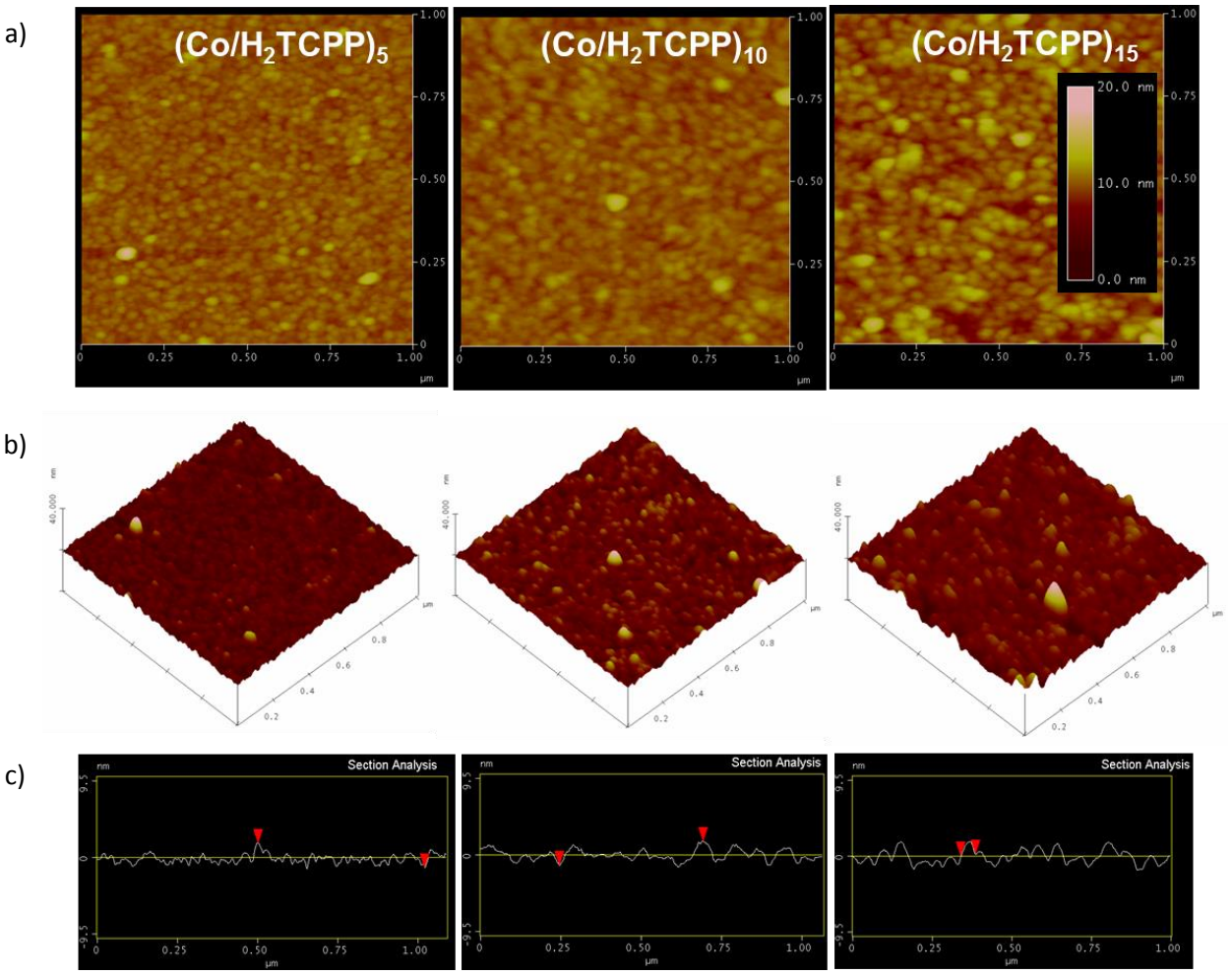

Figure 3.16 (a) surface morphology in 2D, (b) 3D AFM height image of $(Co/H_2TCPP)_5$, $(Co/H_2TCPP)_{10}$ and $(Co/H_2TCPP)_{15}$ on the APTMS-modified Si wafer substrate respectively, and (c) section analysis. Scan size = 1µm × 1µm ; Data scale 20 nm.

Table 3.4 Surface roughness and the estimated domain size of $(Co/H_2TCPP)_5$, $(Co/H_2TCPP)_{10}$ and $(Co/H_2TCPP)_{15}$ on the APTMS-modified Si wafer substrate by AFM analysis.

Number of layer	Scan size (μm)	Roughness Analysis : Img RMS, R_q (nm)	Estimated Domain size (nm)
0 (only Si wafer)	5	0.165	N.A.
APTMS-modified Si wafer	5	0.251	N.A.
5	1	0.645	40-50
	500 nm.	0.684	
10	1	0.654	
	500 nm.	0.614	
15	1	1.259	
	500 nm.	1.031	

N.A. = Not applicable

The small increment of surface roughness (Img RMS, R_q) from bare Si wafer to APTMS-modified Si wafer indicated the availability of molecular layer on Si wafer surface, which might be from the APTMS deposition. In comparison with thin film growth, it showed that both of bare Si wafer and APTMS-modified Si wafer surface have lower RMS roughness. This is one evidence to confirm the available of the film growth on the surface.

3.3.2.4 Determination of Chemical Bond by p-MAIRS

p-MAIRS was used to investigate the molecular vibration of chemical bonds in both IP and OP vibrational modes in thin film.[39, 46] The p-MAIR spectra were displayed in Figure 3.17 a and 3.17 c with the number of layers formation. The vibration of C=C aromatic ring of porphyrin skeleton presented as the overlapped peak at 1588 cm^{-1}.[59] The intense peaks at 1600 and 1400 cm^{-1} referred to asymmetric and symmetric stretching of carboxylate (O–C=O) in thin film.[28, 60, 61] The peak at 1540 cm^{-1} may be considered as another asymmetric stretching of carboxylate.[62] These results provided the evidence for the deprotonation of carboxylic group (COOH) due to the assembly with cobalt ion. However, there were some residue peaks of C=O stretching vibration from free carboxylic group of porphyrin unit at 1688 cm^{-1}.[63, 64] Makiura and Motoyama et al. also reported the similar phenomena in porphyrin-MOF nanofilm, NAFS series, that the remained COOH moieties were attributed to the edge of sheet domain.[28, 29] The absorbance increased linearly with the number of deposited layers in both IP and OP spectra, which inferred the well-growth behavior along with multilayer formation (Figure 3.17 b and 3.17 d). Both UV-Vis and p-MAIRS results were well-supported each other which represented the consistent analysis.

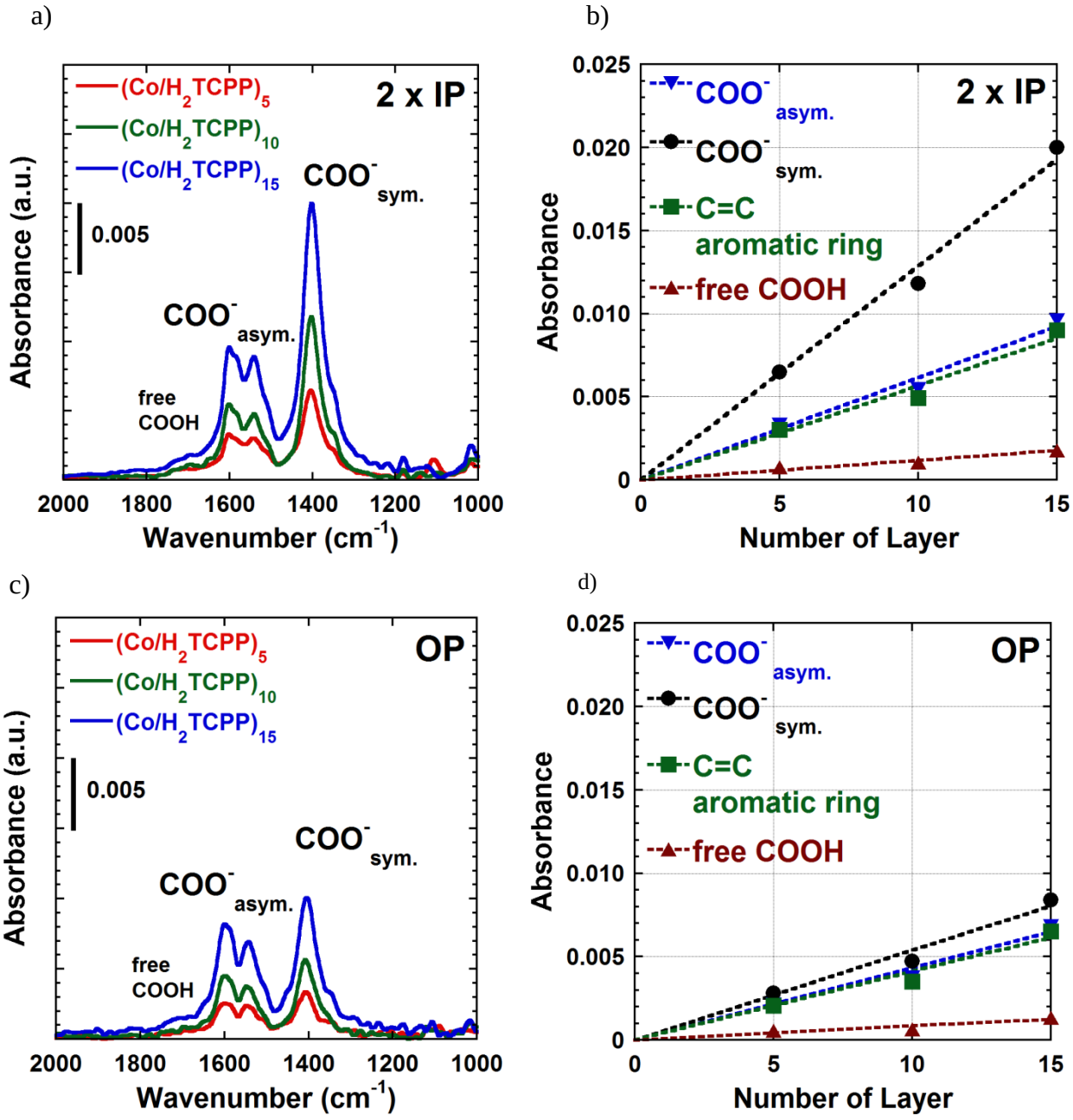

Figure 3.17 p-MAIR spectra of multilayer film as a number of deposited layers $(Co/H_2TCPP)_5$, $(Co/H_2TCPP)_{10}$ and $(Co/H_2TCPP)_{15}$ on the APTMS-modified Si wafer substrates in (a) In-plane (2×IP) and (c) Out-of-plane (OP).

The shoulder peak at 1350 cm^{-1} in both IP and OP of all thin films may assign to the vibration of the pyrrole ring of porphyrin unit (=C-N).[31, 73]

Table 3.5 The ratio of symmetric/ asymmetric COO^- of $(Co/H_2TCPP)_N$ on the APTMS-modified Si wafer substrate.

No. of layer	Ratio of COO^- sym./asym. IP	Ratio of COO^- sym./asym. OP
5	1.9	1.3
10	2.1	1.2
15	2.1	1.2

The IR signal intensity is not only related to the number of functional group, but also the orientation on the surface.[64] The ratio of symmetric/ asymmetric COO^- in all thin films exposed the consistent ratio (Table 3.5), which represented the identical growth character during stepwise film growth.

3.3.2.5 Elemental Composition Analysis by XPS

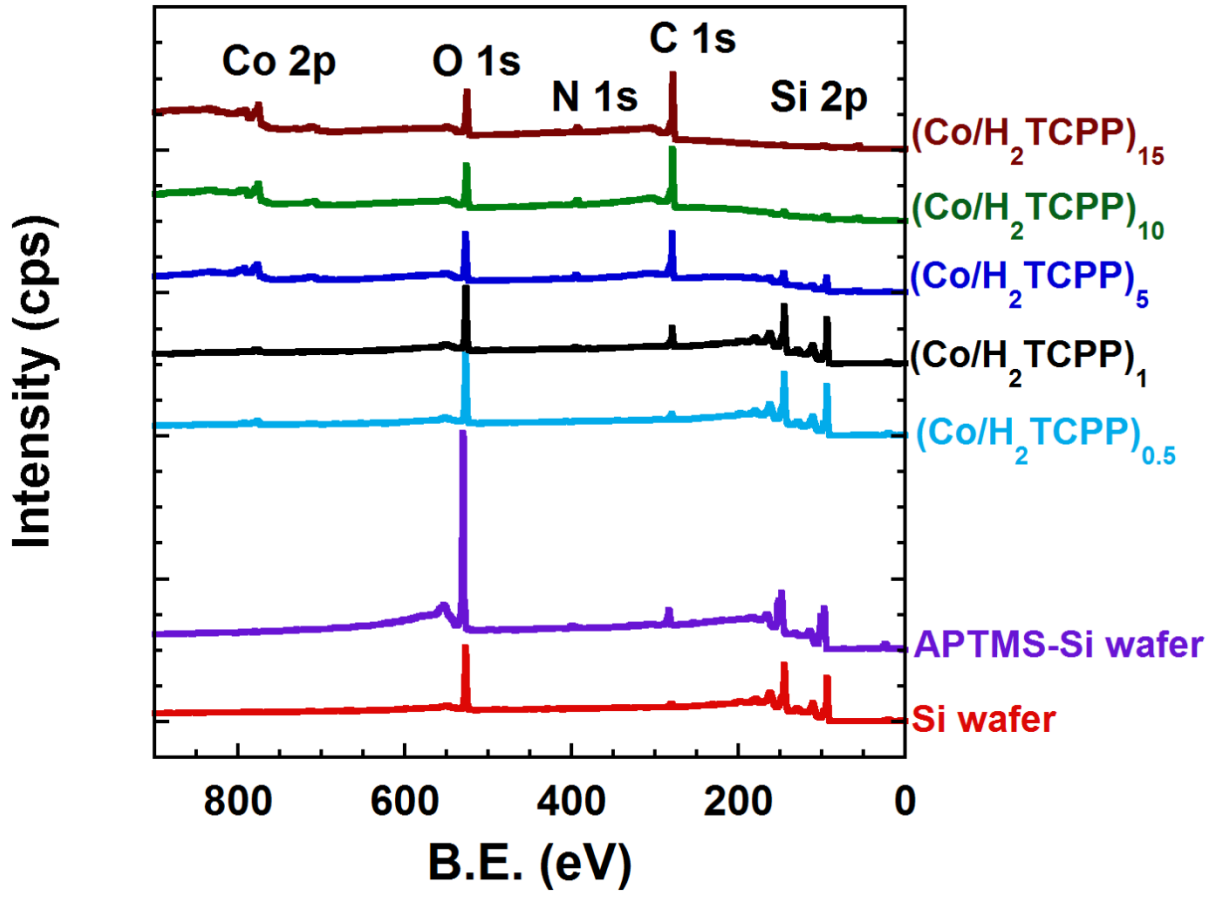

Figure 3.18 XPS survey spectra of $(Co/H_2TCPP)_{0.5}$, $(Co/H_2TCPP)_1$, $(Co/H_2TCPP)_5$, $(Co/H_2TCPP)_{10}$ and $(Co/H_2TCPP)_{15}$ on the APTMS-modified Si wafer substrate.

Figure 3.18 showed that the XPS survey scans of multilayer film on APTMS-modified Si wafer have been primarily examined. The XPS analysis was considered with respect to the multilayer film formation. The trends of Si2p and O1s peak intensities decreased from substrate signal, while the trend of N1s, C1s, and Co2p after multilayer deposition increased. These results suggested the growth of coordination networks on the substrate.[67]

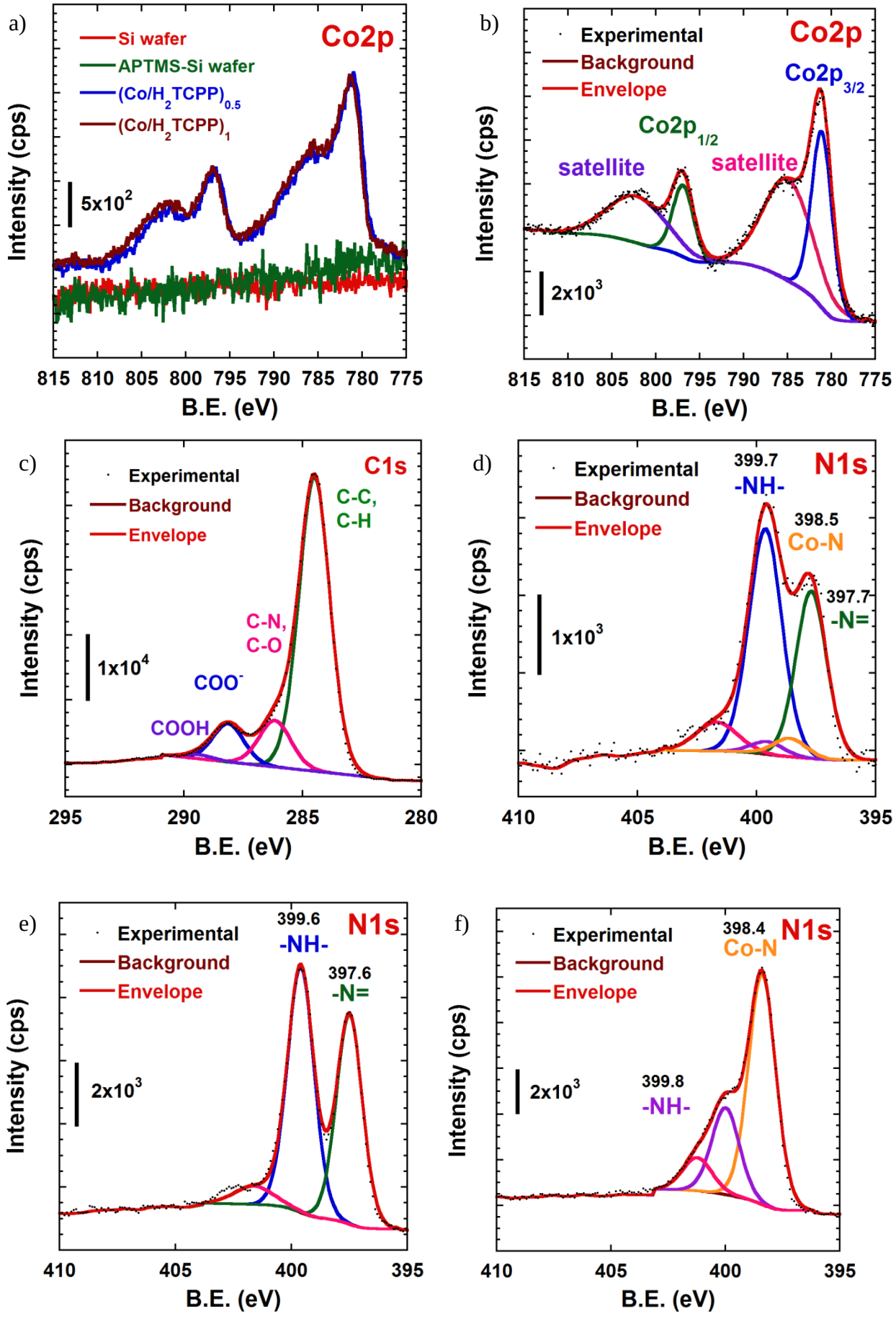
a)
Co2p
Si wafer
APTMS-Si wafer
(Co/H2TCPP)0.5
(Co/H2TCPP)1
5x10^2
Intensity (cps)
815 810 805 800 795 790 785 780 775
B.E. (eV)
b)
Experimental
Background
Envelope
Co2p
Co2p3/2
Co2p1/2
satellite
satellite
2x10^3
Intensity (cps)
815 810 805 800 795 790 785 780 775
B.E. (eV)
c)
Experimental
Background
Envelope
C1s
C-C,
C-H
C-N,
C-O
COO-
COOH
1x10^4
Intensity (cps)
295 290 285 280
B.E. (eV)
d)
Experimental
Background
Envelope
399.7
-NH-
N1s
398.5
Co-N
397.7
-N=
1x10^3
Intensity (cps)
410 405 400 395
B.E. (eV)
e)
Experimental
Background
Envelope
399.6
-NH-
N1s
397.6
-N=
2x10^3
Intensity (cps)
410 405 400 395
B.E. (eV)
f)
Experimental
Background
Envelope
398.4
Co-N
N1s
399.8
-NH-
2x10^3
Intensity (cps)
410 405 400 395
B.E. (eV)

Figure 3.19 (a) Comparison of Co2p spectra in Si wafer, APTMS-modified Si wafer, $(Co/H_2TCPP)_{0.5}$ and $(Co/H_2TCPP)_1$, the deconvolution of (b) Co2p spectrum of $(Co/H_2TCPP)_{10}$, (c) C1s spectrum of $(Co/H_2TCPP)_{10}$, (d) N1s spectrum of $(Co/H_2TCPP)_{10}$ on the APTMS-modified Si wafer substrate, (e) N1s spectrum of H_2TCPP, and (f) Co metalated TCPP.

To observe the availability of cobalt ion on the amine-terminated substrate, the immersion only in cobalt acetate solution (0.5 cycle thin film; $(Co/H_2TCPP)_{0.5}$) was declared (Figure 3.19 a). This result showed the Co2p peak, which indicated the good affinity between amine ($-NH_2$) from APTMS-modified surface and cobalt ion.[35, 36] Furthermore, the similar content of cobalt in $(Co/H_2TCPP)_{0.5}$ and $(Co/H_2TCPP)_1$ indicated that the cobalt species existed in the film after porphyrin immersion.

Figure 3.19 b showed the Co2p spectrum with deconvolution after the 10 layers film formation, the peaks of $Co2p_{3/2}$ and $Co2p_{1/2}$ were located at 781.1 and 796.9 eV, respectively [68, 69] with the presence of the two strong satellite peaks of cobalt at 784.9 and 802.2 eV. This result represented that the oxidation number of cobalt ion was +2.[29, 70, 71] No difference in Co2p spectra were observed, which inferred that cobalt oxidation state was not changed during fabrication process.

For C1s spectrum, the COO^- species presented at 288.1 eV, while the COOH at 289.4 eV was less observed (Figure 3.19 c).[73, 81] This result showed the good agreement with the information from IR spectra.

The availability of porphyrin in the coordination networks was examined by N1s spectrum (Figure 3.19 d). Five peak components were observed in N1s deconvolution. The binding energy at 399.7 eV for pyrrolic (-NH-) and 397.7 eV for iminic (=N-) which can be recognized as the protonated and non-protonated form, respectively.[31] This was well-agreed

with N1s spectrum of H_2TCPP precursor (Figure 3.19 e). Furthermore, two additional peaks were found at 398.5 eV and 399.6 eV. These two peaks were consistent with N1s spectrum of Co metalated TCPP (Figure 3.19 f). The peak at 398.5 eV was assigned to the Co metalated porphyrin (Co-N). These results represented that the partial metalation of Co^{2+} at the porphyrin core (Co-N) occurred in this thin film system. This may be due to the diffusion of Co^{2+} from solution to the porphyrin core during thin film synthesis even at room temperature condition.[74] The small peak at high binding energy around 401.5 eV was contributed to the nitrogen shake-up.[75] We mentioned in section 3.3.2.1 UV-Vis analysis that if the system contains small portion of metalated species (Co metalated TCPP), it cannot be distinguished in UV-Vis spectra. This points out that XPS is an important technique to clarify the metalation stage of porphyrin molecule. The ideal ratio of -NH- and –N= from the molecular stoichiometry should be 1:1. However, the asymmetric ratio of -NH- and –N= was found in both of H_2TCPP (1.2:1) and multilayer thin film $(Co/H_2TCPP)_{10}$ (1.3:1). This phenomenon commonly occurs in the porphyrin system that contains electron withdrawing moieties of porphyrin[31, 76] and also in the multilayer porphyrin system.[74]

From XPS results, it was confirmed that the coordination networks between cobalt ion and H_2TCPP on the surface have been occurred. The binding ratio between Co^{2+} and porphyrin in thin film can be considered from XPS spectra (Figure 3.18). The actual composition using peak areas approximately revealed ratio as $2Co^{2+}$:1Porphyrin, which was in close agreement with the expected value ($2Co^{2+}$:1Porphyrin).

3.3.2.6 Investigation of Structural Alignment in Coordination Networks by GI-SAXS Measurement

The GI-SAXS profiles and d-value of thin film were taken[77] as displayed in Figure 3.20 and Table 3.6, respectively. In the IP direction, the first diffraction peak with a d-value of around 1.9 nm was apparently observed in all thin films. The broad and weak peaks represent the low degree of molecular ordering. While the other weak diffraction peaks in IP and OP were unclearly shown at d-value around 1.2 nm and 1.0 nm, respectively. However, the molecular ordering in thin films improved with increasing deposited layers. The growth manners in these multilayer films showed the reproducibility with anisotropic properties.

a)

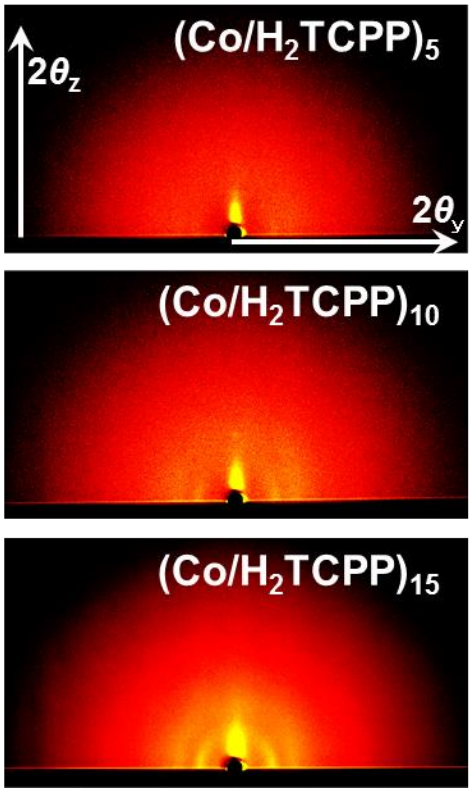

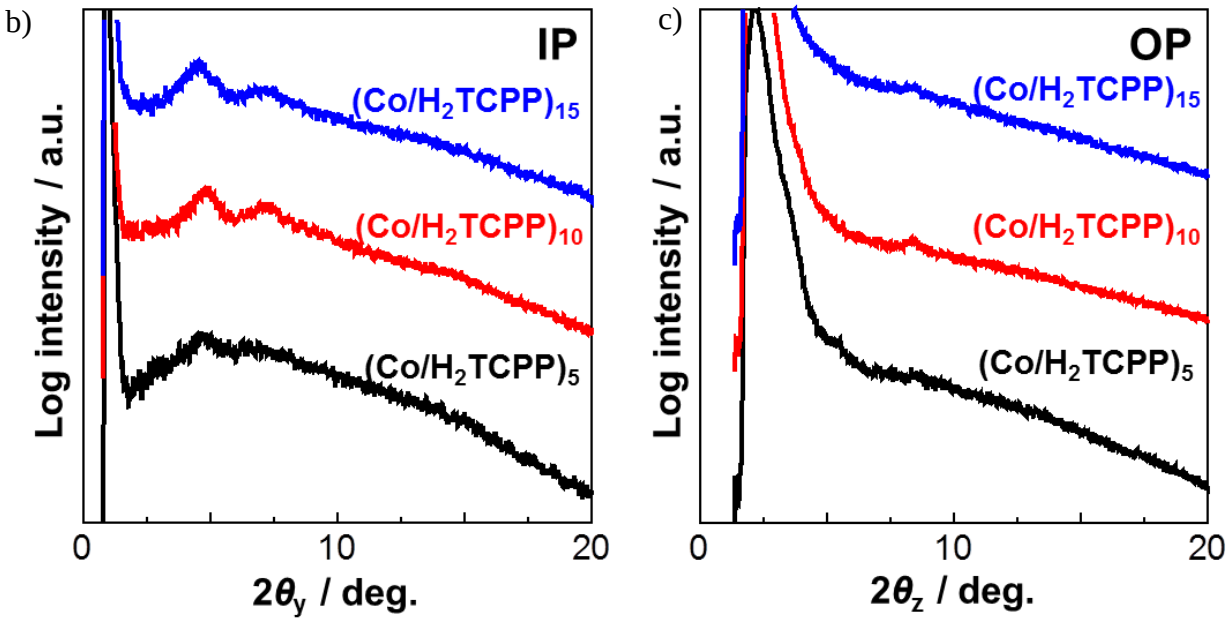

Figure 3.20 (a) 2D GI-SAXS profile of multilayer film $(Co/H_2TCPP)_5$, $(Co/H_2TCPP)_{10}$ and $(Co/H_2TCPP)_{15}$ on the APTMS-modified Si wafer substrates. (b) and (c) 1D GI-SAXS profiles in in-plane (IP) and out-of-plane (OP), respectively.

Table 3.6 The d-value in IP and OP direction from GI-SAXS

Number of layer	IP_2θ$_1$	d_{IP}-value$_1$ (nm)	IP_2θ$_2$	d_{IP}-value$_2$ (nm)	OP_2θ	d_{OP}-spacing (nm)
5	4.66	1.89	N.A.	N.A.	N.A.	N.A.
10	4.92	1.79	7.28	1.21	8.34	1.06
15	4.56	1.94	7.20	1.23	N.A.	N.A.

N.A. = Not applicable

d_{IP} -value$_1$ = d-value of primary diffraction peak in IP direction

d_{IP} -value$_2$ = d-value of secondary diffraction peak in IP direction

The d-value was calculated using Bragg's law equation (equation 3.3)

$$2d \sin\theta = n\lambda \qquad \text{equation 3.3}$$

d = lattice spacing (nm)

θ = diffraction angle

n = integer

λ = wavelength of incident x-ray (0.1542 nm.)

The typical growth types of porphyrin on substrate have been discussed as parallel and perpendicular features with single-anchor or double-anchor configurations[78] (Figure 3.21). The binding geometry of porphyrin on the surface may depend on many factors such as the binding moieties between porphyrin unit and the functionalized surface, and the aggregation behavior of porphyrins.

The possible structure of thin film on the surface was considered using XRR, AFM, and GI-SAXS results. Firstly, the structure of porphyrin with four para-carboxyphenyl groups was considered as shown in Figure 3.21. The high possibility of binding feature at the surface was one or two carboxyl groups[79, 80], rather than the four binding points (parallel or face-on; Figure 3.21 a). This was expected due to the difficulties of binding geometry between cobalt ion and four para-carboxyl groups. Thus, the single and double anchoring modes were concerned (Figure 3.21 b, c, d and e). We further considered the nature of molecular packing of porphyrin. The double-anchor binding mode (Figure 3.21c and e) was considered as more fixable binding geometry on the surface. This geometry might cause more random arrangement than providing the well-organized structure. In contrast, the single-anchor

binding mode made more freely rotate on the surface, indicating the possibility for hexagonal packing (Figure 3.22). To clarify this assumption, we considered the porphyrin dimension with cobalt binding moiety. The rotation diameter was expected to be approximately 2.2-2.3 nm. Figure 3.22 c represented that this proposed model was well supported by the IP diffraction peak of GI-SAXS with a d-value of 1.9 nm. To consider this model with the thickness per layer, the perpendicular (or edge-on) arrangement of single-anchor configuration (2.3 nm) (Figure 3.21 b)) was then discarded because of the higher repeating length of porphyrin unit than the experimental thickness per layer (1 nm) from XRR analysis (Table 3.7). Therefore, the tilting growth with respect to the surface may dominate the structure (Figure 3.21 d)). The tilting angle was calculated based on thickness from XRR approximately 60° with respect to the surface normal (Figure 3.23 and Table 3.8). This result agreed well with some reports of tilted porphyrin arrays thin films.[56, 81-84]

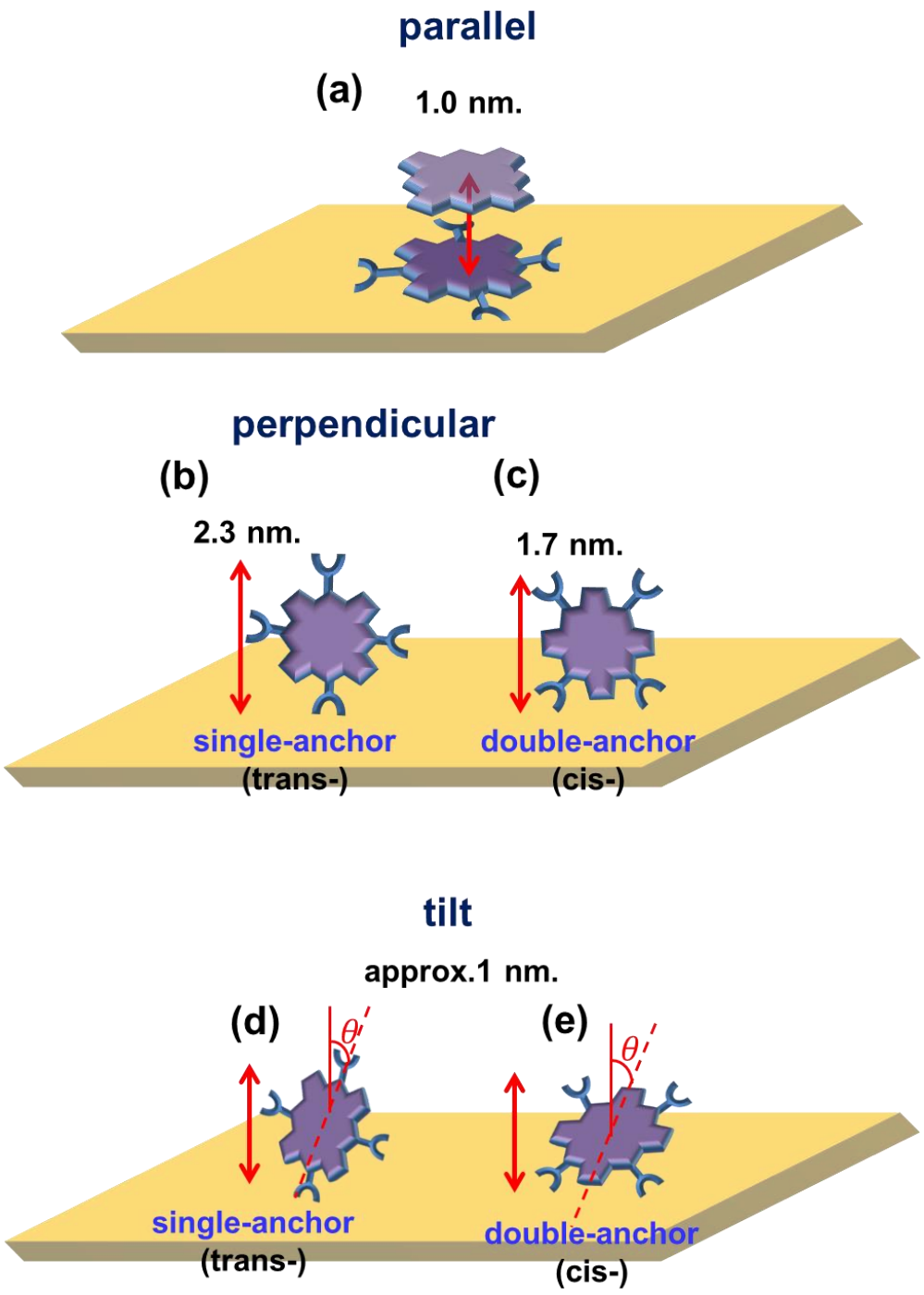

Figure 3.21 The different molecular models aligned on surface with repeating length (nm) of porphyrin unit with cobalt coordination as denoted as (a) parallel, (b) perpendicular with single-anchor (trans-), (c) perpendicular with double-anchor (cis-), (d) tilt with single-anchor (trans-) and (e) tilt with double-anchor (cis-). The cobalt atom has been omitted from the scheme for the clarity.

Table 3.7 Repeating length of porphyrin unit with cobalt coordination in different types of arrangement on surface.

Possible structural arrangement	**Average repeating length (nm)**
Parallel (porphyrin backbone to adjacent porphyrin backbone)	1.0
Perpendicular; single-anchor (trans-)	2.3
Perpendicular; cis-anchor (cis-)	1.7
Tilting	1.0
Experimental data from XRR and AFM	1.0

a)

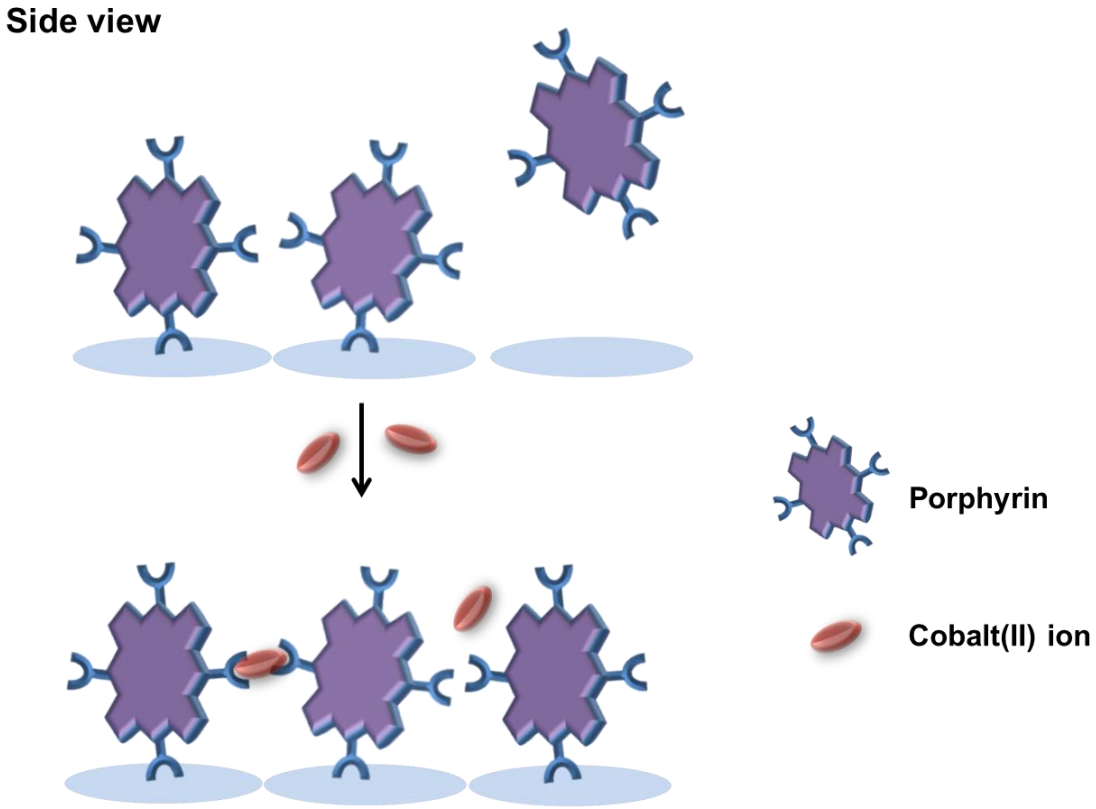

b)

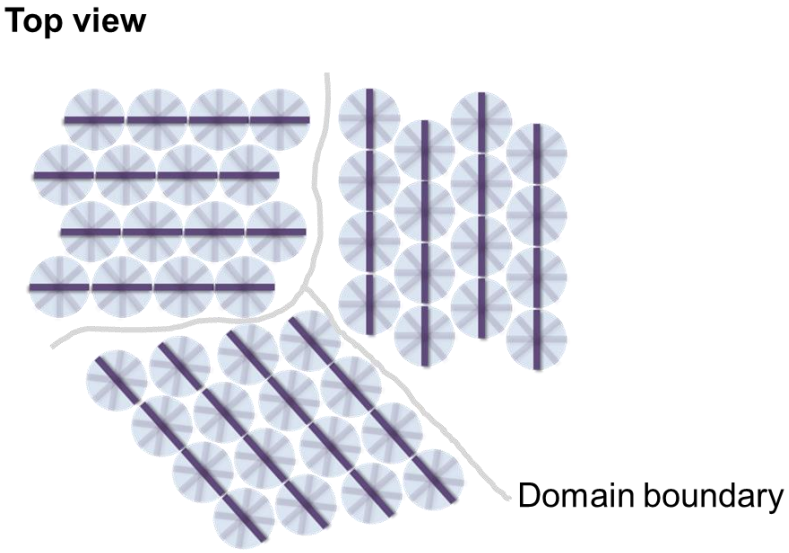

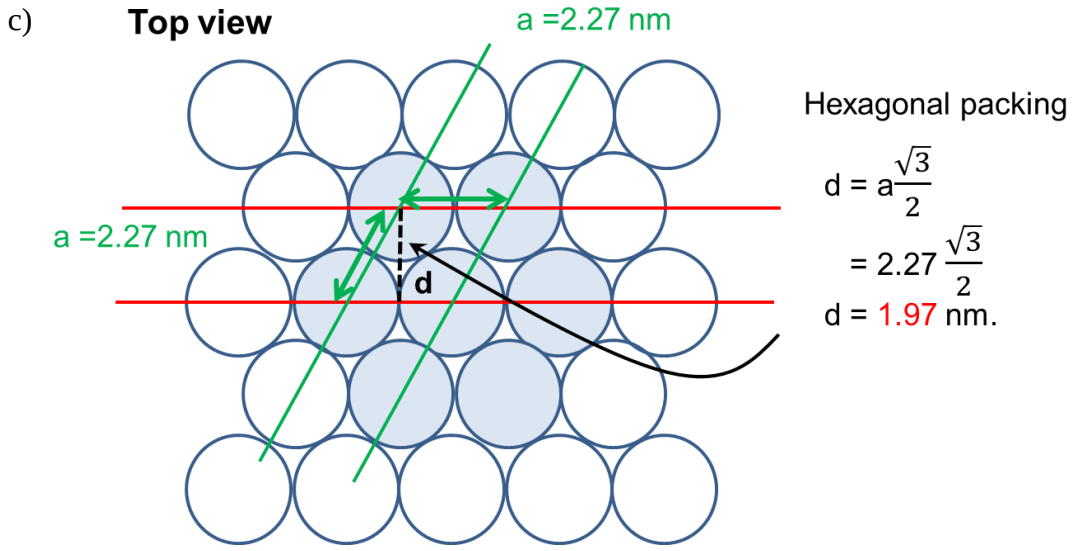

Figure 3.22 Schematic projection for hexagonal packing on the surface (a) side view, (b) and (c) top view. The cobalt atom has been omitted from the scheme for the clarity.

a)

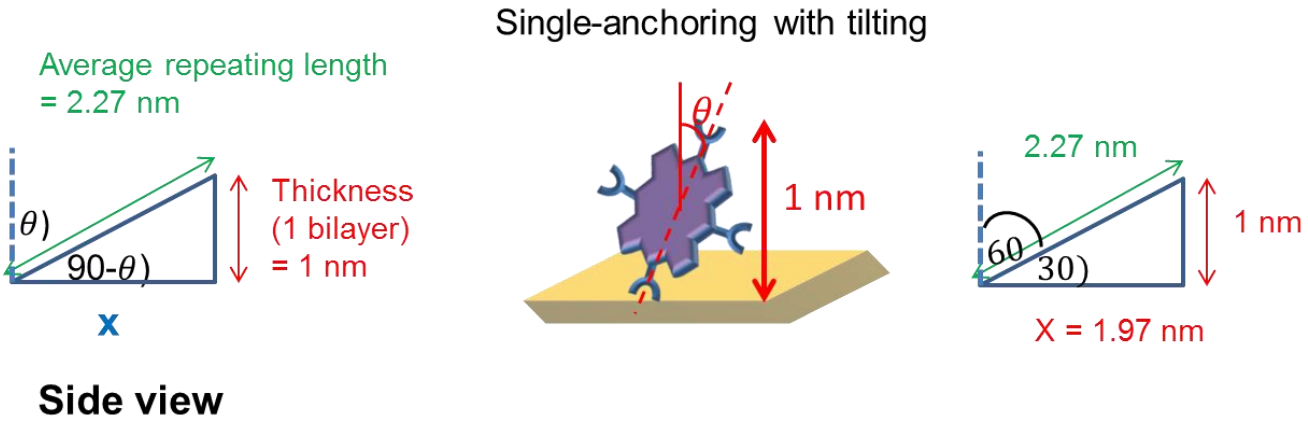

b)

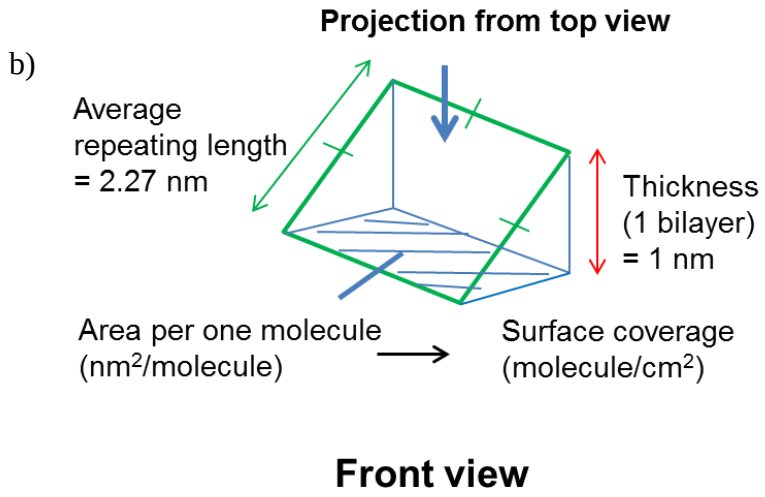

Figure 3.23 Schematic representation for growth angle and surface coverage calculation estimated from XRR results (a) side view and (b) front view

θ (deg.) = Growth angle of coordination networks with respect to normal surface

Table 3.8 The growth angle and surface coverage calculated from XRR results.

Number of layer	**Density; ρ (g/cm^3)**	**Thickness per bilayer; t (nm)**	**Growth angle with respect to surface normal ; θ (deg)**	**Surface coverage ; $\Gamma_{Monolayer}$ (molecule/cm^2)**[85]
5	1.53	5.03/5 = 1.01	64	2.16×10^{13}
10	1.52	9.30/10 = 0.93	66	2.13×10^{13}
15	1.53	15.3/15 = 1.02	63	2.17×10^{13}

The surface coverage (molecule/cm^2) was calculated from the growth model based on XRR result in Si wafer (Figure 3.23 and Table3.8) and absorbance from UV-Vis result in quartz (Table 3.2). Both results showed well-consistent surface coverage approximately with 2×10^{13} molecule/cm^2.

3.3.3 Comparison of Structure Between Bulk and Thin Film

As we compared the experimental data in chapter 2 and chapter 3, we found three different points between bulk and thin film synthesis as following :

3.3.3.1) The remaining of reactive moieties in coordination networks

3.3.3.2) The metalation stage of porphyrin core

3.3.3.3) The structure of coordination networks

3.3.3.1 The Remaining of Reactive Moieties in Coordination Networks

As we mentioned about the IR spectra of bulk sample in the chapter 2, the unreacted COOH groups referred to the incomplete reaction between cobalt ion and carboxylate from porphyrin moieties. Thess COOH reactive sites can be more consumed for network formation by longer reaction time. In contrast, the less amounts of free COOH units were found in the thin film case (Figure 3.24). This can be referred to the more complete reaction within the short period in thin film system. These results apparently showed the advantage of the thin film growth on the surface by SIA approach beyond the defect (unreacted part) in bulk system even in the same reaction condition.

Though the unreacted linker functionalities still remained partly in the traditional bulk MOFs, it can be considered for furnishing the chemically heterogeneous properties of the framework. This can also provide more variety of material, which widens the area of applications.[86]

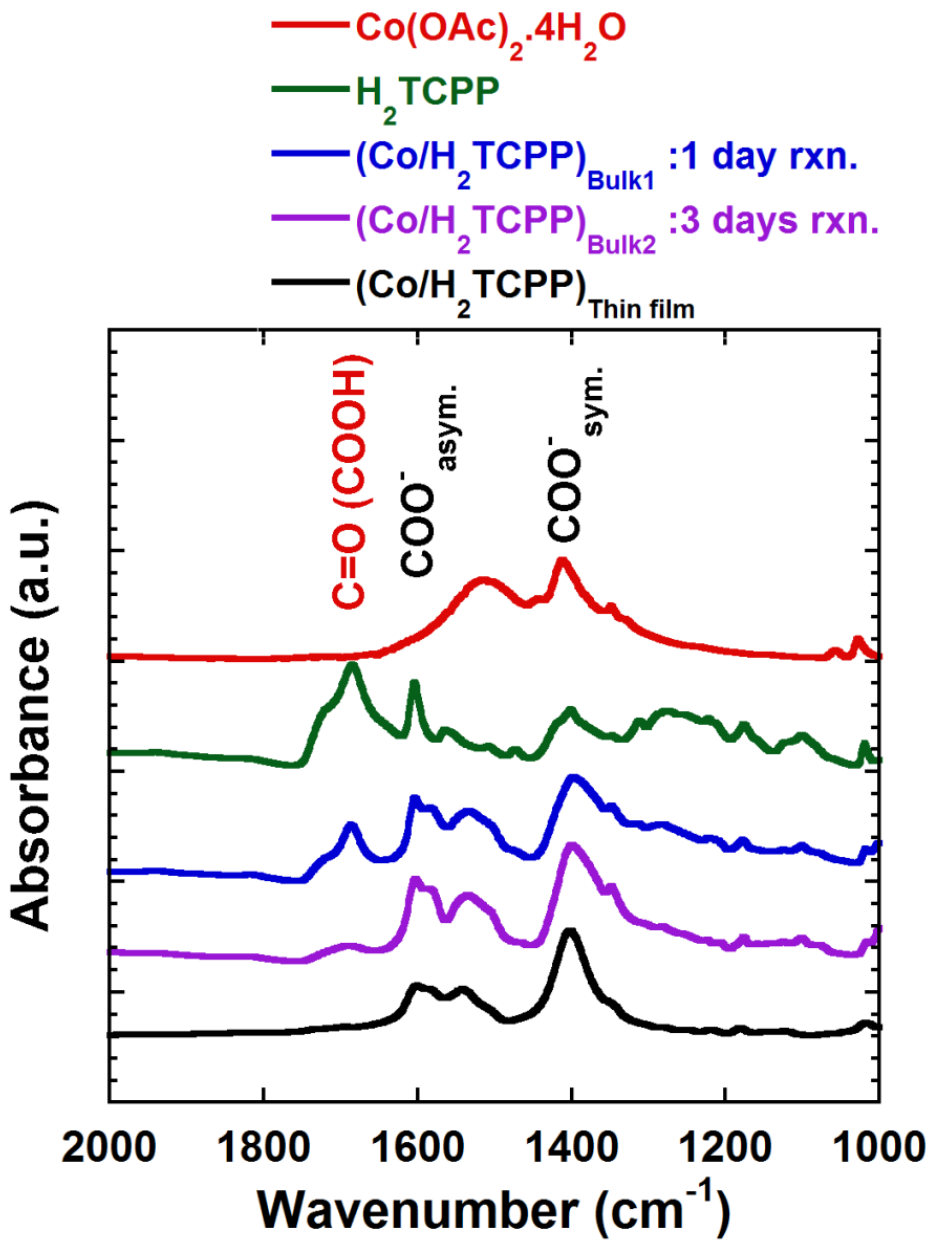

Figure 3.24 ATR-IR spectra of $Co(OAc)_2.4H_2O$, H_2TCPP, bulk samples(($Co/H_2TCPP)_{Bulk-1}$)) , (($Co/H_2TCPP)_{Bulk-2}$)), comparing with p-MAIR spectra of thin film on APTMS-modified Si wafer substrate (($Co/H_2TCPP)_{Thin\ film}$).

Table 3.9 The peak assignment of characteristic bands in IR spectra.

	C=O (COOH)	**C=C aromatic ring**	**C-O (COOH)**	**COO^- asym**	**COO^- sym**
H_2TCPP	1685 [63, 64]	1605	1401	N.A.	N.A.
$Co(OAc)_2 .4H_2O$	N.A.	N.A.	N.A.	1513	1412
$(Co/H_2TCPP)_{Bulk}$	1688 (unreacted COOH)[87, 88]	1582 [60]	N.A.	1530 [80], 1603 [60]	1389 [60, 80]
$(Co/H_2TCPP)_{Thin\ film}$	1688 (unreacted COOH)	1588	N.A.	1540, 1600	1400

N.A. = Not applicable

3.3.3.2 Metalation Stage of Porphyrin Core

The metalation stage of porphyrin center in the coordination networks between bulk and thin film was different. The N1s spectra were mainly focused to notify the metalation stage of porphyrin.[89, 90] As mentioned in last chapter, the synthesized bulk showed the presence of metalated porphyrin core from the N1s of XPS result (Figure 3.25 a and b). In contrast, the partial metalated state at the center of porphyrin unit was observed in thin film case, which was confirmed by XPS analysis (Figure 3.25 c and d). From these results, we supposed that the metalated core in our bulk may occur due to the longer time synthesis, while the short time operation in thin film synthesis provides the partial metalated core.

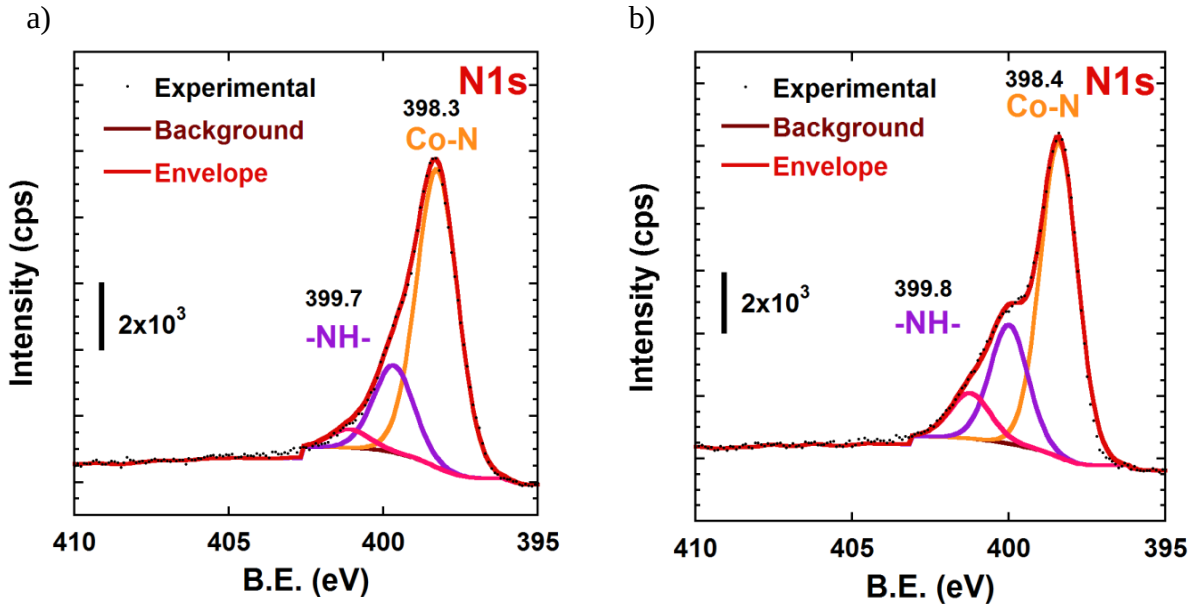

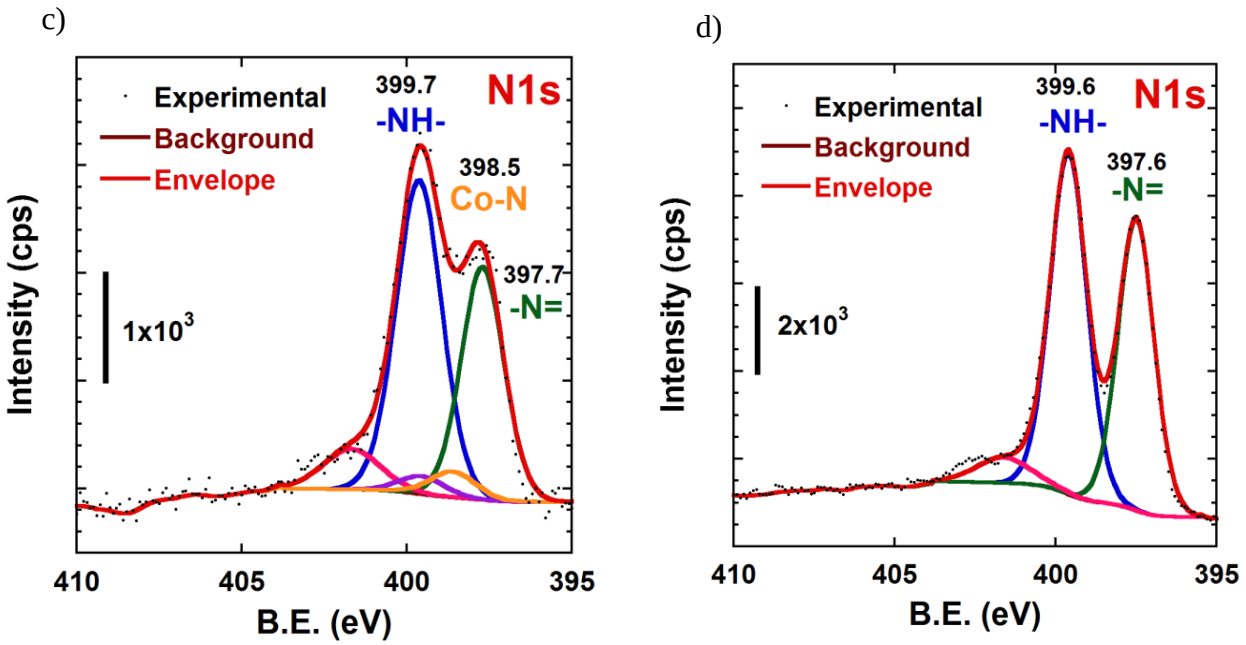

Figure 3.25 Comparison of N 1s spectra between (a) $(Co/H_2TCPP)_{Bulk}$, (b) Co metalated TCPP, (c) $(Co/H_2TCPP)_{Film}$, and (d) TCPP

3.3.3.3 Structure of Coordination Networks

The thin film was compared with bulk sample in the viewpoint of the structure. We found that the coordination network structure in thin film was different from bulk. This was concerned based on GI-SAXS and PXRD analysis.

The peak positions of the thin films were completely different from that of the bulk (Table 3.10). This result indicated the distinction in structural networks between thin film and bulk. This was probably due to the dissimilarity in growth mechanisms or molecular arrangements during network formation between film on the surface by SIA and bulk in solution. For the sequential growth process of SIA, the organic molecules and metal ions separately reach to the surface in the different deposition steps. During the dipping process, porphyrin molecules diffuse to the surface to react with the cobalt (II) species that are available on the surface. It might be possible that this deposited porphyrin on the surface can make the reorganization or rearrangement in this porphyrin deposition step. Another possibility is that this porphyrin molecular layer may reorganize at the time of next cobalt (II) immersion step in order to make the coordination binding with the cobalt (II) ion. These phenomena are distinct from the bulk situation, which the coordination manner between organic molecule and metal ion can occur concurrently.

Table 3.10 The comparison of d-value (nm) between thin film and bulk sample

Sample Type	Peak1	Peak2	Peak3
Thin Film $(Co/H_2TCPP)_{10}$	1.9	1.2	1.0
Bulk $(Co/H_2TCPP)_{Bulk}$	1.67	1.13	1.00

In very recent, Kitagawa *et al.*[91] reported the lattice shrinkage phenomena in MOF thin film compared with the bulk. The guest free thin film showed relatively smaller lattice parameters than that bulk. However, the film lattice can expand after guest vapor absorption, compared with nearly unchanged lattice in bulk one.[91] They also mentioned about the relation between SAMs and MOF lattice that the lattice mismatch can contribute to the lattice shrinkage.

The idea to explain for lattice distortion or shrinkage was derived from the relationship between bulk and nanoparticle, which was reported by Gilbert and co-workers.[92] Comparing the structural bulk and nanoparticle material, the deviation of structures can occur. The structural investigation by x-ray scattering technique indicated the broad and less peak intensity of nanoparticle rather than the bulk one. This can be explained by the strain in nanoparticle leading to the distortion in structure. Although the local structure is preserved in the strain-driven distortion manner, the atom is slightly located far from the expected lattice position.

Base on the above idea, we supposed that one possibility of dissimilarity between thin film and bulk may concern as the distortion or shrinkage phenomena such as strain of structure on the surface. However, we obtained the contrast phenomena comparing with

result from Kitagawa group. Our thin film structure expanded to be larger than the bulk structure. One of the plausible ideas to explain this distinction result is the size of organic ligand. We used porphyrin as the organic ligand, which is the macromolecule that can present the distortion character such as stretching or bending to make the flexibility in this molecule.[93] Thus, we supposed that the size and the flexibility of organic ligand are also important factors for surface phenomena. The flexibility of macrocycle ligand may consider as an advantage for this thin film preparation by SIA technique, which may increase the opportunity for finding the unique and variable structures.

One idea to explain the reorganization of molecular array on the surface is derived from the SAMs on the surface, reported by Ulman.[1] The packing and ordering of molecules in SAMs are determined by the intramolecular and intermolecular interactions. Thus, the reorganization of the SAMs array can minimize the energy for the optimum arrangement. Figure 3.26 represented the reorganization (tilting) of molecular array to reduce the free volume of the system, causing the tilting arrangement for the final structure of SAMs.

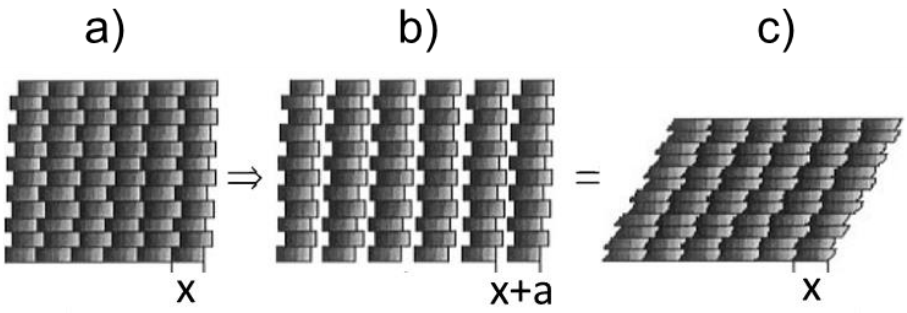

Figure 3.26 A schematic representations (a) The close packing of block array (b) The perturbation from close packing by introducing a block with large spacing than the block size. (c) The tilting of the block array to eliminate the free volume. The shape of the bricks changed, while the volume is no change.[1]

Another idea to explain the different structures in film and bulk is the reorientation of molecule during the deposition process on the surface.[94] This concept can be considered as the coverage of molecule on the surface. In case of low coverage, the molecule can deposit nearly lying down to the surface. At the high coverage, the molecules deposit and then can reorient to make some tilting geometry, thus the more dense packing character can occur.

From the above phenomena, it might be possible that the reorientation of porphyrin may occur in our thin film synthesis to make the tilting structural film. Furthermore, we supposed that the reorientation phenomena may not be found in the bulk case due to absence of substrate. This result strongly suggests how importance of surface for the coordination chemistry on the surface. Based on our results, the variety of coordination networks on the surface can be feasible via SIA strategy.

We also compared our film and bulk structures with the related bulk and thin film reports, which were synthesized from the same H_2TCPP unit and cobalt ion. In the bulk case, our bulk structure was different from the simulated XRD pattern of PIZA-1 built from the same H_2TCPP unit and cobalt ion (Figure 3.27) by solvothermal process.[45] In PIZA-1 system, pyridine was used in the synthesis. In contrast, our synthetic system has no pyridine in synthesis procedure. Moreover, the different synthesis conditions such as temperature also affect to these distinct structures. In the thin film case, the peak positions of our GI-SAXS data were also distinct from PXRD of the recent report in CoPIZA/FTO MOF thin film[18], which were synthesized from the similar H_2TCPP and cobalt ion by solvothermal on FTO surface. One of the reasons may contribute to the dissimilarity in preferential growth direction regarding to the different functionalized substrates and also the synthesis condition. In case of CoPIZA/FTO, the network directly was deposited on the surface without the functionalized-surface, while we used APTMS as the initial functionalized surface for film growth.

a)

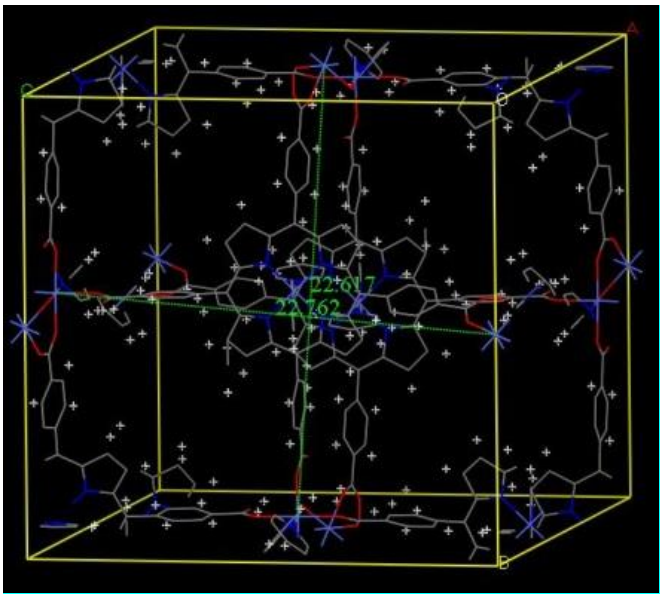

b)

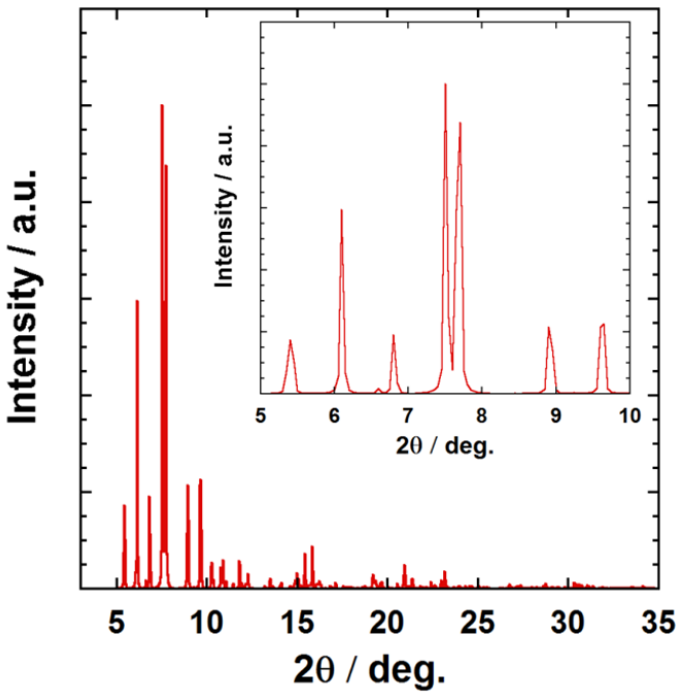

Figure 3.27 (a) The PIZA-1 structure, obtained from crystal data[45] with Material Studio v6.0.0 (Accelrys software), (b) The simulated XRD of PIZA-1. (λ= 0.1541 nm.). The inset represented the zoom-in of 2θ in range 5-10 degree.

The detail in coordination mechanism on the surface, especially in nanoscale level is likely complicated comparing to the bulk material. This is needed to make more studied and further investigation to understand the important factors for network formation on the surface and improve the technique to prepare the coordination networks on the surface with high efficiency. From our results, SIA is considered as an effective method to control the structural arrangement on the surface.

3.3.4 Opportunity to Extend This Research for Further Applications

As we mentioned about the retaining of non-metalated porphyrin center, this provides the opportunity to extend the material application by the post-metalation. This post-synthetic modification (PSM) process can provide the accessibility of metal ion to the center of porphyrin ring after the thin film preparation. The variety of metal ion species is highly possible for porphyrin unit such as iron, cobalt, copper, zinc, nickel, etc. This can promote the tremendous applications due to the variation of metal properties. Recently, the post-metalation method was mentioned in some porphyrin-based MOFs materials in both bulk and thin film.[95, 96]

In some bulk porphyrin-based MOFs, the center of porphyrin unit in the frameworks can be *in situ* metalated by the similar metal ions as the metal nodes during the framework formation. This phenomenon can provide the increasing of catalytic active sites in the frameworks which can promote the high efficiency for catalytic properties.

Gao *et.al.* reported a metalloporphyrin framework, MMPF-9 (Figure 3.28), which has high copper (II) active sites due to the metalation of copper(II) to the center of porphyrin ligand during synthesis using free base porphyrin derivative and copper(II) ion under solvothermal method. The high metal active sites enhanced the catalytic activity for CO_2

fixation under room temperature condition with higher performance than the benchmark MOF catalyst, HKUST-1. This points out that the metalated frameworks can improve the catalytic application.[97]

a)

b)

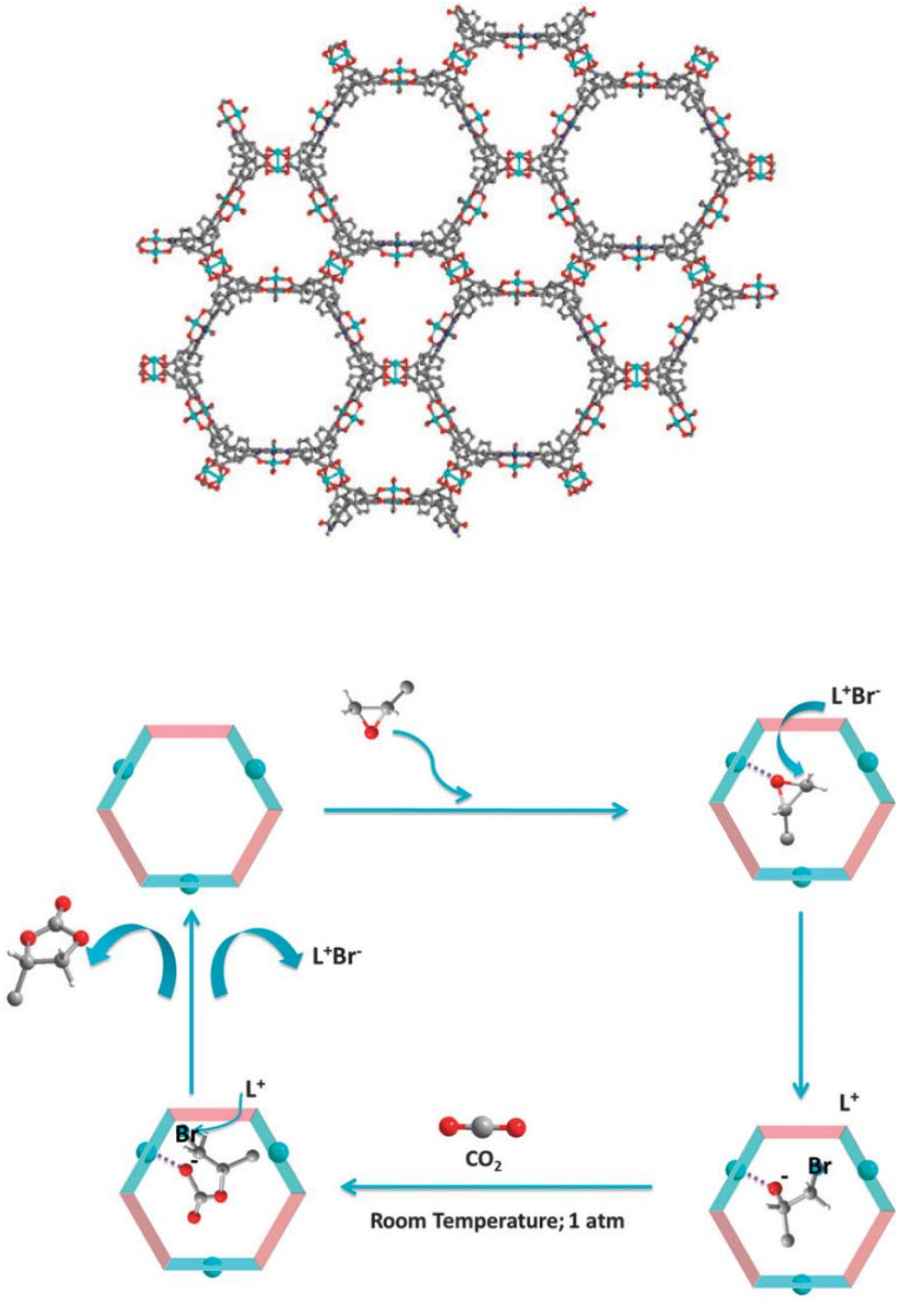

Figure 3.28 (a) The MMPF-9 channel (C, gray; O, red; and Cu, blue; and H is omitted for the clarity) (b) The proposed scheme for catalytic process of MMPF-9. The blue spherical shape represented the copper(II) active site from both center of porphyrin unit and copper node.[97]

So *et al.* demonstrated the post-metalation process of magnesium(II) to the porphyrin-based MOF thin film, L2-MOF, which was fabricated by LbL method[26] (Figure 3.29). They pointed out the advantage of LbL approach with post-metalation that the mild synthetic condition of this method can preserve the weakly bound of Mg(II) in the porphyrin center. In contrast, the Mg(II) in pre-metalated porphyrin cannot retain in the harsh synthetic condition such as solvothermal process. This research provides the great chance to prepare the sensitive material that cannot be obtained in the conventional process.

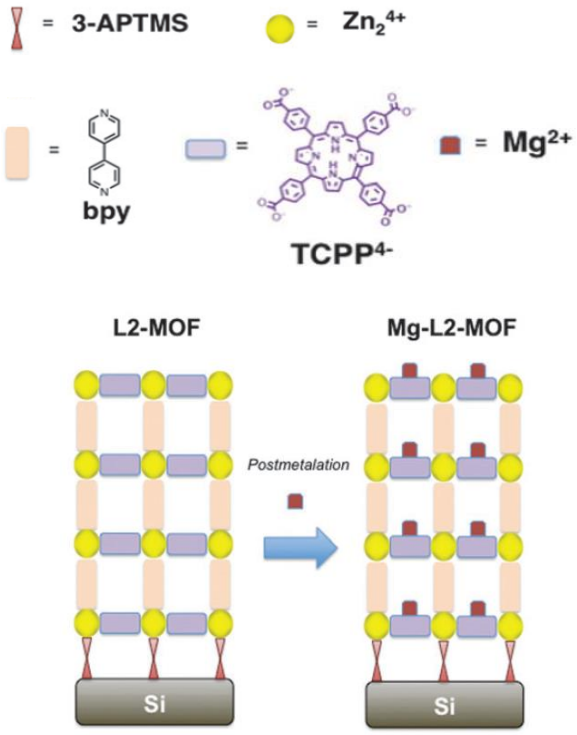

Figure 3.29 The porphyrin-based MOF thin film, L2-MOF with post-metalation process by Mg(II) ion. [26]

Metal-organic coordination network thin film can facilitate the redox reaction due to the better contact between electrolyte and metal ion moieties in the film.[98] Thus, the heterogeneous electrocatalyst can be achieved by thin film synthesis on surface. The variety of metals can be applied to the porphyrin units, which provides the variation of catalytic properties toward the reactions.

Hod *et al.* reported the Fe-porphyrin-based MOFs film as a heterogeneous catalyst for CO_2 reduction (Figure 3.30). Due to the structural ordering in MOFs leading to the less aggregation of catalytic species, the electrolyte and CO_2 reactant can efficiently access to the catalytic sites in the framework of the film. Thus, the well-arranged structure in thin film is needed to improve the catalytic performance for using as electrodcatalyst.[99]

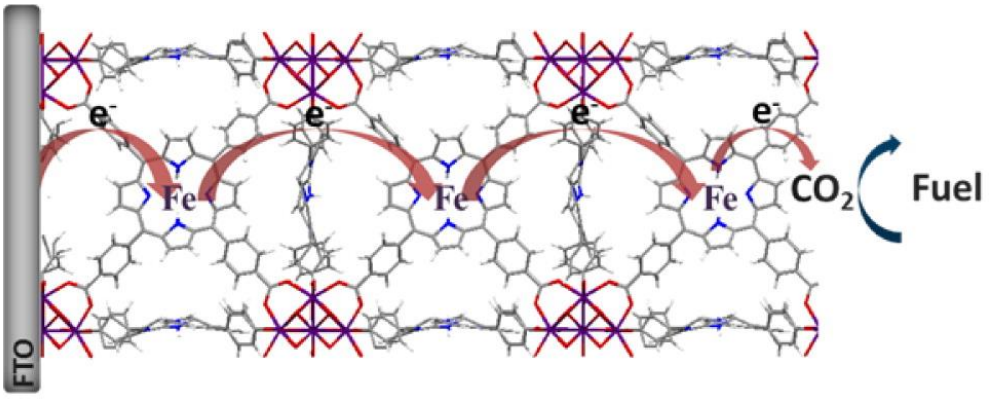

Figure 3.30 The schematic representation of electrocatalytic CO_2 reduction by Fe-porphyrin-based MOFs film.[99]

3.4 Conclusion

In this chapter, the multilayer film formation of porphyrin-based coordination networks on amine-functionalized surface has been promoted using surface-induced assembly (SIA) method under room temperature synthesis. The stepwise growth with homogeneous and smooth surface was confirmed by UV-Vis, XRR, AFM and XPS analysis. GI-SAXS and XRR results indicated the periodic structure in in-plane (IP) direction with the consistent mass density (ca.1.5 g/cm^3) along the multilayer formation. We proposed that the orientation of the porphyrin plane with a hexagonal packing model via single anchoring mode was tilted approximately 60° with respect to the surface substrate. This result indicated that SIA technique has a powerful capability to control the structural arrangement on the surface. Furthermore, there are some different points between thin film and bulk synthesis such as the remaining of reactive carboxylic moieties (-COOH) in the coordination networks, the different metalation stages at porphyrin core and especially the structural dissimilarity. The distinction in structural networks between thin film and bulk was probably due to the dissimilarity in growth mechanisms or molecular arrangements during network formation between film on the surface by SIA method and bulk in solution. Some of the phenomena such as the partial distortion, shrinkage or reorientation of network on the surface and the functionalized group on substrates might be considered to explain the discriminated structures between bulk and film system. The exact reason for this difference is still needed to have further study which may provide the valuable information for the material development in future.

References

1. Ulman, A. Formation and Structure of Self-Assembled Monolayer. *Chem. Rev.* **1996**, *96*, 1533-1554.
2. Kobayashi, S.; Nishikawa, T.; Takenobu, T.; Mori, S.; Shimoda, T.; Mitani, T.; Shimotani, H.; Yoshimoto, N.; Ogawa, S.; Iwasa, Y. Control of Carrier Density by Self-Assembled monolayers in Organic Field-Effect Transistors. *Nat. Mater.* **2004**, *3*, 317-322.
3. Love, J. C.; Estroff, L. A.; Kriebel, J. K.; Nuzzo, R. G.; Whitesides, G. M. Self-Assembled Monolayers of Thiolates on Metals as a Form of Nanotechnology. *Chem. Rev.* **2005**, *105*, 1103-1170.
4. Ashkenasy, G.; Cahen, D.; Cohen, R.; Shanzer, A.; Vilan, A. Molecular Engineering of Semiconductor Surface and Devices. *ACC. Chem. Res.* **2002**, *35*, 121-128.
5. Nuzzo, R. G.; Allara, D. L. Adsorption of Bifunctional Organic Disulfides on Gold Surfaces. *J. Am. Chem. Soc.* **1983**, *105*, 4481-4483.
6. Sagiv, J. Organized Monolayers by Adsorption. 1. Formation and Structure of Oleophobic Mixed Monolayers on Solid Surfaces. *J. Am. Chem. Soc.* **1980**, *102*, 92-98.
7. Herzer, N.; Hoeppener, S.; Schubert, U. S. Fabrication of Patterned Silane Based Self-Assembled Monolayers by Photolithography and Surface Reactions on Silicon-Oxide Substrates. *Chem. Commun.* **2010**, *46*, 5634-5652.
8. Haensch, C.; Hoeppener, S.; Schubert, U. S. Chemical Modification of Self-Assembled Silane Based Monolayers by Surface Reactions. *Chem. Soc. Rev.* **2010**, *39*, 2323-2334.

9. Sugimura, H.; Nakagiri, N. Nanoscopic Surface Architecture Based on Scanning Probe Electrochemistry and Molecular Self-Assembly. *J. Am. Chem. Soc.* **1997**, *119*, 9226-9229.
10. Crego-Calama, M.; Reinhoudt, D. N. New Materials for Metal Ion Sensing by Self-Assembled Monolayers on Glass. *Adv. Mater.* **2001**, *13*, 1171-1174.
11. Jakša, G.; Štefane, B.; Kovač, J. XPS and AFM Characterization of Aminosilanes with Different Numbers of Bonding Sites on a Silicon Wafer. *Surf. Interface Anal.* **2013**, *45*, 1709–1713.
12. Acres, R. G.; Ellis, A. V.; Alvino, J.; Lenahan, C. E.; Khodakov, D. A.; Metha, G. F.; Andersson, G. G. Molecular Structure of 3-Aminoprpyltriethoxysilane Layers Formed on Silanol-Terminated Silicon Surfaces. *J. Phys. Chem. C* **2012**, *116*, 6289-6297.
13. Chiang, C.-H.; Liu, N.-I.; Koenig, J. L. Magic-angle cross-polarization carbon 13 NMR study of aminosilane coupling agents on silica surfaces. *J. Colloid Interface Sci.* **1982**, *86*, 26-34.
14. Ariga, K.; Yamauchi, Y.; Mori, T.; Hill, J. P. 25th Anniversary Article: What Can Be Done with the Langmuir-Blodgett Method? Recent Developments and its Critical Role in Materials Science. *Adv. Mater.* **2013**, *25*, 6477-6512.
15. Bétard, A.; Fischer, R. A. Metal-Organic Framework Thin Films: From Fundamentals to Applications. *Chem. Rev.* **2012**, *112*, 1055–1083.
16. Zhuang, J.-L.; Terfort, A.; Wöll, C. Formation of Oriented and Patterned Films of Metal-Organic Frameworks by Liquid Phase Epitaxy: A Review. *Coord. Chem. Rev.* **2016**, *307*, 391-424.
17. Gliemann, H.; Wöll, C. Epitaxially Grown Metal-Organic Frameworks. *Mater. Today* **2012**, *15*, 110-116.

18. Ahrenholtz, S. R.; Epley, C. C.; Morris, A. J. Solvothermal Preparation of an Electrocatalytic Metalloporphyrin MOF Thin Film and its Redox Hopping Charge-Transfer Mechanism. *J. Am. Chem. Soc.* **2014**, *136*, 2464–2472.

19. Shekhah, O. Layer-by-Layer Method for the Synthesis and Growth of Surface Mounted Metal-Organic Frameworks (SURMOFs). *Materials* **2010**, *3*, 1302-1315.

20. Munuera, C.; Shekhah, O.; Wang, H.; Wöll, C.; Ocal, C. The Controlled Growth of Oriented Metal-Organic Frameworks on Functionalized Surfaces as Followed by Scanning Force Microscopy. *Phys. Chem. Chem. Phys.* **2008**, *10*, 7251-7261.

21. So, M. C.; Jin, S.; Son, H.-J.; Wiederrecht, G. P.; Farha, O. K.; Hupp, J. T. Layer-by-Layer Fabrication of Oriented Porous Thin Films Based on Porphyrin-Containing Metal-Organic Frameworks. *J. Am. Chem. Soc.* **2013**, *135*, 15698-15701.

22. Hou, C.; Xu, Q.; Peng, J.; Ji, Z.; Hu, X. (110)-Oriented ZIF-8 Thin Films on ITO with Controllable Thickness. *Chem. Phys. Chem.* **2013**, *14*, 140-144.

23. Liu, B.; Fischer, R. A. Liquid-Phase Epitaxy of Metal-Organic Framework Thin Films. *Sci. China Chem.* **2011**, *54*, 1851-1866.

24. Krawicz, A.; Palazzo, J.; Wang, G.-C.; Dinolfo, P. H. Layer-by-Layer Assembly of Zn(II) and Ni(II) 5,10,15,20-tetra(4-ethynylphenyl)porphyrin Multilayers on Au Using Copper Catalyzed Azide-Alkyne Cycloaddition. *RSC Adv.* **2012**, *2*, 7513-7522.

25. Gao, W-Y.; Chrzanowski, M.; Ma, S. Metal-Metalloporphyrin Frameworks: a Resurging Class of Functional Materials. *Chem. Rev. Soc.* **2014**, *43*, 5841–5866.

26. So, M. C.; Beyzavi, M. H.; Sawhney, R.; Shekhah, O.; Eddaoudi, M.; Al-Juaid, A. S.; Hupp, J. T.; Farha, O. K. Post-Assembly Transformations of Porphyrin-Containing Metal-Organic Framework (MOF) Films Fabricated via Automated Layer-by-Layer Coordination. *Chem. Commun.* **2015**, *51*, 85–88.

27. Makiura, R.; Kitagawa, H. Porous Porphyrin Nanoarchitectures on Surfaces. *Eur. J. Inorg. Chem.* **2010**, 3715-3724.

28. Motoyama, S.; Makiura, R.; Sakata, O.; Kitagawa, H. Highly Crystalline Nanofilm by Layering of Porphyrin Metal-Organic Framework Sheets. *J. Am. Chem. Soc.* **2011**, *133*, 5640–5643.

29. Makiura, R.; Motoyama, S.; Umemura, Y.; Yamanaka, H.; Sakata, O.; Kitagawa, H. Surface Nano-Architecture of a Metal-Organic Framework. *Nat. Mater.* **2010**, *9*, 565–571.

30. Gough, D. V.; Lambert, T. N.; Wheeler, D. R.; Rodriguez, M. A.; Brumbach, M. T.; Allendorf, M. D.; Spoerke, E. D. Controlled Nucleation and Growth of Pillared Paddlewheel Framework Nanostacks onto Chemically Modified Surfaces. *ACS Appl. Mater. Interfaces* **2014**, *6*, 1509-1514.

31. Joyce, J. T.; Laffir, F. R.; Silien, C. Layer-by-Layer Growth and Photocurrent Generation in Metal-Organic Coordination Films. *J. Phys. Chem. C* **2013**, *117*, 12502–12509.

32. Wijesekera, T.; Dolphin, D. Synthtic Aspect of Porphyrin and Metalloporphyrin Chemistry. In *Metalloporphyrins in Catalytic Oxidations*; Sheldon, R. A.., Ed.; Marcel Dekker Inc., 1994, Chapter 7, pp 193-239.

33. Josefsen, L. B.; Boyle, R. W. Photodynamic Therapy and the Development of Metal-Based Photosensetisers. *Met.-Based Drugs*. **2008**.

34. Gottfried, J. M.; Marbach, H. Surface-Confined Coordination Chemistry with Porphyrins and Phthalocyanines: Aspects of Formation, Eletronic Structure, and Reactivity. *Z. Phys. Chem.* **2009**, *223*, 53-74.

35. Yokoi, T.; Yoshitake, H.; Yamada, T.; Kubota, Y.; Tatsumi, T. Amino-Functionalized Mesoporous Silica Synthesized by an Anionic Surfactant Templating Route. *J. Mater. Chem.* **2006**, *16*, 1125–1135.

36. Ansell, M. A.; Zeppenfeld, A. C.; Yoshimoto, K.; Cogan, E. B.; Page, C. J. Self-Assembled Cobalt-Diisocyanobenzene Multilayer Thin Films. *Chem. Mater.* **1996**, *8*, 591–594.

37. Rubio-Giménez, V; Tatay, S.; Volatron, F.; Martí-Gastaldo, C.; Cororado, E. High-Quality Metal-Organic Framework Ultrathin Films for Electronically Active Interfaces. *J. Am. Chem. Soc.* **2016**, *138*, 2576-2584.

38. Hasegawa, T. Advanced Multiple-Angle Incidence Resolution Spectrometry for Thin-Layer Analysis on a Low-Refractive-Index Substrate. *Anal. Chem.* **2007**, *79*, 4385–4389.

39. Hasegawa, T. A New Spectroscopic Tool for Surface Layer Analysis: Multiple-Angle Incidence Resolution Spectrometry. *Anal. Bioanal. Chem.* **2007**, *388*, 7–15.

40. Zhang, Z.; Hu, R.; Liu, Z. Formation of a Porphyrin Monolayer Film by Axial Ligation of Protoporphyrin IX Zinc to an Amino-Terminated Silanized Glass Surface. *Langmuir* **2000**, *16*, 1158–1162.

41. Krawicz, A.; Palazzo, J.; Wang, G.-C.; Dinolfo, P. H. Layer-by-Layer Assembly of Zn(II) and Ni(II) 5,10,15,20-tetra(4-ethynylphenyl)porphyrin Multilayers on Au Using Copper Catalyzed Azide-Alkyne Cycloaddition. *RSC Adv.* **2012**, *2*, 7513–7522.

42. Castillero, P.; Sánchez-Valencia, J. R.; Cano, M.; Pedrosa, J. M.; Roales, J.; Barranco, A.; González-Elipe, A. R. Active and Optically Transparent Tetracationic Porphyrin/ TiO2 Composite Thin Films. *ACS Appl. Mater. Interfaces* **2010**, *2*, 712–721.

43. Sakuma, T.; Sakai, H.; Hasobe, T. Preparation and Structural Control of Metal Coordination-Assisted Supramolecular Architectures of Porphyrins. Nanocubes to Microrods. *Chem. Commun.* **2012**, *48*, 4441–4443.

44. So, M. C.; Jin, S.; Son, H.-J.; Wiederrecht, G. P.; Farha, O. K.; Hupp, J. T. Layer-by-Layer Fabrication of Oriented Porous Thin Films Based on Porphyrin-Containing Metal-Organic Frameworks. *J. Am. Chem. Soc.* **2013**, *135*, 15698–15701.

45. Kosal, M. E.; Chou, J.-H.; Wilson, S. R.; Suslick, K. S. A Functional Zeolite Analogue Assembled From Metalloporphyrins. *Nat. Mater.* **2002**, *1*, 118–121.

46. Wang, X.-S.; Chrzanowski, M.; Wojtas, L.; Chen, Y.-S.; Ma, S. Formation of a Metalloporphyrin-Based Nanoreactor by Postsynthetic Metal-Ion Exchange of a Polyhedral-Cage Containing a Metal-Metalloporphyrin Framework. *Chem. Eur. J.* **2013**, *19*, 3297–3301.

47. Richardson, T. H.; Dooling, C. M.; Jones, L. T.; Brook, R. A. Development and Optimization of Porphyrin Gas Sensing LB Films. *Adv. Colloid Interface Sci.* **2005**, *116*, 81–96.

48. Palomaki, P. K. B.; Civic, M. R.; Dinolfo, P. H. Photocurrent Enhancement by Multilayered Porphyrin Sensitizers in a Photoelectrochemical Cell. *ACS Appl. Mater. Interfaces* **2013**, *5*, 7604–7612.

49. Khairutdinov, R. F. Photoluminescence and Transient Spectroscopy of Free Base Porphyrin Aggregates. *J. Phys. Chem. B* **1999**, *103*, 761–769.

50. Qian, D.-J.; Nakamura, C.; Miyake, J. Multiporphyrin Array from Interfacial Metal-Mediated Assembly and its Langmuir-Blodgett Films. *Langmuir* **2000**, *16*, 9615–9619.

51. Araki, K.; Wagner, M. J.; Wrighton, M. S. Layer-by-Layer Growth of Electrostatically Assembled Multilayer Porphyrin Films. *Langmuir* **1996**, *12*, 5393–5398.

52. Liu, B.; Qian, D.-J.; Huang, H.-X.; Wakayama, T.; Hara, S.; Huang, W.; Nakamura, C.; Miyake, J. Controllable Growth of Well-Defined Regular Multiporphyrin Array Nanocrystals at the Water-Chloroform Interface. *Langmuir* **2005**, *21*, 5079–5084.

53. Otte, F. L.; Lemke, S.; Schütt, C.; Krekiehn, N. R.; Jung, U.; Magnussen, O. M.; Herges, R. Ordered Monolayers of Free-Standing Porphyrins on Gold. *J. Am. Chem. Soc.* **2014**, *136*, 11248–11251.

54. Drain, C. M.; Varotto, A.; Radivojevic, I. Self-Organized Porphyrinic Materials. *Chem. Rev.* **2009**, *109*, 1630–1658.

55. Zhu, M.; Aryal, G. H.; Zhang, N.; Zhang, H.; Su, X.; Schmehl, R.; Liu, X.; Hu, J.; Wei, J.; Jayawickramarajah, J. Host-Guest Interactions Derived MultilayerPerylene Diimide Thin Film Constructed on a Scaffolding Porphyrin Monolayer. *Langmuir* **2015**, *31*, 578–586.

56. Palomaki, P. K. B.; Krawicz, A.; Dinolfo, P. H. Thickness, Surface Morphology, and Optical Properties of Porphyrin Multilayer Thin Films Assembled on Si(100) Using Copper(I)-Catalyzed Azide-Alkyne cycloaddition. *Langmuir* **2011**, *27*, 4613–4622.

57. Kojima, I.; Li, B. Structural Characterization of Thin Film by X-Ray Reflectivity. *The Rigaku Journal* **1999**, *16*, 31–42.

58. Krawicz, A.; Palazzo, J.; Wang, G.-C.; Dinolfo, P. H. Layer-by-Layer Assembly of Zn(II) and Ni(II) 5,10,15,20-tetra(4-ethynylphenyl)porphyrin Multilayers on Au Using Copper Catalyzed Azide-Alkyne Cycloaddition. *RSC Adv.* **2012**, *2*, 7513–7522.

59. Fateeva, A.; Clarisse, J.; Pilet, G.; Grenèche, J.-M.; Nouar, F.; Abeykoon, B. K.; Guegan, F.; Goutaudier, C.; Luneau, D.; Warren, J. E.; Rosseinsky, M. J.; Devic, T. Iron and Porphyrin Metal-Organic Frameworks: Insight into Structural Diversity, Stability, and Porosity. *Cryst. Growth Des.* **2015**, *15*, 1819–1826.

60. Fateeva, A.; Clarisse, J.; Pilet, G.; Grenèche, J.-M.; Nouar, F.; Abeykoon, B. K.; Guegan, F.; Goutaudier, C.; Luneau, D.; Warren, J. E.; Rosseinsky, M. J.; Devic, T. Iron and Porphyrin Metal-Organic Frameworks: Insight into Structural Diversity, Stability, and Porosity. *Cryst. Growth Des.* **2015**, *15*, 1819–1826.

61. Zhuang, J. L.; Lommel, K.; Ceglarek, D.; Andrusenko, I.; Kolb, U.; Maracke, S.; Sazama, U.; Fröba, M.; Terfort, A. Synthesis of a New Copper-Azobenzene Dicarboxylate Framework in the Form of Hierarchical Bulk Solids and Thin Films Without and With Patterning. *Chem. Mater.* **2011**, *23*, 5366–5347.

62. Rochford, J.; Chu, D.; Hagfeldt, A.; Galoppini, E. Tetrachelate Porphyrin Chromophores for Metal Oxide Semiconductor Sensitization: Effect of the Spacer Length and Anchoring Group Position. *J. Am. Chem. Soc.* **2007**, *129*, 4655–4665.

63. Alben, J. O. Infrared Spectroscopy of Porphyrins. In The Porphyrins, Physical Chemistry Part A; Dolphin, D., Ed.; Academic Press Inc.: New York, 1978; Vol.3, Chapter 7, pp 323–345.

64. Zhuang, J. L.; Lommel, K.; Ceglarek, D.; Andrusenko, I.; Kolb, U.; Maracke, S.; Sazama, U.; Fröba, M.; Terfort, A. Synthesis of a New Copper-Azobenzene Dicarboxylate Framework in the Form of Hierarchical Bulk Solids and Thin Films without and with Patterning. *Chem. Mater.* **2011**, *23*, 5366–5347.

65. Wen, L.; Li, M.; Schlenoff, J. B. Polyporphyrin Thin Films from the Interfacial Polymerization of Mercaptoporphyrin. *J. Am. Chem. Soc.* **1997**, *119*, 7726-7733.

66. Thomas, D. W.; Martell, A. E. Metal Chelates of Tetraphenylporphine and of Some p-Substituted Derivatives. *J. Am. Chem. Soc.* **1959**, *81*, 5111-5119.

67. Li, D.; Buscher, T.; Swanson, B. I. Synthesis, Characterization, and Properties of Covalently Bound, Self-Assembled Porphyrin Multilayer Thin Film. *Chem. Mater.* **1994**, *6*, 803-810.

68. Tang, H.; Yin, H.; Wang, J.; Yang, N.; Wang, D.; Tang, Z. Molecular Architecture of Cobalt Porphyrin Multilayer on Reduced Graphene Oxide Sheets for High-Performance Oxygen Reduction Reaction. *Angew. Chem.* **2013**, *125*, 5695–5699.

69. Jiang, L.; Cui, L.; He, X. Cobalt-Porphyrin Noncovalently Functionalized Graphene as Nonprecious-Metal Electrocatalyst for Oxygen Reduction Reaction in an Alkaline Medium. *J. Solid State Electrochem.* **2015**, *19*, 497–506.

70. González, T.; Salazar, R.; Marco, J. F.; Gutiérrez, C.; Ureta-Zañartu, M. S. Electrooxidation of 2,4,6-Trichlorophenol on Glassy Carbon Electrodes Modified with Composite $Ni(OH)_2$-$Co(OH)_2$ Films. *J. Chil. Chem. Soc.* **2013**, *58*, 2043–2047.

71. Bi, L.; Kim, H.-S.; Dionne, G. F.; Ross, C. A. Structure, Magnetic Properties and Magnetoelastic Anisotropy in Epitaxial $Sr(Ti_{1-x}Co_x)O_3$ films. *New J. Phys.* **2010**, *12*, 043044.

72. Pellegrino, G.; Condorelli, G. G.; Privitera, V.; Cafra, B.; Marco, S. D.; Alberti, A. Dye-Sensitizing of Self-Nanostructured Ti(:Zn)O_2/AZO Transparent Electrodes by Self-Assembly of 5,10,15,20-Tetrakis(4-carboxyphenyl)porphyrin. *J. Phys. Chem. C* **2011**, *115*, 7760–7767.

73. Gulino, A. Structural and Electronic Characterization of Self-Assembled Molecular Nanoarchitectures by X-Ray Photoelectron Spectroscopy. *Anal. Bioanal. Chem.* **2013**, *405*, 1479–1495.

74. Franke, M.; Marchini, F.; Steinrück, H.-P.; Lytken, O.; Williams, F. J. Surface Porphyrins Metalate with Zn Ions from Solution. *J. Phys Chem. Lett.* **2015**, *6*, 4845–4849.

75. Pellegrino, G.; Alberti, A.; Condorelli, G. G.; Giannazzo, F.; Magna, A. L.; Paoletti, A. M.; Pennesi, G.; Rossi, G.; Zanotti, G. Study of the Anchoring Process of Tethered Unsymmetrical Zn-Phthalocyanines on TiO_2 Nanostructured Thin Films. *J. Phys. Chem. C* **2013**, *117*, 11176–11185.

76. Yamashige, H.; Matsuo, S.; Kurisaki, T.; Perera, R. C. C.; Wakita, H. Local Structure of Nitrogen Atoms in Porphine Ring of meso-Phenyl Substituted Porphyrin with an Electron-Withdrawing Group Using X-Ray Photoelectron Spectroscopy and X-Ray Absorption Spectroscopy. *Anal. Sci.* **2005**, *21*, 635–639.

77. Müller-Buschbaum, P. The Active Layer Morphology of Organic Solar Cells Probed with Grazing Incidence Scattering Techniques. *Adv. Mater.* **2014**, *26*, 7692–7709.

78. Palomaki, P. K. B.; Krawicz, A.; Dinolfo, P. H. Thickness, Surface Morphology, and Optical Properties of Porphyrin Multilayer Thin Films Assembled on Si(100) Using Copper(I)-Catalyzed Azide-Alkyne cycloaddition. *Langmuir* **2011**, *27*, 4613–4622.

79. Roales, J.; Pedrosa, J. M.; Guillén, M. G.; Lopes-Costa, T.; Castillero, P.; Barranco, A.; González-Elipe, A. R. Free-Base Carboxyphenyl Porphyrin Films Using a TiO_2 Columnar Matrix: Characterization and Application as NO_2 Sensors. *Sensors* **2015**, *15*, 11118–11132.

80. Rochford, J.; Chu, D.; Hagfeldt, A.; Galoppini, E. Tetrachelate Porphyrin Chromophores for Metal Oxide Semiconductor Sensitization: Effect of the Spacer Length and Anchoring Group Position. *J. Am. Chem. Soc.* **2007**, *129*, 4655−4665.

81. Palomaki, P. K. B.; Dinolfo, P. H. Structural Analysis of Porphyrin Multilayer Films on ITO Assembled Using Copper(I)-Catalyzed Azide-Alkyne Cycloaddition by ATR IR. *ACS Appl. Mater. Interfaces* **2011**, *3*, 4703−4713.

82. Libera, J. A.; Gurney, R. W.; Schwartz, C.; Jin, H.; Lee, T.-L.; Nguyen, S.-T.; Hupp, J. T.; Bedzyk, M. J. Comparative X-Ray Standing Wave Analysis of Metal-Phosphonate Multilayer Films of Dodecane and Porphyrin Molecular Square. *J. Phys. Chem. B* **2005**, *109*, 1441−1450.

83. Qian, D.-J.; Nakamura, C.; Ishida, T.; Wenk, S.-O.; Wakayama, T.; Takeda, S.; Miyake, J. Palladium-Mediated Stepwise Assembly of Three-Dimensional Organized Multiporphyrin Arrays Directly on Solid Substrates. *Langmuir* **2002**, *18*, 10237−10242.

84. Kira, A.; Umeyama, T.; Matano, Y.; Yoshida, K.; Isoda, S.; Park, J. K.; Kim, D.; Imahori, H. Supramolecular Donor-Acceptor Heterojunctions by Vectorial Stepwise Assembly of Porphyrins and Coordination-Bonded Fullerene Arrays for Photocurrent Generation. *J. Am. Chem. Soc.* **2009**, *131*, 3198−3200.

85. Qian, D.-J.; Nakamura, C.; Ishida, T.; Wenk, S.-O.; Wakayama, T.; Takeda, S.; Miyake, J. Palladium-Mediated Stepwise Assembly of Three-Dimensional Organized Multiporphyrin Arrays Directly on Solid Substrates. *Langmuir* **2002**, *18*, 10237−10242.

86. Furukawa, H.; Müller, U.; Yaghi, O. M. Heterogeneity Within Order in Metal-Organic Frameworks. *Angew. Chem. Int. Ed.* **2015**, *54*, 3417-3430.

87. Ambre, R.; Chen, K.-B.; Yao, C.-F.; Luo, L.; Diau, E. W.-G,; Hung, C.-H. Effect of Porphyrinic *meso*-Substituents on the Photovoltaic Performance of Dye-Sensitized Solar Cells: Number and Position of *p*-Carboxyphenyl and Thienyl Groups on Zinc Porphyrins. *J. Phys. Chem. C* **2012**, *116*, 11907-11916.

88. Ambre, R. B.; Mane, S. B.; Chang, G.-F.; Hung, C.-H. Effects of Number and position of Meta and Para Carboxyphenyl Group of Zinc Porphyrin in Dye-Sensitized Solar Cells: Structure-Performance Relationship. *ACS Appl. Mater. Interfaces* **2015**, *7*, 1879-1891.

89. Gottfried, J. M.; Flechtner, K.; Kretschmann, A.; Lukasczyk, T.; Steinrück, H.-P. Direct Synthesis of a Metalloporphyrin Complex on a surface. *J. Am. Chem. Soc.* **2006**, *128*, 5644-5645.

90. Karweik, D. H.; Winograd, N.; Nitrogen Charged Distributions in Free-Base Porphyrins, Metalloporphyrins, and Their Reduced Analogues Observed by X-Ray Photoelectron Spectroscopy. *Inorg. Chem.* **1976**, *15*, 2336-2342.

91. Haraguchi, T.; Otsubo, K.; Sakata, O.; Fujiwara, A.; Kitagawa, H. Remarkable Lattice Shrinkage in Highly Oriented Crystalline Three-Dimensional Metal-Organic Framework Thin Films. *Inorg. Chem.* **2015**, *54*, 11593-11595.

92. Gilbert, B.; Huang, F.; Zhang, H.; Waychunas, G. A.; Banfield, J. F. Nanoparticles: Strained and Stiff. *Science* **2004**, *305*, 651-654.

93. Senge, M. O.; MacGowan, S. A.;O'Brien, J. M. Conformational Control of Cofactors in Nature-the Influence of Protein-Induced Macrocycle Distortion on the Biological Function of Tetrapyrroles. *Chem. Commun.* **2015**, *51*, 17031-17063.

94. Werner, K.; Mohr, S.; Schwarz, M.; Xu, T.; Amende, M.; Döpper, T.; Görling, A.; Libuda, J. Functionalized Porphyrins on an Atomically Defined Oxide Surface: Anchoring and Coverage-Dependent Reorientation of MCTPP on Co_3O_4(111). *J. Phy. Chem. Lett.* **2016**, 7, 555-560.

95. Morris, W.; Volosskiy, B.; Demir, S.; Gándara, F.; McGrier, P. L.; Furukawa, H.; Cascio, D.; Stoddart, J. F.; Yaghi, O. M. Synthesis, Structure, and Metalation of Two New Highly Porous Zirconium Metal-Organic Frameworks. *Inorg. Chem.* **2012**, *51*, 6443–6445.

96. Kung, C.-W.; Chang, T.-H.; Chou, L.-Y.; Hupp, J. T.; Farha, O. K.; Ho, K.-C. Post Metallation of Solvothermally Grown Electroactive Porphyrin Metal-Organic Framework Thin Films. *Chem. Commun.* **2015**, *51*, 2414-2417.

97. Gao, W.-Y.; Wojtas, L.; Ma, S. A porous metal-metalloporphyrin framework featuring high density active sites for chemical fixation of CO_2 under ambient conditions. *Chem. Commun.* **2014**, *50*, 5316–5318.

98. Nishihara, H.; Kanaizuka, K.; Nishimori, Y.; Yamanoi, Y. Construction of Redox- and Photo-Functional Molecular Systems on Eletrode Surface for Application to Molecular Devices. *Coord. Chem. Rev.* **2007**, *251*, 2674-2687.

99. Hod, I.; Sampson, M. D.; Deria, P.; Kubiak, C. P.; Farha, O. K.; Hupp, J. T. Fe-Porphyrin-Based Metal-Organic Framework Films as High-Surface Concentration,

Heterogeneous Catalysts for Electrochemical Reduction of CO_2. *ACS Catal.* **2015**, *5*, 6302–6309.

Chapter 4

General Conclusion and Future Prospects

4.1 General Conclusion

My study was conducted to achieve the research objectives. These are the conclusion, achievement and prospect of this research.

1.) The bulk of metal-organic coordination networks was successfully synthesized through 5,10,15,20-tetrakis(4-carboxyphenyl)-porphyrin and cobalt (II) ions. The single crystal was not obtained from this bulk at room temperature synthesis. The bulk product provided not only the crystalline phase but also the amorphous phase at this mild condition. This may due to quick precipitation of bulk product. Furthermore, it was found that the cobalt (II) ions can bind to porphyrin not only at the carboxylic acid group of porphyrin to generate the coordination network, but cobalt (II) ions also metalate at the center of porphyrin core. The finding results in bulk synthesis indicated that the metal-organic coordination networks based on this system can be obtained even in room temperature condition which encouraged the study of thin film preparation on the surface using the similar chemical precursors.

2.) Metal-organic coordination network thin films were effectively prepared through 5,10,15,20-tetrakis(4-carboxyphenyl)-porphyrin and cobalt (II) ions by surface-induced assembly (SIA) method at room temperature synthesis. The surface modification of solid substrate was prior prepared on the surface to act as platform for the growth of

coordination structure on this surface. The multilayer thin films exhibited the stepwise growth with compact packing and homogeneous surface morphology with low surface roughness. The linear increase of thickness in multilayer film was controlled by the number of layers. The mass density of film was almost constant throughout the multilayer formation along with the existence of periodic structure in in-plane (IP) direction. These results indicated a well-organized structure of film growth. The alignment of the porphyrin macrocycle plane of the framework has been proposed as a hexagonal packed model using single-anchor binding with tilting of approximately 60° relative to the surface substrate. This result suggested that structural arrangement on the surface can be efficiently controlled by SIA technique.

3.) We found the dissimilar characteristics between thin film and bulk materials in several points including the remaining of reactive moieties (-COOH) in the coordination networks, the different metalation stage at the center of porphyrin core and the most important point is the structural dissimilarity. This may due to the distinct growth mechanisms or molecular arrangements during network formation between film on the surface by SIA method and the bulk in solution. More complete reaction within the short time in thin film synthesis represented the advantage of SIA technique to sequentially control the assembly between cobalt (II) ions and porphyrin in step-by-step fashion. In contrast with bulk system, the defect (unreacted -COOH part) was existed in the bulk product even in long time synthesis process. Some of the phenomena such as the partial distortion, shrinkage or reorientation of network on the surface and the functionalized moiety on substrates might be considered to explain the discriminated structures between bulk and film system. The exact reason for this difference is still needed to have further study which may provide the valuable information for the development of surface science in future.

4.) The finding in this research can contribute to the study of coordination chemistry on the surface which may promote the understanding in solid state phenomena and extend to prepare the variety of nanostructures for application in nanoscale devices.

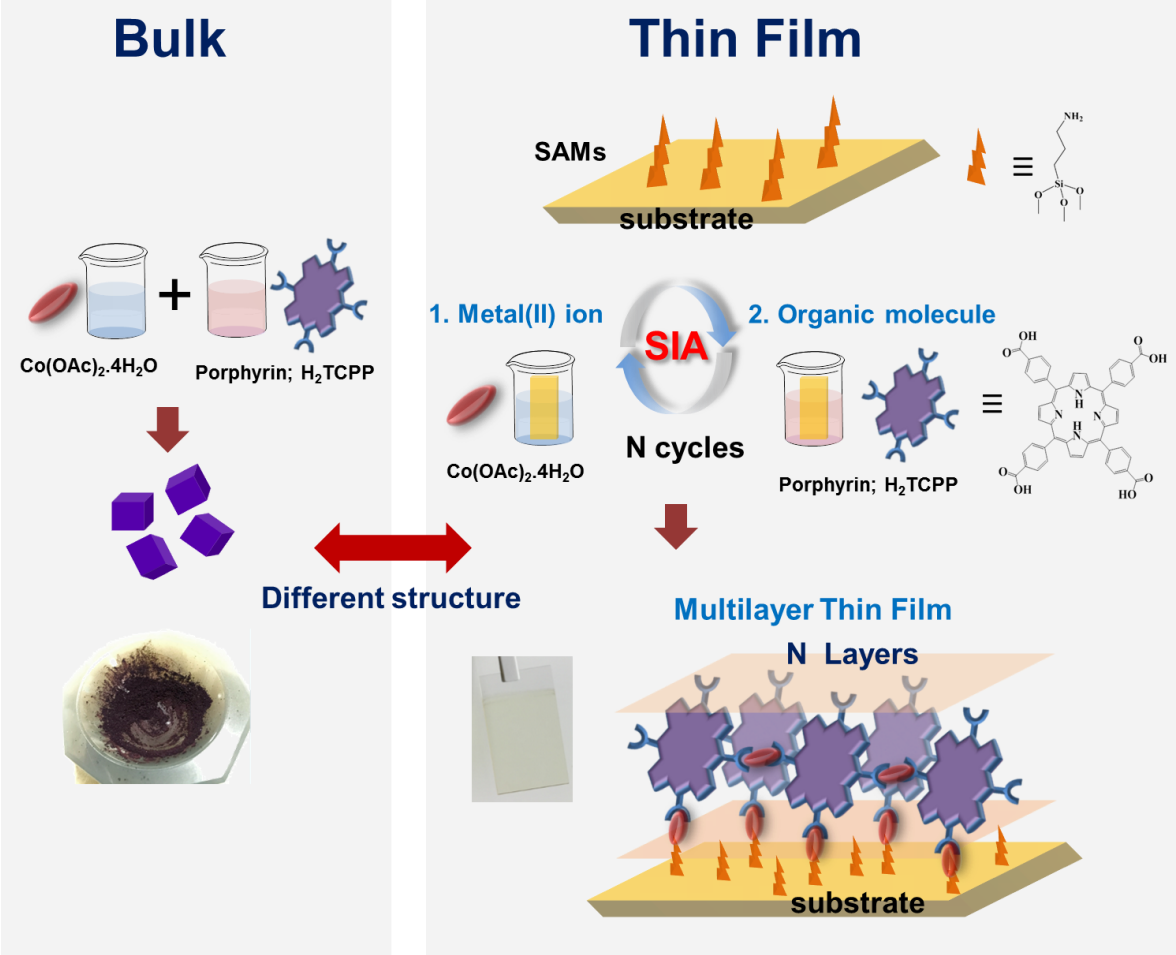

4.2 Future Prospects

From our thin film research, the results suggest that the role of surface and the SIA process can provide the controlling of molecular arrangement for the coordination chemistry on the surface. The future prospects are mentioned as following aspects:

1. Based on our results, the variety of coordination networks on the surface can be anticipated using this SIA technique with other chemical components.

2. The different types of SAMs terminal group and the density of SAMs should be investigated to understand the relationship between SAMs and structure of coordination networks on the surface.

3. The retaining of non-metalated porphyrin center in thin film (even partial metalation) provides the opportunity to extend the material application by the post-metalation process, which can provide the accessibility of metal ion to the center of porphyrin ring after the thin film preparation. The variety of metal ion species is highly possible for porphyrin unit such as iron, cobalt, copper, zinc, nickel, etc. This advantage can promote the tremendous applications such as sensing, catalyst due to the variation of metal properties.

4. The understanding of growth mechanism via interior growth phenomena is very necessary and needed to develop the desirable properties of metal-organic coordination network thin film.

The design of metal-organic coordination network thin film with controllable growth manner is the key challenge that must be addressed to promote these solid state phenomena for nanoscale device.

Acknowledgement

I would like to express my deepest gratitude to my supervisor, Associate Professor Yuki Nagao for his valuable suggestion, kind encouragement, supervision, and great supporting in research throughout my doctoral study.

I also express my grateful thank to Professor Noriyoshi Matsumi for being my second supervisor and his kind guidance in this study.

I would like to gratefully thank to Associate Professor Tsutomu Hamada to provide me a great opportunity to proceed subtheme research under his supervision, which widen my knowledge in another research field. I also express my special thanks to Ms. Shino Mizuno for her kind support in this subtheme research.

I would like to sincerely express my appreciation to Associate Professor Shusaku Nagano and Assistance Professor Mitsuo Hara in Nagoya University for great research collaboration and valuable discussion. I also acknowledge Mr. Ryosuke Goto for his kind support in experiments at Nagoya University.

I am very grateful to Associate Professor Masashi Akabori for his kind guidance and valuable suggestion for AFM measurement.

I also deeply appreciate all referees including Professor Kohki Ebitani and Professor Donglin Jiang of JAIST, and Associate Professor Tatsuya Nishimura of Kanazawa University for their valuable comments and suggestion.

I would like to thank all of the present and former members in Nagao laboratory for kind supporting and beneficial discussion.

Finally, I profoundly appreciate the encouragement, understanding and support from my parents and all of friends.

SALINTHIP LAOKROEKKIAT

September 2016

Achievements

[Research Publications]

1. Salinthip Laokroekkiat, Mitsuo Hara, Shusaku Nagano and Yuki Nagao. "Metal-Organic Coordination Network Thin Film by Surface-Induced Assembly", *Langmuir*, **2016**, *32*, 6648-6655.

[Other Research Publications]

1. Md. A. Rashed, Salinthip Laokroekkiat, Mitsuo Hara, Shusaku Nagano and Yuki Nagao. "Fabrication and Characterization of Cross-Linked Organic Thin Films with Nonlinear Mass Densities", *Langmuir*, **2016**, *32*, 5917-5924.

[Conferences]

Oral Presentation

1. Salinthip Laokroekkiat, Mitsuo Hara, Shusaku Nagano and Yuki Nagao, "Nanostructure Fabrication of Porphyrin-based Metal Organic Frameworks (MOFs) Thin Film" 第 64 回高分子学会北陸支部研究発表会, 14-15 November 2015, Ishikawa High-Tech Center, Japan

2. Salinthip Laokroekkiat, Mitsuo Hara, Shusaku Nagano and Yuki Nagao, "Oriented Multilayer Nanofilm of Metal-Organic Coordination Networks based on Porphyrin Architecture" 96th CSJ Annual Meeting 2016, 24-27 March 2016, Kyoto, Japan

Poster Presentation

1. Salinthip Laokroekkiat, Mitsuo Hara, Shusaku Nagano and Yuki Nagao, "Porphyrin-based Metal-Organic Coordination Network Thin Films via Layer-by-Layer Approach" IISc-JAIST Joint Workshop on Functional Inorganic and Organic Materials, 7 March 2016, JAIST, Japan

2. Salinthip Laokroekkiat, Mitsuo Hara, Shusaku Nagano and Yuki Nagao, " Fabrication of Nanoscale Thin Film Using Porphyrin-based SURMOFs Concept" 2015 International Chemical Congress of Pacific Basin Societies, 15-20 December 2015, Hawaii, USA

3. Salinthip Laokroekkiat, Mitsuo Hara, Shusaku Nagano and Yuki Nagao, "Multilayer Growth of Porphyrin-based Metal Organic Frameworks on substrate" 25th Annual Meeting of MRS-J (2015), 8-10 December 2015, Yokohama, Japan

4. Salinthip Laokroekkiat, Mitsuo Hara, Shusaku Nagano and Yuki Nagao, "Nanofabrication of Porphyrin-based Metal-Organic Frameworks (MOFs) thin film on Solid Surface" 平成 27 年度北陸地区講演会と研究発表会, 27 November 2015, Kanazawa, Japan

5. Salinthip Laokroekkiat, Mitsuo Hara, Shusaku Nagano and Yuki Nagao, "Nanostructure Fabrication of Porphyrin-based Metal Organic Frameworks (MOFs) Thin Film" 平成 27 年度北陸地区高分子若手研究会, 13 November 2015, Ishikawa High-Tech Center, Japan

6. Salinthip Laokroekkiat, Mitsuo Hara, Shusaku Nagano and Yuki Nagao, "Porphyrin-based Metal-Organic Frameworks (MOFs) Multilayer Thin Film on Solid Surface" JAIST-SAST 2015, 11 November 2015, JAIST, Japan

7. Salinthip Laokroekkiat, Tomoyuki Ihara, Takahiro Ohyama, Banjongsak Lamlua and Yuki Nagao, "Metalloporphyrin-based Multilayer Molecular Assembly Using Layer-by-Layer Technique" 平成 26 年度北陸地区講演会と研究発表会, 21 November 2014, Toyama, Japan

8. Salinthip Laokroekkiat, Tomoyuki Ihara, Takahiro Ohyama, Banjongsak Lamlua and Yuki Nagao, "Multilayer of Metalloporphyrin-based Coordination Network Via Layer-by-Layer Assembly For Oxygen Reduction Reaction" 4th International Conference on Metal-Organic Frameworks & Open Framework Compounds, 28 September - 1 October 2014, Kobe, Japan

[Award]

1. Poster award in SPSJ Young Scientist Conference in Hokuriku. 13 November 2015, Ishikawa High-Tech Center, Japan

Abstract of Subtheme Research

The creation of an artificial ion channel in material is still challenging issue. Prussian blue (PB) is one of coordination polymer compound which shows the proton transport property. The hybrid material of lipid bilayer and the prussian blue nanoparticle (PB NP) may provide the proton transport channel through the PB NP. In this research, the preliminary results suggested some evidences about the proton transport phenomena and the reversibility of this phenomenon in the PB NP-embedded liposome. The observation was proceeded by the phase-contrast microscopy with dye fluorescence. The pH adjustment between inside and outside liposome was used to control the proton gradient. As the present results, it seems difficult to exactly determine the proton transport phenomena by the present method. Thus, more experiments are needed to be conducted for clarifying in this issue. This research opens up the opportunity to discover the artificial material for controlling the proton transport properties.

Keywords: Prussian Blue Nanoparticle (PB NP), Lipid Bilayer, Liposome, Proton transport property